ARPA/NRL X-RAY LASER PROGRAM - SEMIANNUAL TECHNICAL REPORT TO DEFENSE ADVANCED RESEARCH PROJECTS AGENCY, 1 JANUARY 1974 - 30 JUNE 1974

R. A. Andrews, et al

Naval Research Laboratory

Prepared for:

Office of Naval Research
Defense Advanced Research Projects Agency

October 1974

UNCLASSIFIED

SECURITY CLASSIFICATION OF THIS PAGE (When Data Entered)

REPORT DOCUMENTATION PAGE		READ INSTRUCTIONS BEFORE COMPLETING FORM
1. REPORT NUMBER NRL Memorandum Report 2910	2. GOVT ACCESSION NO.	3. RECIPIENT'S CATALOG NUMBER AD 787626
4. TITLE (and Subtitle) ARPA/NRL X-Ray Laser Program - Semiannual Technical Report to Defense Advanced Research Projects Agency - 1 January 1974 - 30 June 1974		5. TYPE OF REPORT & PERIOD COVERED Semi-Annual Technical Report; work continuing 6. PERFORMING ORG. REPORT NUMBER
7. AUTHOR(s) Interaction Physics Branch Optical Sciences Division		8. CONTRACT OR GRANT NUMBER(s)
9. PERFORMING ORGANIZATION NAME AND ADDRESS Naval Research Laboratory Washington, D.C. 20375		10. PROGRAM ELEMENT, PROJECT, TASK AREA & WORK UNIT NUMBERS NRL Prob. N01-43, N01-33 ARPA Order 2694, Program Code 4D10
11. CONTROLLING OFFICE NAME AND ADDRESS Defense Advanced Research Projects Agency Washington, D.C. 20375		12. REPORT DATE October 1974 13. NUMBER OF PAGES 142
14. MONITORING AGENCY NAME & ADDRESS(if different from Controlling Office)		15. SECURITY CLASS. (of this report) UNCLASSIFIED 15a. DECLASSIFICATION/DOWNGRADING SCHEDULE

16. DISTRIBUTION STATEMENT (of this Report)

Approved for public release; distribution unlimited.

17. DISTRIBUTION STATEMENT (of the abstract entered in Block 20, if different from Report)

18. SUPPLEMENTARY NOTES

19. KEY WORDS (Continue on reverse side if necessary and identify by block number)

X-Ray Lasers
Lasers
Ultraviolet Lasers
Laser-Plasma Interactions

20. ABSTRACT (Continue on reverse side if necessary and identify by block number)

The ARPA/NRL x-ray laser program is concerned with demonstrating gain in the soft x-ray region. The program is jointly supported by ARPA and NRL. The approaches include electron-collisional pumping in picosecond laser pumped plasma, resonant charge transfer pumping, optical parametric mixing to short wavelengths, traveling wave e-beam pumping, and analysis and numerical modeling. This report covers the progress made during the second half of FY-74.

DD FORM 1 JAN 73 1473 EDITION OF 1 NOV 65 IS OBSOLETE S/N 0102-014-6601

UNCLASSIFIED

SECURITY CLASSIFICATION OF THIS PAGE (When Data Entered)

TABLE OF CONTENTS

FORWARD

The Interaction Physics Branch of the Optical Sciences Division, Naval Research Laboratory, Washington, D. C. prepared this semiannual report on work sponsored jointly by the Defense Advanced Research Projects Agency, DARPA Order 2694, and the Naval Research Laboratory. Co-authors of the report were R. A. Andrews, R. C. Elton, J. Reintjes. R. C. Eckardt, R. H. Lehmberg, R. Waynant, T. N. Lee, L. J. Palumbo, J. M. McMahon, D. Nagel, and W. Jones.

SEMI-ANNUAL TECHNICAL REPORT

Reporting Period
1 Jan 1974 - 30 June 1974

1.	DARPA Order	2694
2.	Program Code No.	4D10
3.	Name of Contractor	Naval Research Laboratory Optical Sciences Division
4.	Effective Date of Contract	1 January 1974
5.	Contract Expiration Date	Continuing
6.	Amount of Contract	$125K (FY74) $250K (FY75)
7.	Contract No.	N/A
8.	Principal Investigator	Dr. R. A. Andrews
9.	Telephone No.	202-767-3528
10.	Scientific Officer	Dr. C. M. Stickley
11.	Title of Work	X-Ray Lasers

Sponsored by

DEFENSE ADVANCED RESEARCH PROJECTS AGENCY
DARPA Order No. 2694

I. INTRODUCTION

The x-ray laser program at NRL was initiated as an in-house funded effort in July of 1972. Its goal is to demonstrate gain in the soft x-ray region. The total program is one of several approaches that look about equally promising of achieving this goal. The guiding premise is that multiple approaches will be followed until one or more approaches stand out as being less promising than the others, at which point the program is narrowed and concentrated on the remaining approaches. The program was augmented by ARPA support in January 1974. It is currently a jointly funded program with four experimental approaches. The ARPA/NRL x-ray laser program currently consists of the following efforts to achieve gain and/or coherent radiation in the soft x-ray region:

(1) Electron collisional pumping using picosecond laser pumping of a cold plasma,

(2) Traveling wave (TW) high energy electron beam pumping,

(3) Nonlinear optical mixing starting with intense 1600 Å radiation,

(4) Resonant charge transfer pumping in a plasma expanding into neutral helium, and

(5) Theory, analysis, and numerical modeling in support of the above and other approaches.

All these efforts are interrelated and, in fact, no one segment can be separated from the program as an individual, distinct effort. That is, all of the professionals and experimental facilities are common to two or more of the program segments. However, for administrative purposes only, a distinction has been made. Hence approaches (1) and (2) have been designated NRL supported efforts, (3) and (4) ARPA supported efforts, and (5) a jointly supported effort.

This progress report will treat the x-ray laser program in its entirety. The reasons are many. First, the approaches were selected as the most promising that would cover all possibilities considering NRL's expertise and what is being done at other laboratories. Second, work centers around large laser facilities and the professionals involved are involved with all aspects of the program to some extent. Third, results from each approach relate to and affect the work on the other approaches. Hence in order to present a complete and coherent picture of the program, this report will cover the entire effort. The approaches that were initiated with ARPA support (3, 4, 5 above) will report six months progress. The other efforts (1, 2, 5 above) will include background on progress made prior to January 1974.

Manuscript submitted September 27, 1974.

The x-ray laser program, since it relies heavily on short pulse lasers and laser plasma interactions, is aided by the work done at NRL on the larger Laser-Matter Interaction (LMI) program. This program has been in existence for several years and is supported by the AEC (laser fusion related experiments) and DNA (laser x-ray generation experiments). That program centers around the NRL Glass Laser Facility which was developed under ARPA support (ARPA Order 2062). Experimental results and expertise in the areas of lasers, laser plasmas, and numerical modeling have, in the past, influenced this program and continue to do so.

The selection of the above listed approaches in this program is based not only on analyses of the feasibility of various pumping schemes, given today's technology, but on an analysis of potential applications. Technological limits realistically put the goal of the program under 1 keV. Generally speaking applications that can be identified as really needing an x-ray laser depend on two unique characteristics of the potential "laser". These are coherence and ultra short pulses. Most approaches to an "x-ray laser" are really high gain single pass ASE devices. This is due to the difficulty of providing a resonator in this spectral region. ASE devices are of limited coherence at best and are generally considered incoherent laser sources. This very important consideration of coherence is the reason why the nonlinear mixing approach to shorter wavelengths is being pursued in this program. This technique preserves the coherence and beam quality of the initial laser, which in this case is a mode-locked, single transverse mode, Nd:YAG laser. To obtain significant or ultra high power densities in the soft x-ray region using this approach, amplifiers will probably be required somewhere in the cascade from 1.06 μ to the region of 100 Å. The hydrogen amplifier at 1600 Å is one very real possibility. The other approaches in this program offer other possibilities for amplifiers at shorter wavelengths.

The electron collisional pumping and resonant charge transfer approaches use two state-of-the-art laser facilities at NRL. Both of these facilities are described in detail in this report. Also, both of these approaches use laser produced plasmas and have goals in the soft x-ray region. Laser-plasma studies are involved in both of these approaches. The experiments are similar. The experimental parameters and conditions can easily be varied to study the physics of either scheme. In principle these two efforts could be combined into a "laser-plasma" approach to achieving gain in the soft x-ray region.

The TW e-beam pumping device is limited to about 1000 Å. However it represents an effort to understand the concept of TW pumping which is important for short-lived soft x-ray transitions. The technology and experimental devices also lend themselves to the study of UV lasing in high pressure gases.

Finally, the theory and analysis cover a variety of topics. This

is consistent with the overall program concept of pursuing only those approaches that offer the highest potential for success. Hence efforts are modified, dropped, or initiated based on the best current understanding of the mechanisms and physics involved.

The following sections of this report cover each approach in the program in detail. This is followed by a summary of the important results of the past six months. Appendices are included for completeness. These include reports on work closely related to this effort but which are parts of other programs with other goals. However, this work has had a significant impact on the program. Pulse compression studies offer the possibility of shorter, laser pulses to pump laser plasma and in principle make inversions easier to attain. The other appendix describes the NRL Glass Laser Facility and its capability.

II. E-COLLISIONAL PUMPING VIA PICOSECOND LASER PUMPING OF PLASMAS

II. A. BACKGROUND

One of the potential techniques for pumping a soft x-ray laser is to use electron-collisional pumping of a plasma where 1) the electron temperature is much greater than the ion temperature and, 2) the population of the potential laser ion species has been maximized in the preformed plasma. As a first approach the laser levels can be isoelectronic with known lasers in the visible/UV, using atoms and ions with low levels of ionization. Then as one goes to higher Z ions in the same isoelectronic sequence, the laser levels become more energetic. To make this technique work one must create a plasma which has a large population of the desired ion species at some point in time. This plasma should have as low an ion temperature as possible to reduce the Doppler broadening of the laser levels. Also to obtain the high electron temperatures required for pumping, the laser pulse which heats the electrons should be as short as possible, i.e., picosecond pulses for high pumping power.

The first step in this general experimental approach is to develop a laser system which is capable of producing two synchronized energetic pulses--the first a nanosecond pulse for producing the "target" plasma and a second picosecond pulse at a specific time later to heat the electrons and pump the laser transition. This laser development is described in the next section. The second step is to characterize laser produced plasmas in order to develop the capability of predicting the time history of electron and ion temperatures, and ionic species and their populations. Once this can be done, then a target plasma of known parameters can be reproduceably created for the two step laser experiments. These experiments are on-going and are described in this section.

The experiments to date have utilized three distinct NRL laser facilities:

(1) The short-pulse laser facility (25 psec, 10 GW) which will be used to heat laser-generated plasmas.

(2) The NRL Glass Laser Facility which produces pulses of various widths between 50 and 900 picoseconds with ouput on the order of 100 GW. (This facility is described in detail in Appendix B.)

(3) A Korad Q-switched ruby laser (20 nsec, 0.5 GW) which is also used for diagnostics development.

The long pulse experiments were the first in the series. Shorter pulse experiments were done as the laser facilities became available. Results obtained from x-ray diagnostics of plasmas produced by each of these lasers are discussed separately in the following three subsections. Some comparison of these results with numerical modeling work has been done and is also discussed. The goal of the experiments done to date has been to characterize the laser produced plasmas in order that plasmas pertinent to the x-ray laser problem can be predictably created.

II. B. PICOSECOND LASER/PLASMA EXPERIMENTS

The mode-locked Nd:YAG laser beam of 25 ps in pulse duration is directed into a vacuum chamber ($p \leq 10^{-4}$ torr) and then focused onto various slab targets (Na, Mg, Al and Si) using a 30 cm focal length lens. The focal spot has an elliptical shape of 30 μm by 70 μm and the laser power density at the focus is estimated to be 10^{14} Watts/cm^2. X-ray pinhole images and spectra from plasmas produced by this power density were measured. An expanding, x-ray emitting plasma (aluminum) is photographed using a double-pinhole x-ray camera. Figure 1 shows microdensitometer scans (showing density contour) of such x-ray photographs taken simultaneously, one through 0.5 mil and the other through 1.5 mil beryllium absorbers. The size of the initial hot plasma is estimated to be 50 μm in diameter.

The plasma radiation is spectrally analyzed using a flat Rubidium Acid Phthalate (RAP) crystal (2d = 26.121 Å) and the spectra are recorded on No Screen medical x-ray film through 12 μm beryllium foil to protect the film from visible radiation. Although the potential lasing wavelengths conceivable with the laser power density available here would lie well above 100 Å, the spectral region of 5 Å - 12 Å is relatively clear of line radiation, and consequently more convenient for line identification. Figures 2 through 5 indicate microdensitometer scans of the x-ray spectra thus obtained from Na-, Mg-, Al-, and Si - plasmas, respectively. All four spectra show very strong $1s2p \rightarrow 1s^2$ resonance transition lines and the other Rydberg series lines of He-like ion species, i.e., Na X, Mg XI, Al XII, and Si XIII. Free-to-bound recombination edges are also seen at the series limits. For Na-, Mg-, and Al- plasmas, even H-like (Na XI, Mg XII, and Al XIII) Lyman-α lines

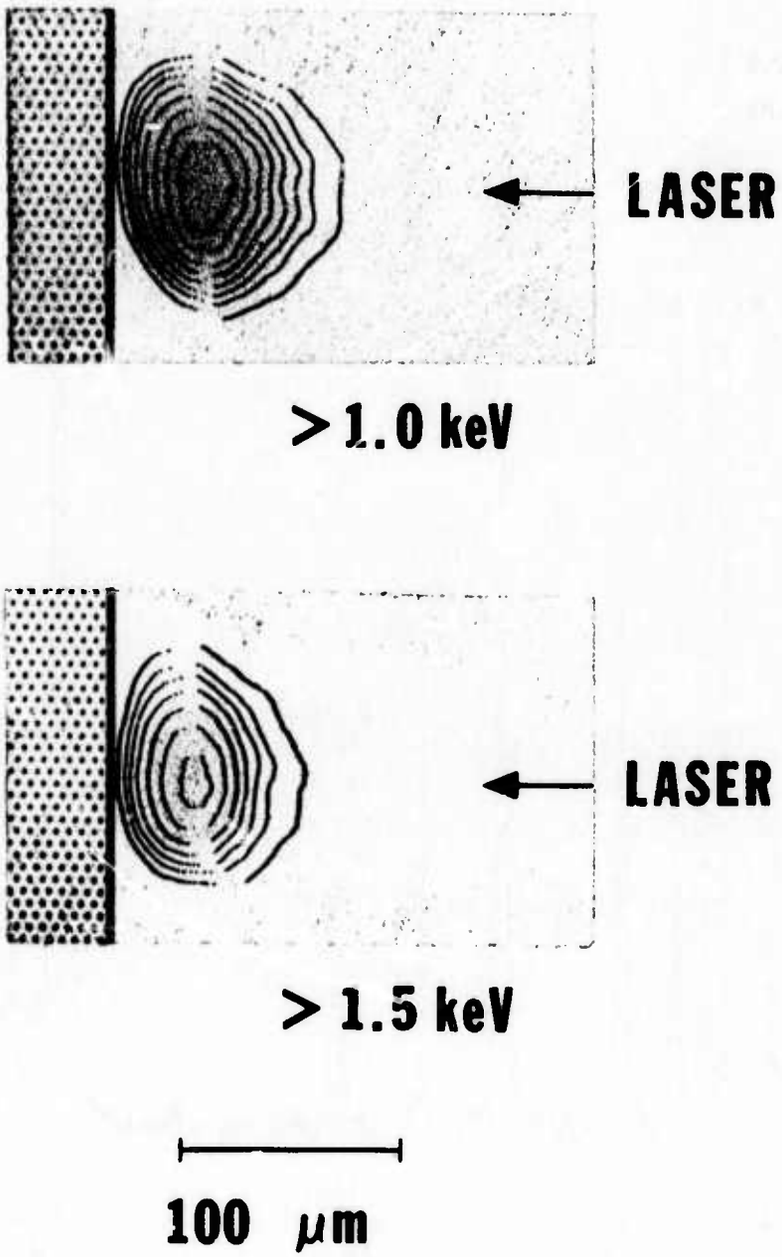

Figure 1 Pinhole x-ray photographs taken simultaneously with two different absorbers to detect the x-ray energies indicated in keV.

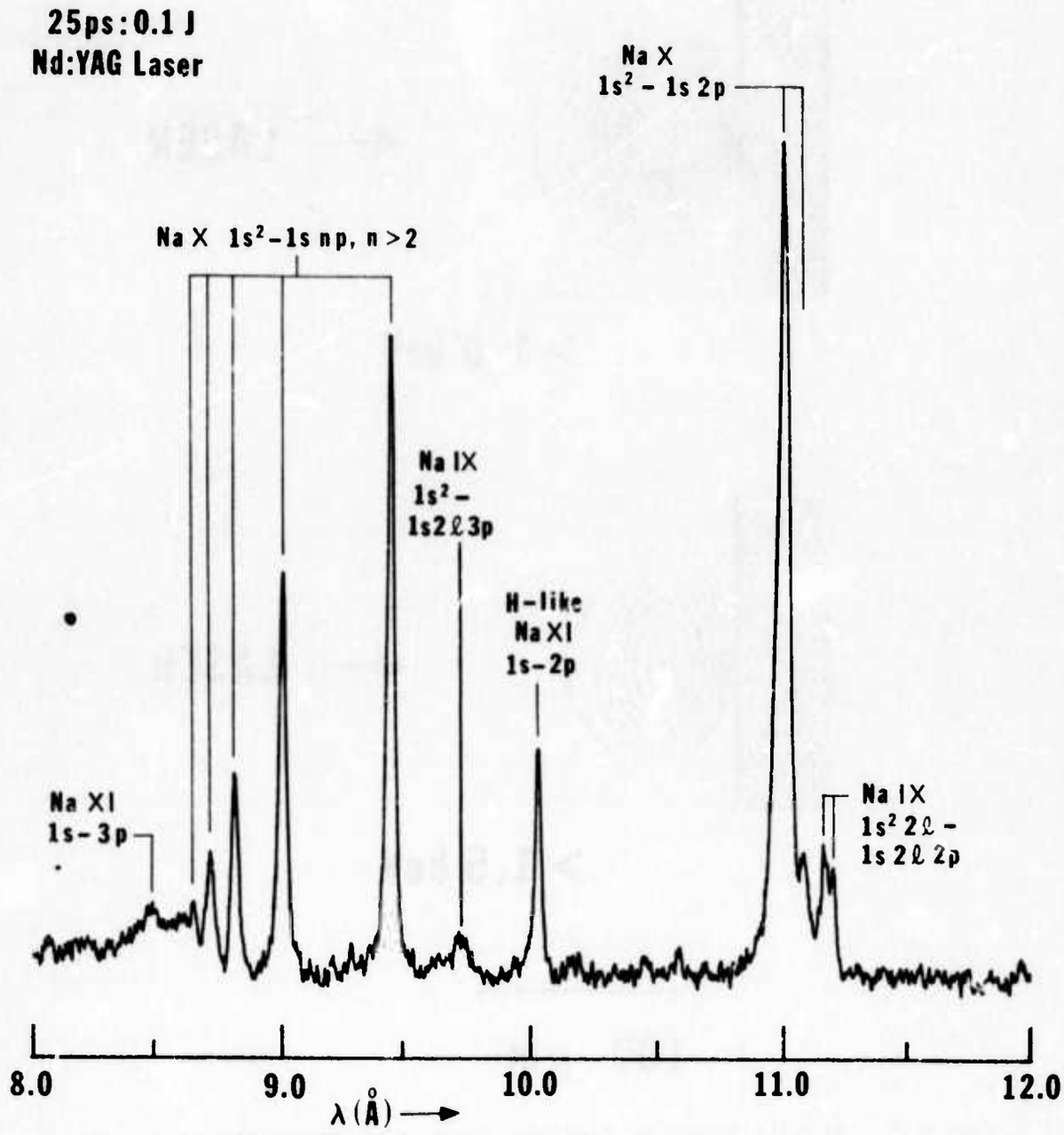

Figure 2 X-ray spectrum taken with Na-target.

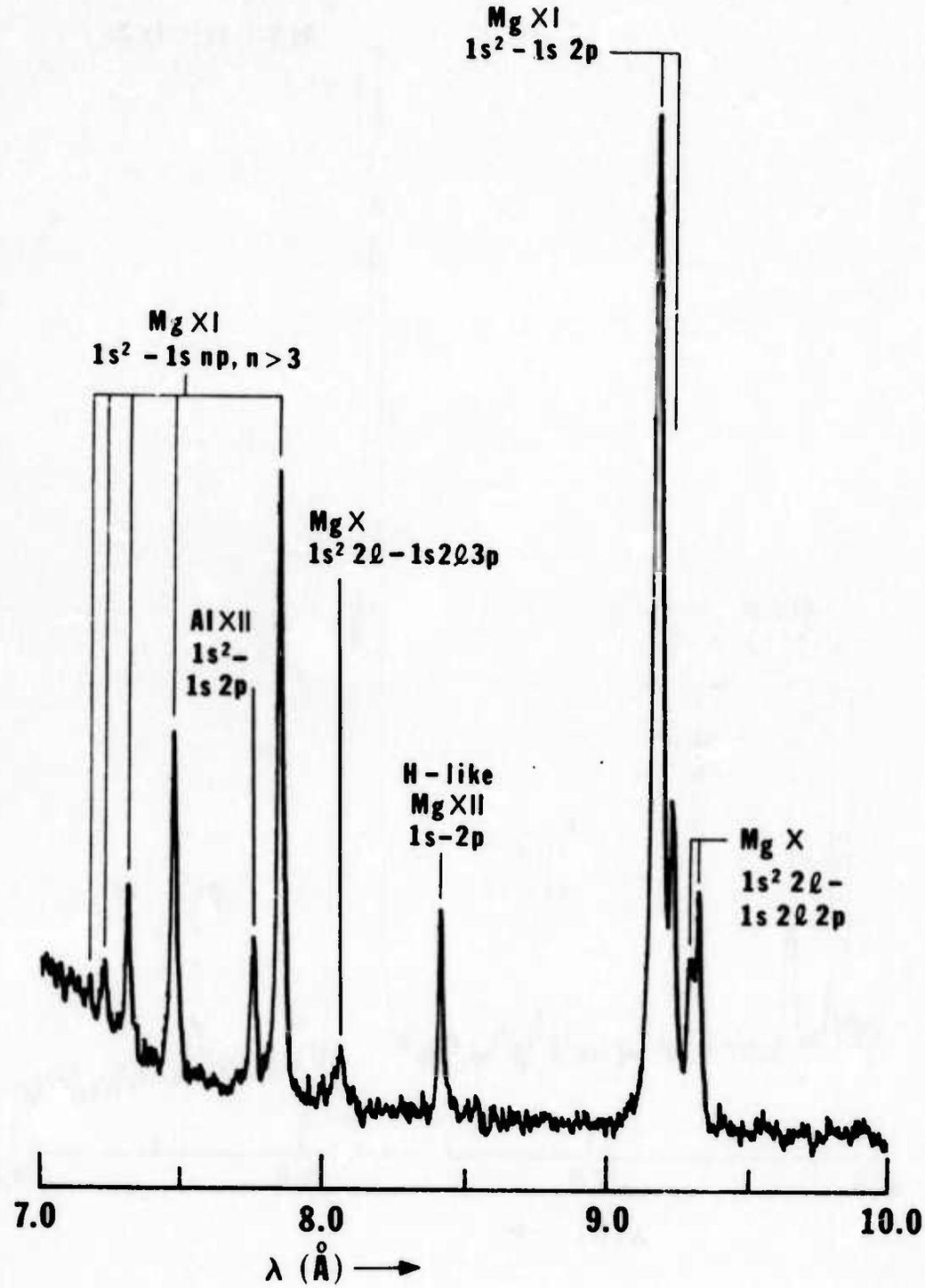

Figure 3 X-ray spectrum taken with Mg-target.

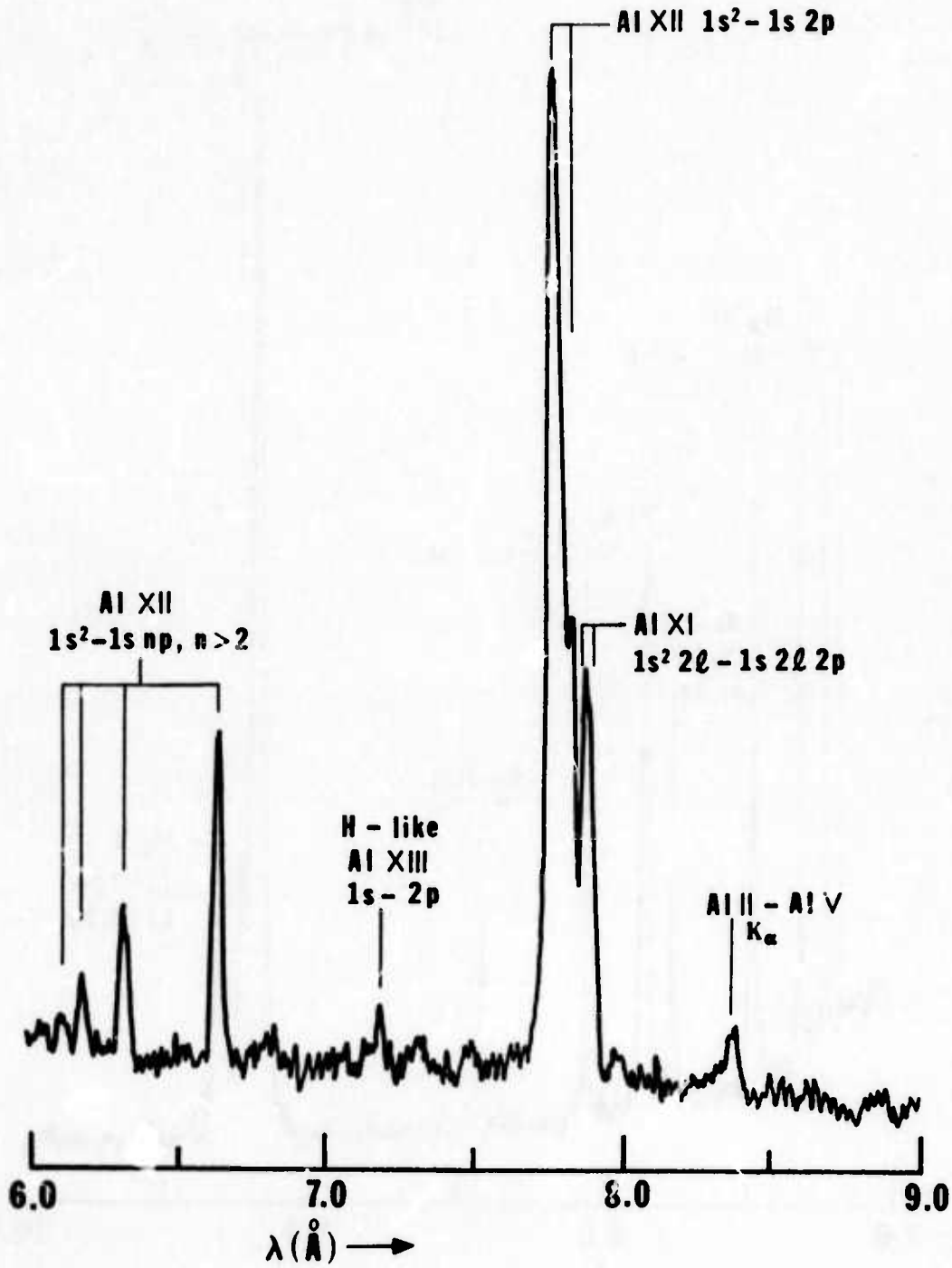

Figure 4 X-ray spectrum taken with Aℓ-target.

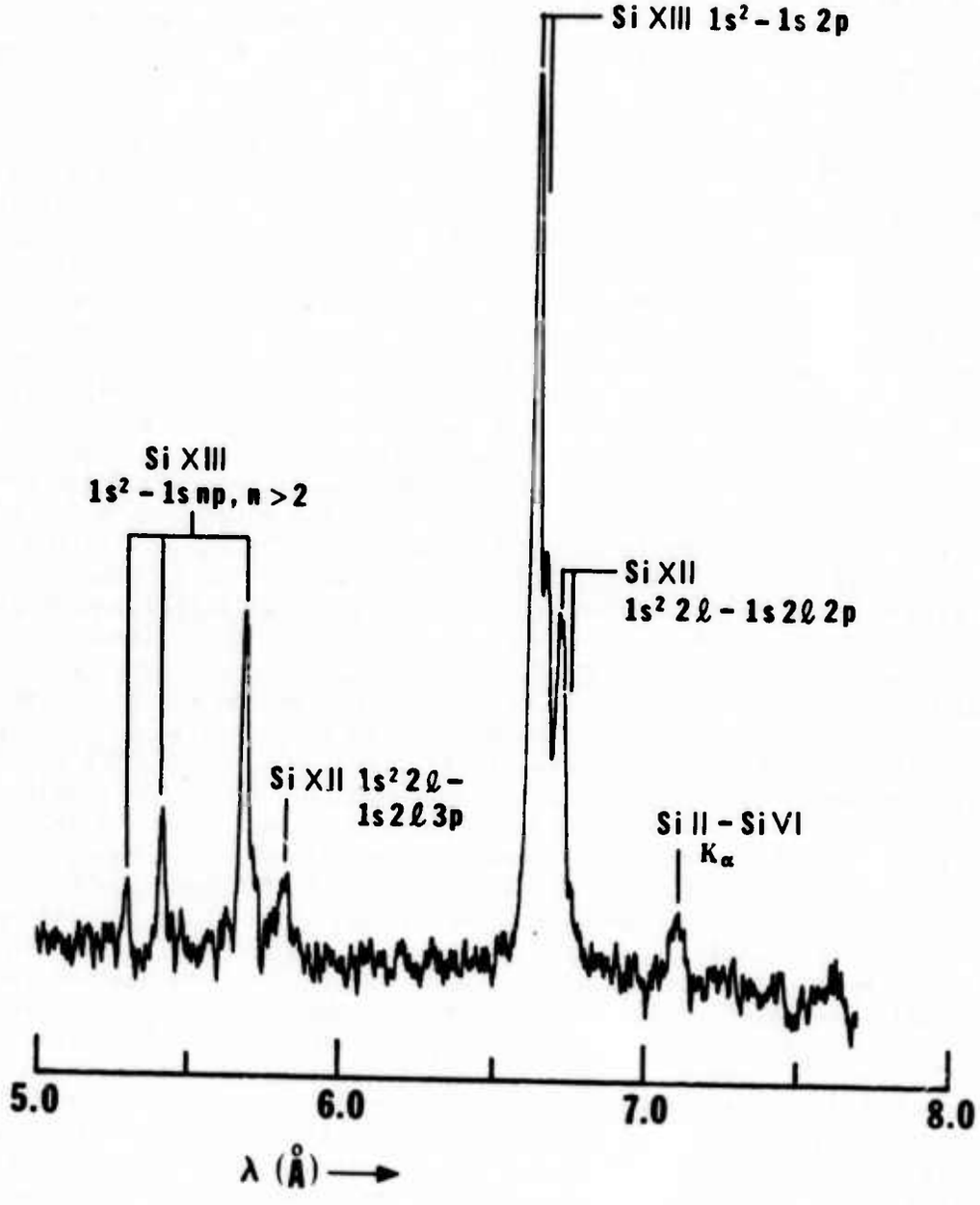

Figure 5 X-ray spectrum taken with Si-target.

appear, decreasing in intensity with increasing atomic number. But the trend is reversed for blends of long wavelength satellite lines of the He-like resonance line, $1s2\ell 2p \rightarrow 1s^2 2\ell$. This is understandable in a view that, when the laser heated plasma temperature is high enough to ionize up to H-like ion species for lower Z atoms, the temperature is too high for Li-like ion species to be highly populated (burn out).

Assuming that the electron density does not exceed the critical value ($\simeq 10^{21}$ cm^{-3}) for laser light penetration, the high stages of ionization observed with such a short heating pulse are difficult to understand using a thermal model of the plasma, because the thermal ionization time required is longer than the laser pulse. The situation here may be explained however using a spherical "hot spot" model*. This numerical model assumes a stationary, uniform plasma sphere at the laser focus (neglecting magnetohyrodynamic plasma motion during the time of interest) and also assumes that the major plasma cooling is by radiative and thermal-conductive mechanisms. It is also assumed that the laser light is absorbed in a small volume of $\sim 10^{-6}$ cm^{-3} predominantly through the process of inverse bremsstrahlung, and its energy is deposited directly as thermal energy into the electron gas. The electrons then share their energy with the ions through collisions that heat, excite, and ionize the ions. The excitation and subsequent radiative decay of the hyrogen-like and helium-like ionization stages are modeled in some detail to allow computation of the K-line ($np \rightarrow 1s$, $n \geq 2$) emission spectrum that is observed in the laser heated plasma. Figure 6 indicates the computed electron and ion temperatures as a function of time for Al-plasma. One notes that a large T_e/T_i with $kT_e \sim 1$ keV exists for an initial time period of ~ 50 ps. The temporary non-equilibrium situation which exists here is desirable, because the high T_e is most effective in producing a high inversion, whereas a lower T_i reduces the Doppler linewidth — both effects increasing any gain. Figure 7 shows ground population densities of Al XI, Al XII, Al XIII, and Al XIV, where the populations of electrons and Al XII are nearly constant due to the assumptions made. Li-like Al XI, however, dips sharply after a peak due to the burn-out and then gradually increases, caused mainly by the recombination of Al XII ions. Time resolved power densities of line radiation due to Al XII $1s^2$-$1s2p$, Al XII $1s^2$-$1s3p$, and H-like Al XIII 1s-2p transitions are shown in Figure 8 and a time integated K-x-ray spectrum of Al XII and Al XIII ions is compared with that of the experimentally obtained spectrum in Figure 9. The experimental points are relative values with arbitrary units and are normalized to the computed value of the $1s^2$-$1s4p$ line overall agreement is good between the two; however, a definite tendency towards lower experimental values in $1s^2$-$1s3p$, $1s^2$-$1s2p$, is noted. This discrepancy is interpreted to be due to the fact these lines may be optically thick, an effect not yet included in the numerical model.*

* Details of this model are presented in Section VI B.

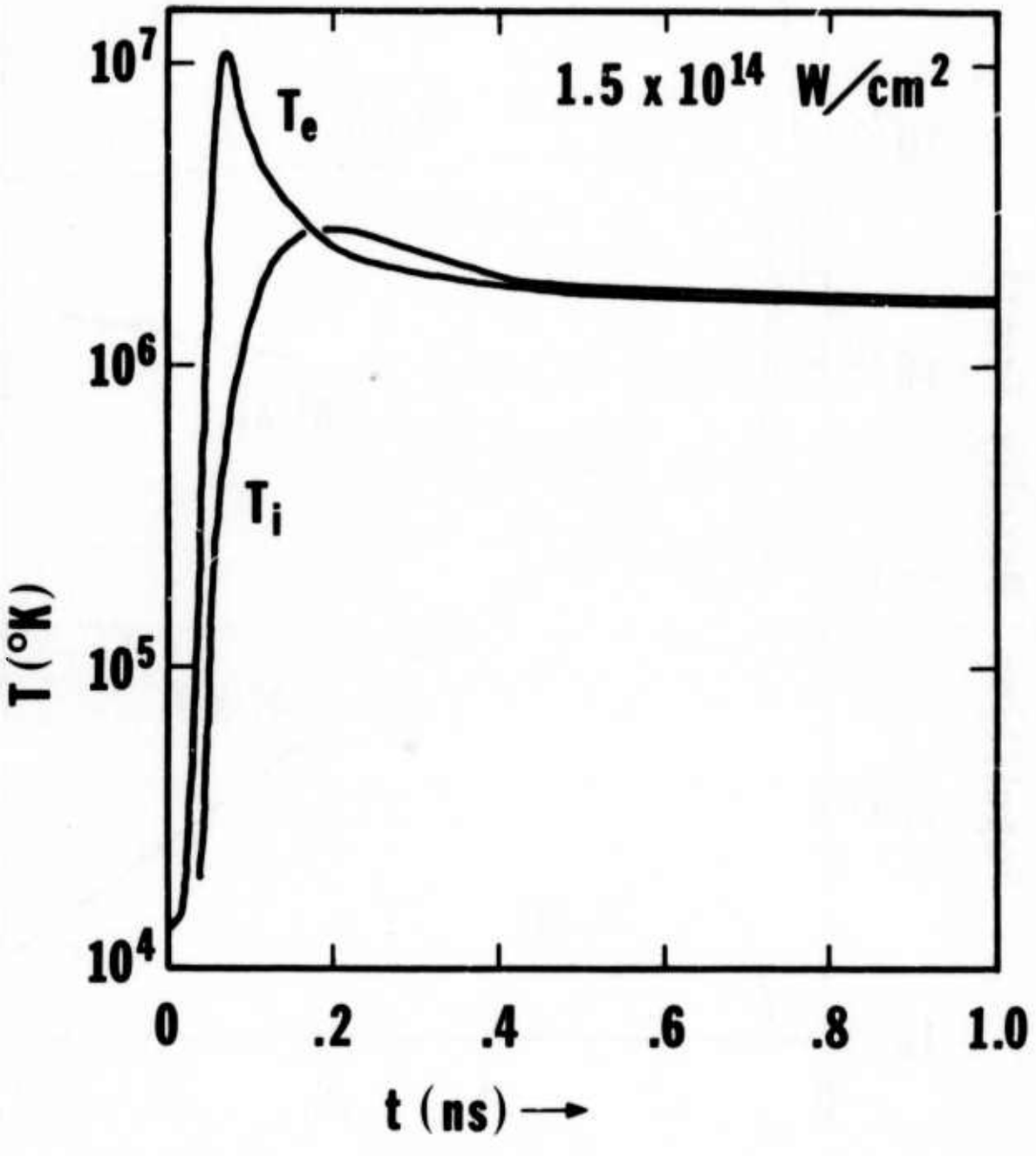

Figure 6 Computed electron and ion temperatures as a function of time.

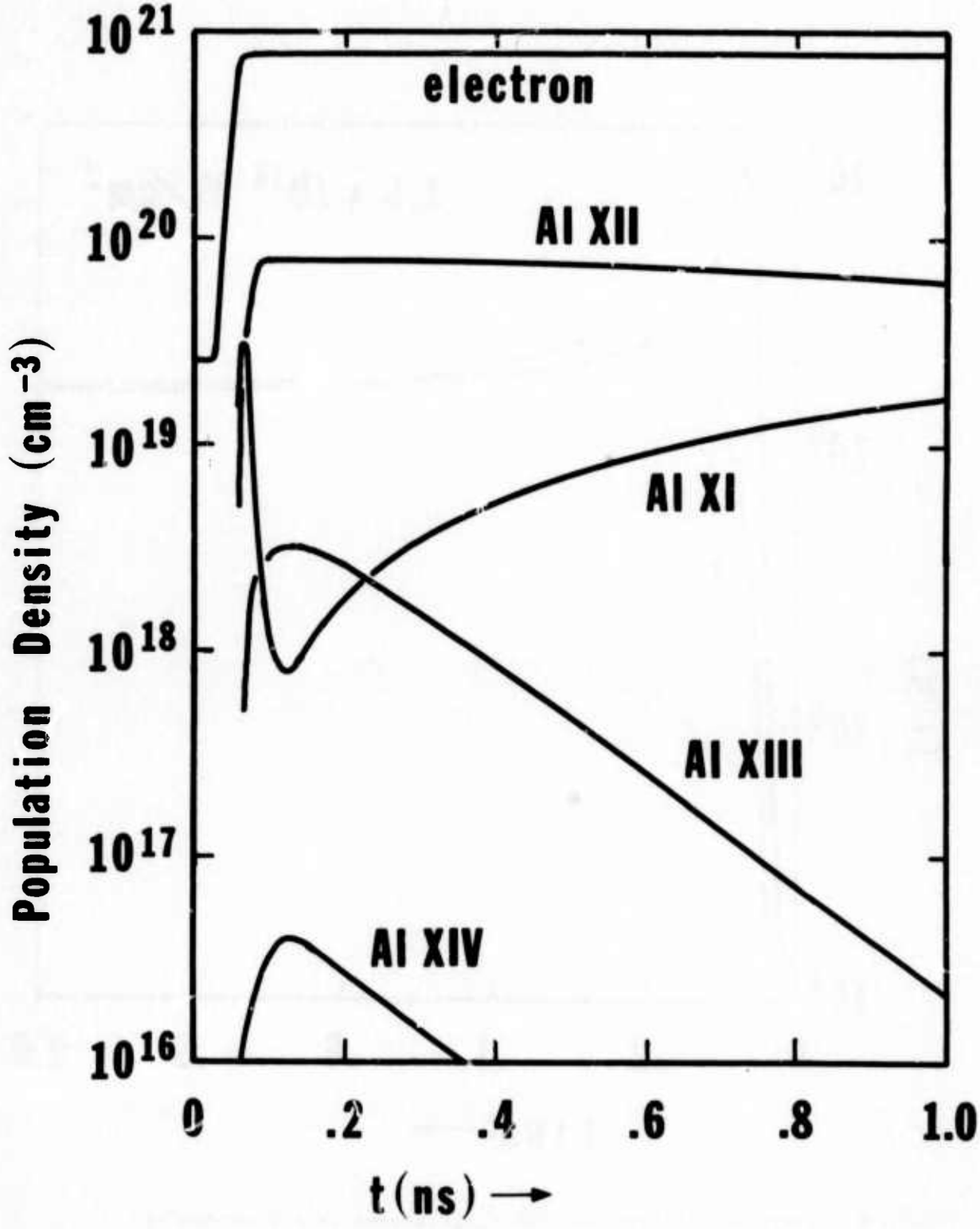

Figure 7 Ground state population densities of Aℓ XI, Aℓ XII, Aℓ XIII and Aℓ XIV ions.

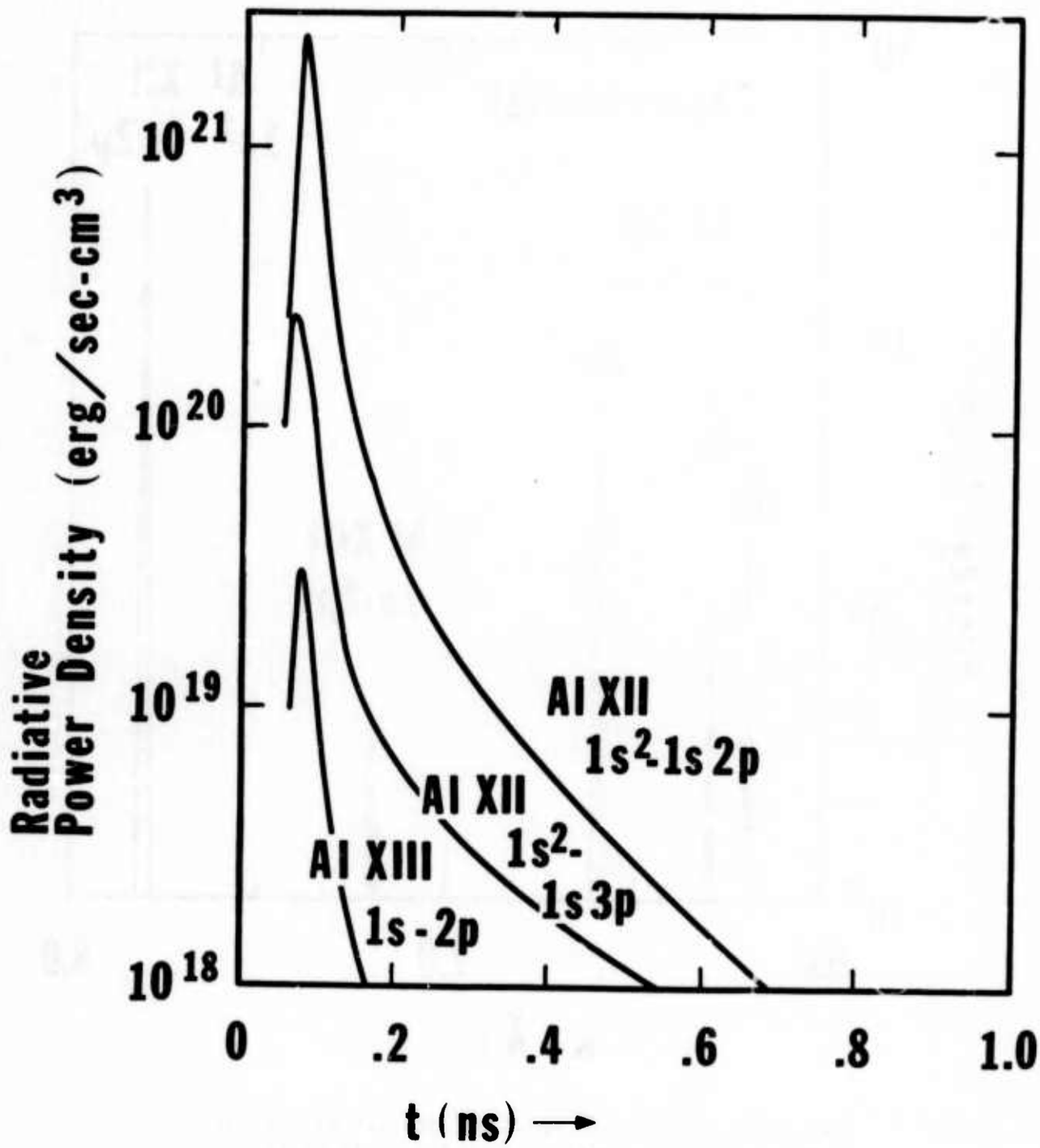

Figure 8 Computed time histories of Aℓ XII $1s^2$-1s2p, Aℓ XII $1s^2$-1s3p, and Aℓ XIII 1s-2p transition line.

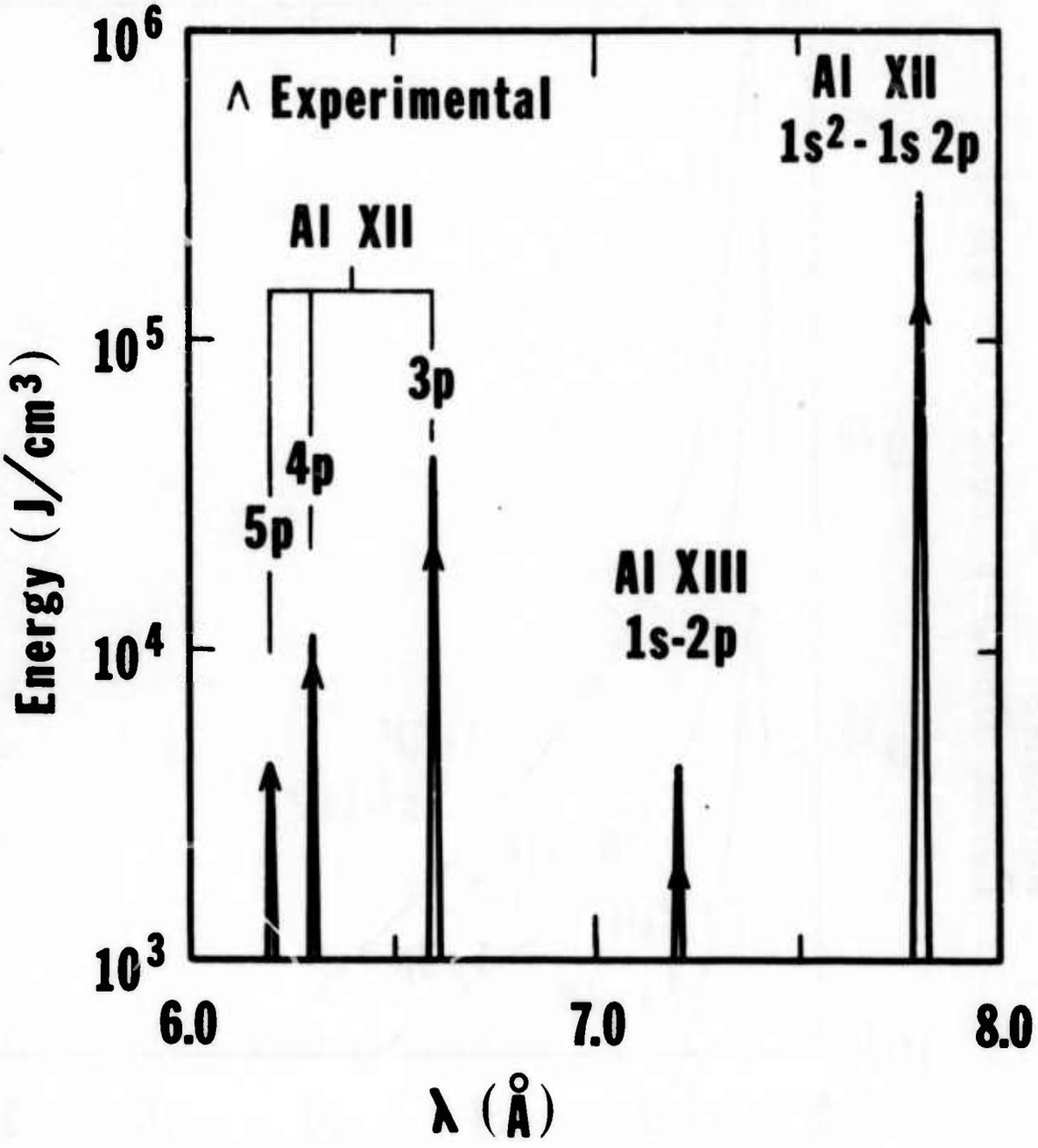

Figure 9 Comparison of computed spectral line intensities of aluminum and that obtained from the experiment.

The spectral features observed so far indicate that the plasma electrons are heated to a temperature somewhere between 300-600 eV. However, precise temperature measurement is essential for further investigation. This will be done using two approaches, i.e., from the intensity ratio of He-like $1s^2$-1s2p to H-like 1s-2p resonance lines and by using the x-ray absorption method. The latter technique may also be used to obtain the bremsstrahlung profile of the plasma.

The original experimental scheme proposed is to make a line focus on a slab target so that a cylindrical expanding plasma is formed. This plasma is subsequently heated and pumped by an axial laser beam of short pulse duration. Detailed plasma diagnostics and spectroscopic study in the two-laser-beam operation will be made using low Z targets. The spectroscopic study will be extended to the vacuum UV region where 3p→3s lasing is likely to occur.

II. C. SUBNANOSECOND LASER/PLASMA EXPERIMENTS*

The NRL Glass Laser Facility has produced pulses ranging from 50 to 900 psec for plasma x-ray experiments. Pulses with up to 100 GW (e.g., 10 J in 100 psec or 100 J in 900 psec) were focused to power densities exceeding 10^{15} W/cm^2. Plasmas containing many of the elements from Li through U were studied using a wide variety of x-ray plasma diagnostic equipment. Grating and crystal spectrographs were used to measure spectra in the 50-5000 eV range. Several active detectors (e.g., thermoples, Si/p-i-n detectors) as well as calibrated crystal spectrographs gave absolute intensity data. A pyroelectric detector determined a limit on the x-ray emission time; and, pinhole cameras were used to obtain plasma x-ray images. Highlights of these results which are relevant to the ARPA/NRL x-ray laser program are summarized in this section.

Grazing-incidence grating spectra in the 50-1000 eV range were measured for a wide range of elements. Figure 10 shows the carbon K spectrum obtained from 30 GW irradiation of a CH_2 target. Two Rydberg series of resonance lines, plus associated satellite lines, are evident in the spectrum, similar to the spectra from Na through Si shown in the last section. Line profile analysis for 6p and 7p to 1s transitions in one-electron carbon ions yielded an electron density value of 10^{19} cm^{-3}. A similar F spectrum from a LiF target gave a similar electron density result and an electron temperature of 400 eV. Analysis of the intensities of three-electron satellites in the F spectrum showed that the laser-plasma was only approximately in ionization equilibrium. This underscores the necessity for a rate-equation approach to computation of the time-evaluation of ionization stages with plasmas produced by subnanosecond lasers. Data from the grating spectrograph were also used to classify non-resonant lines at

*The majority of the work described here was done as part of the NRL-LMI program, but is included since it is directly relevant.

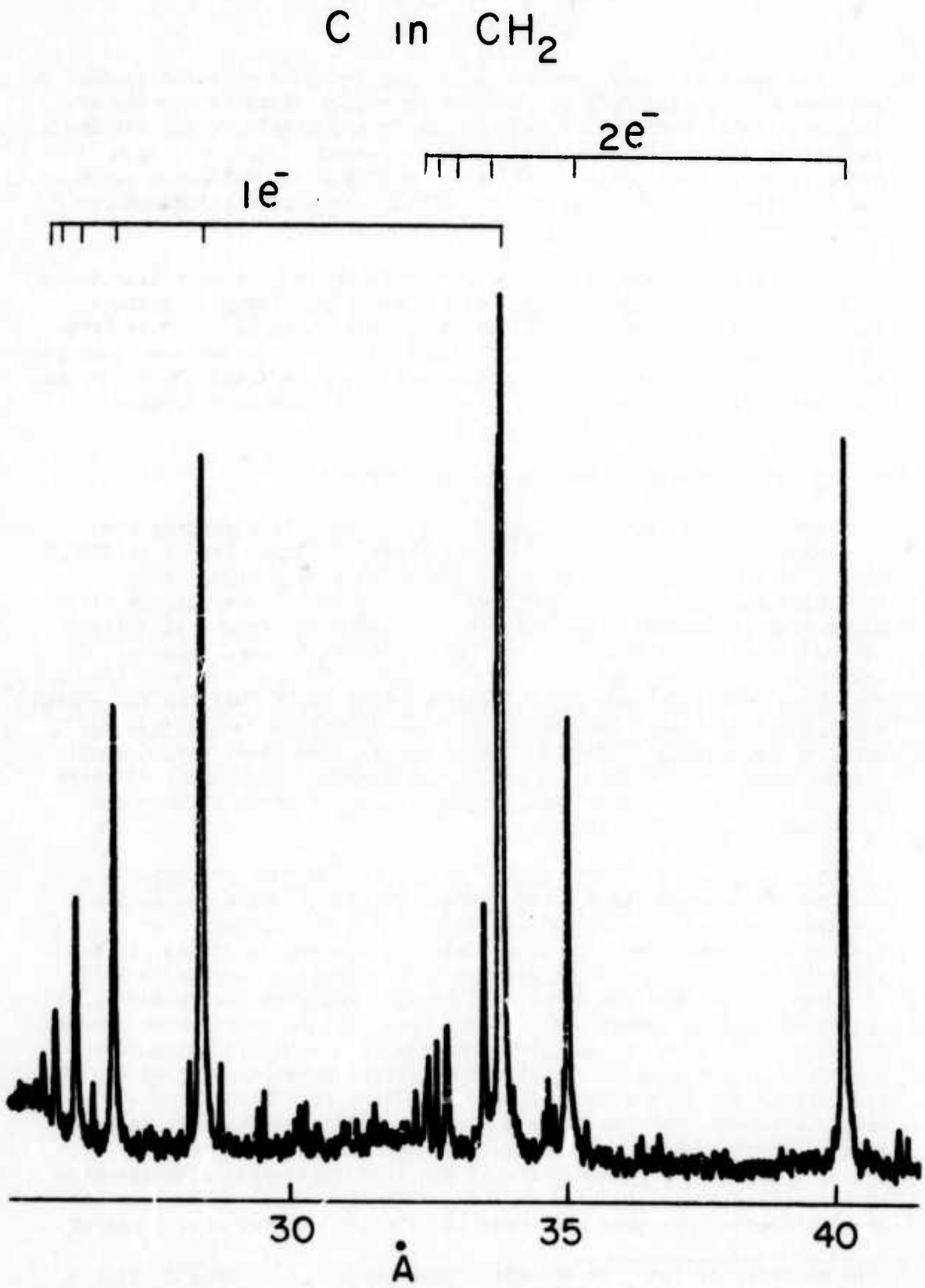

Figure 10 Carbon K resonance spectrum from one- and two-electron ions in a plasma produced by a 0.9 ns, 30 GW pulse.

lower photon energies (~ 100 eV) in 8 and 9-electron ions from medium weight elements. Completion of such isolectronic sequences may prove useful to approaches which attempt to produce lasers of increasingly higher photon energies using plasmas containing heavier ions.

Crystal spectrographs were used to obtain spectra in the 0.8-5 keV region from elements in the range $10 < Z < 67$. In particular, Al K-spectra were studied as a function of increasing laser power. Figure 11 shows one of the spectra obtained. Using line intensity ratios, it was found that 900 psec pulses generate plasmas which increase from 600 eV at 2 J to 900 eV at 10 J. The temperature appears to saturate near 1 keV for pulses in excess of 20 J, possibly due to thermal conduction losses. Satellite spectra were obtained with crystals for elements from Na through Ti. The spectra, which are widely used for density and temperature determination, exhibited intensity anomalies when compared with existing theory. This emphasizes caution when using rate-equation computations of laser-plasma spectra. Isoelectronic sequence studies for 10-electron ions which emit L-radiation and 28-electron ions which emit M-radiation were also performed using heavier elements.

Measurements of the atomic number (Z) and laser power dependence of the integrated x-ray intensity transmitted by a 1 mil Be window (800 eV cutoff) were made with a thermopile. For 1 ns, 35 J pulses, a strong Z-dependence was found with peaks near Al, Cu and Gd. The x-ray intensity from these targets also varied (went through low peaks) as the laser energy was increased from 2 to 60 J. Efficiencies for conversion of laser-pulse energy into x-rays approaching 20% were measured.

A limit on the x-ray emission time was measured using a fast electronic detector. It was found that the FWHM of the x-ray pulse was very close to the laser pulse length of 1 nsec.

The measured size of the x-ray-emitting region in laser-generated plasmas was found to depend on target and pulse conditions as well as on the sensitivity of the pinhole-film instrument. In general, the most intense emission came from a volume with dimensions somewhat larger than the focal spot diameter which was $(100\ \mu m)^3 = 10^{-6}\ cm^3$.

II. D. NANOSECOND LASER/PLASMA EXPERIMENTS

Investigations were made of some characteristics of the plasma x-ray emission generated by a relatively long pulse laser (10 J at 18 ns) in comparison with short pulse (< 1ns), high power lasers. The study includes the determination of plasma electron temperature, x-ray conversion efficiency, x-ray line emission spectrum, and x-ray yield as a function of lens-target distance; and a close observation of target craters. The experimental arrangement is shown in Figure 12. A Korad K-2 ruby laser system consisting of Q-switched oscillator produces pulses with energies of up to 9 J. The laser beam is focused

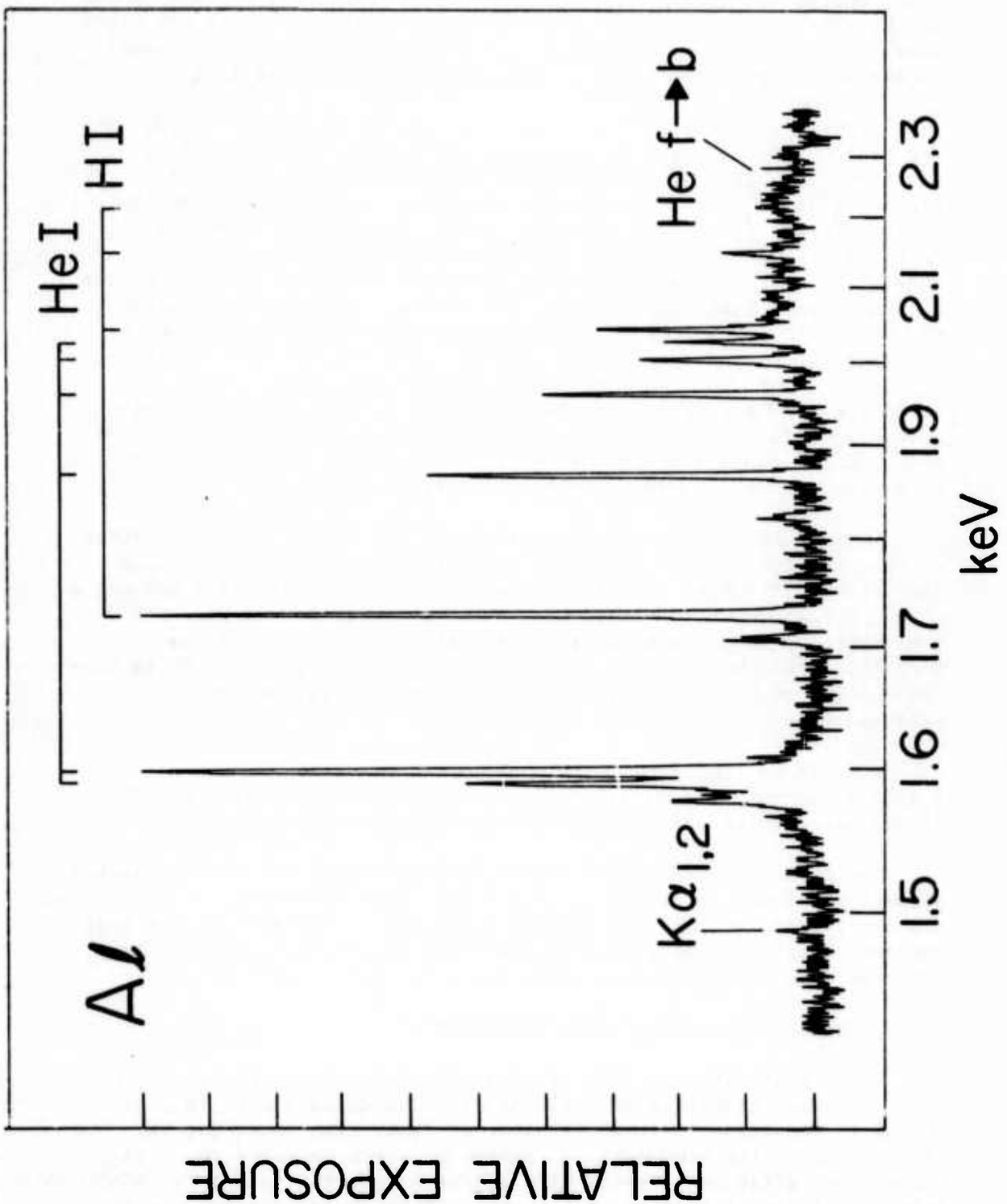

Figure 11 Aluminum K resonance spectrum from a plasma produced by 0.25 ns, 7 GW pulse.

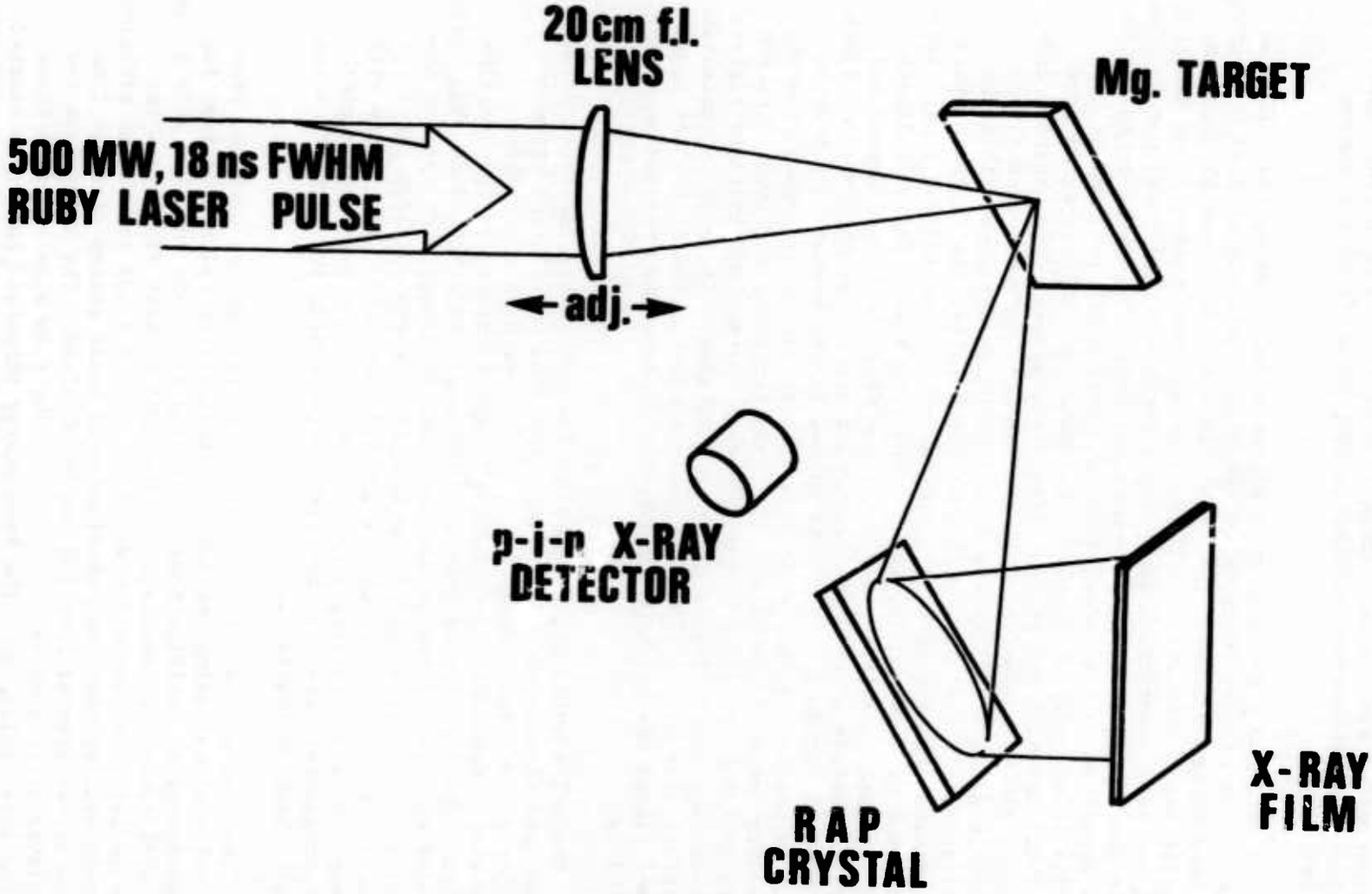

Figure 12 Schematic Diagram of experimental arrangement.

onto magnesium slab targets using a 20 cm focal length lens, which is mounted on a micrometer translation stage outside of the vacuum chamber.

In order to provide as much plasma x-radiation as possible, the effect of laser beam focusing on the x-ray yield was studied by varying the lens-target spacing. The result is shown in Figure 13 where the relative x-ray intensity ($h\nu > 1$keV) as measured with a p-i-n detector is given as a function of lens displacement near the focal point. The curve has a single, roughly-symmetrical peak. The x-ray intensity is very sensitive to the focusing, and the half width ($\sim$ 2 mm) of the profile is an order of magnitude narrower than that expected from the focal depth of the present laser-lens system. This apparent discrepancy can be rationalized if one assumes that most of the x-radiation detected originates from a much smaller area within the focal spot. In order to check this possibility, the target craters are examined under a scanning electron microscope and a typical microphotograph is shown in Figure 14. The target spot indeed indicates that the laser intensity is not uniform over the beam diameter and that it consists of a larger crater and one or two much smaller spots (hot spots) within it. The size of the larger crater ($\sim$ 1.5 mm in dia.) is consistent with a focal spot size one would expect from the beam divergence (8 mrad.) and the focal length of the lens. The hot spots ($\sim$ 100 μm in dia.) are much deeper craters and indicate higher-than-average power density at these locations. It is quite conceivable therefore that mainly the laser power concentration at the hot spots caused plasma heating high enough to produce x-ray emission of $h\nu > 1$ keV.

The p-i-n detector, cables, and Tektronix 7904 oscilloscope have a combined risetime of about 2 ns. The time correlation between the laser and x-ray signals are made by feeding a common high frequency sinusoidal signal to the Z-axis terminals of two oscilloscopes. The two signals peak simultaneously to within 3 ns (Fig. 15). The FWHM of the x-ray pulse is much narrower ($\sim$ 11 ns) than that of the laser pulse. This suggests the absence of x-ray emission until the laser light intensity reaches a certain threshold. For lasers with 1 ns pulses and intensity greater than 1 GW, the x-ray pulse width is approximately equal to the laser pulse width, in contrast to the result shown in Figure 15.

The approximate x-ray conversion efficiency was obtained from the p-i-n signal using the detector sensitivity calculated from the manufacturer's specifications. Assuming isotropic emission into 4π ster., the efficiency for conversion of the 6943 Å laser light to x-ray line radiation at about 9 Å was 0.07%. This x-ray conversion efficiency is much smaller than that obtained with laser pulses of about 1 ns, where values greater than 10% can be obtained. The main cause for the lower efficiency is the slow rise and fall times of the laser pulse, as the beam energy threshold has to be reached for the x-ray emission. The total energy in the radiation is 7×10^4

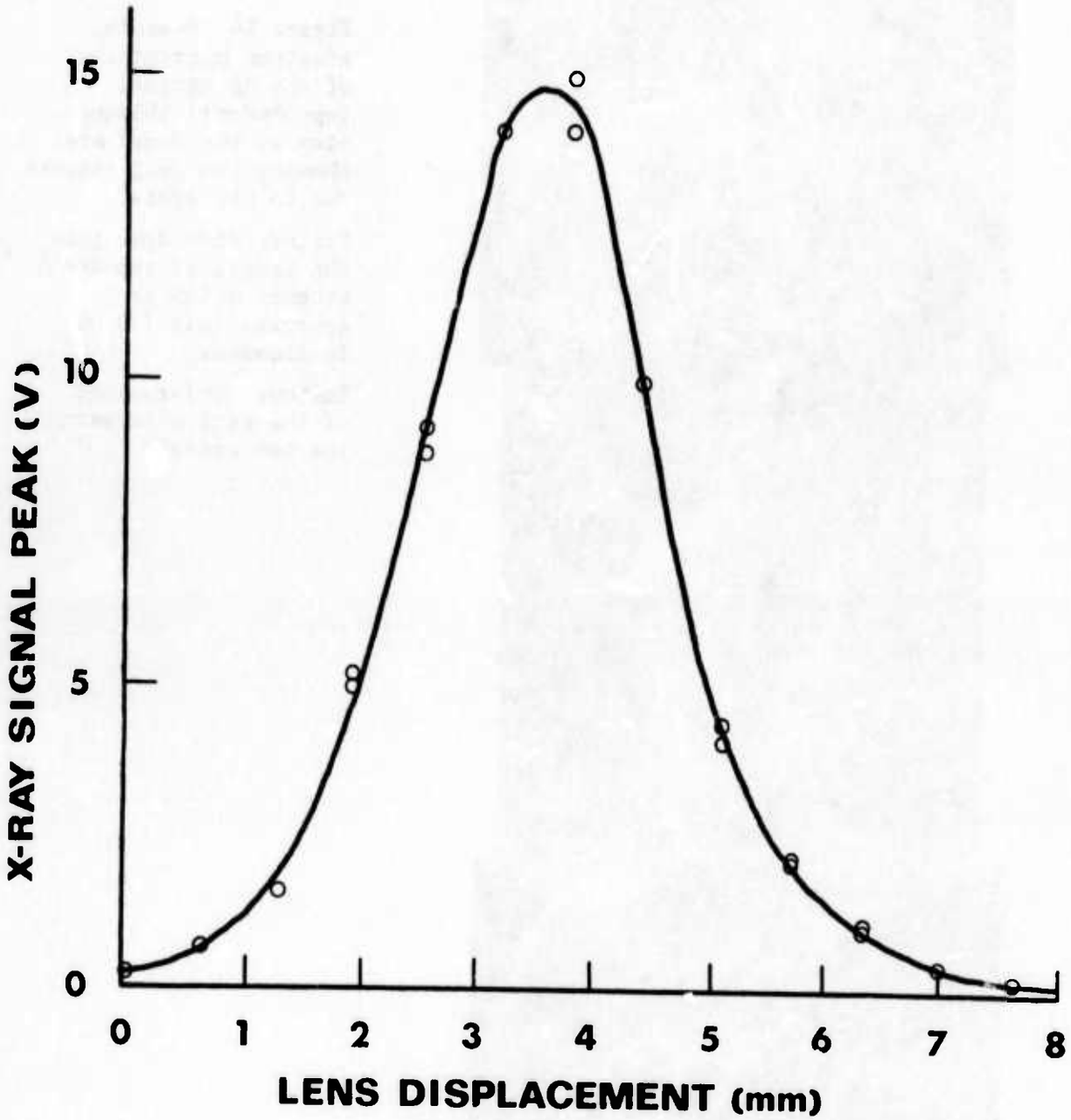

Figure 13 X-Ray signal measured with p-i-n detector vs. lens displacement.

Figure 14 Scanning electron micrographs of the Mg target.
Top: Overall oblique view of the focal area showing two deep craters due to hot spots.

Center: View down into the larger of the two craters which is approximately 175 μm in diameter.

Bottom: Enlargement of the region between the two craters.

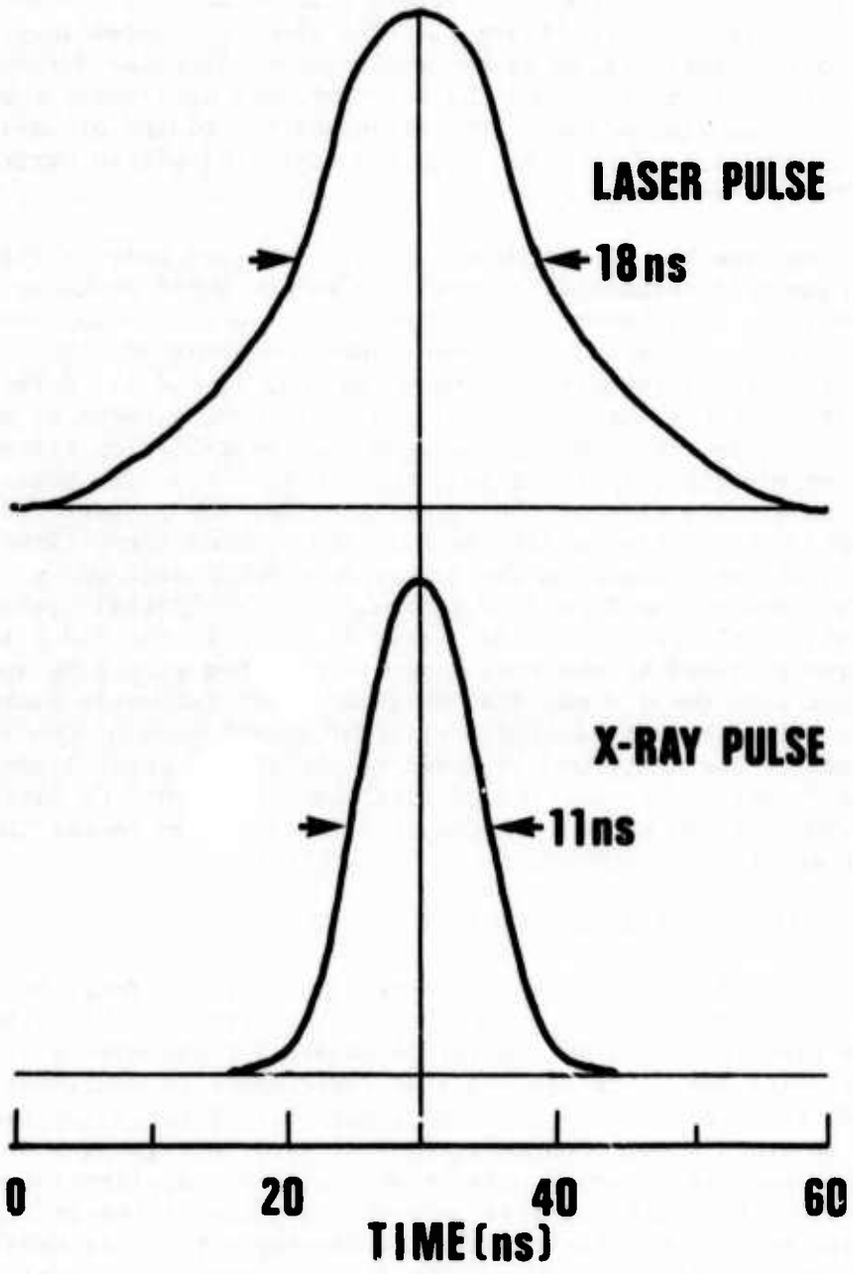

Figure 15 Time histories and correlation between laser and x-ray pulses. The peak alignment is uncertain to $\pm$ 1.5 nsec.

ergs compared to 10^7 ergs of x-rays from a 1 ns, 10 J laser pulse.

X-ray pinhole photographs were taken through 25 μm pinholes with a single exposure on Kodak No-Screen film behind a 12 μm Be window. An example is shown in Figure 16. The time integrated image consists of a more intense region which is elongated along the direction of the incident laser beam and the less intense, apparently more tenuous, radially expanding plasma. The elongated hot region probably results from interaction of the beam with the expanding plasma during the relatively long pulse.

X-ray spectra of the Mg-plasma are obtained using a flat RAP (rubidium acid phthalate) crystal and are recorded on Kodak No-Screen x-ray film behind 12 μm Be-foil. Figure 17 (top) shows a microdensitometer scan of an x-ray spectrum obtained with a 25 shot exposure. Three transitions ($np \rightarrow 1s$, n=2, 3, and 4) in two ionization states, He-like Mg XI and Li-like Mg X, make up most of the spectrum. Free-to-bound Mg XI recombination radiation appears at the short-wavelength end of the spectrum. One of the weak peaks to the short wavelength side of the Mg XI $1s^2$-1s2p line is ascribed to a transition in doubly excited Mg XI. The remaining two lines in this region, the weak lines on the longer wavelength side of Mg X $1s^2 2\ell$ - $1s2\ell 2p$ lines, may be from Zn which was found by optical spectrographic analysis to be present in the target material at the 0.2 % level. The spectrum produced by the ruby laser is compared with a Mg-spectrum obtained with the 0.9 ns, 2.2 GW glass laser (shown in lower part of Figure 17). The H-like Lyman α-line of Mg XII, one of the prominent features in the spectrum produced by the higher power laser, is absent in the spectrum obtained with the 1.8 ns, 0.5 GW laser. The spectrum obtained here indicates that the electron temperature of the Mg-plasma is about 300 eV.

II. E. PICOSECOND LASER FACILITY

This section describes of the picosecond laser facility used in the X-ray Laser Program. Although this is the primary application, the lasers discussed here are versatile research tools with a broad area of potential use. For example, some experiments in nonlinear optics have already been performed. The long range goal of the X-ray Laser Program is to generate population inversions at x-ray wavelengths in laser produced and laser pumped plasmas with ultimate application to an x-ray laser. For this application, a unique state-of-the-art laser is required which necessitates in-house development. This development is continuing with portions of the facility now operational. Currently x-ray spectroscopy and other characterization of laser produced plasmas are being performed using this facility.

Controlled studies of interactions between laser pulses and laser generated plasma requires a laser system to meet relatively unusual requirements. In particular, several synchronized pulses with durations on different time scales are required for purposes of prepulsing,

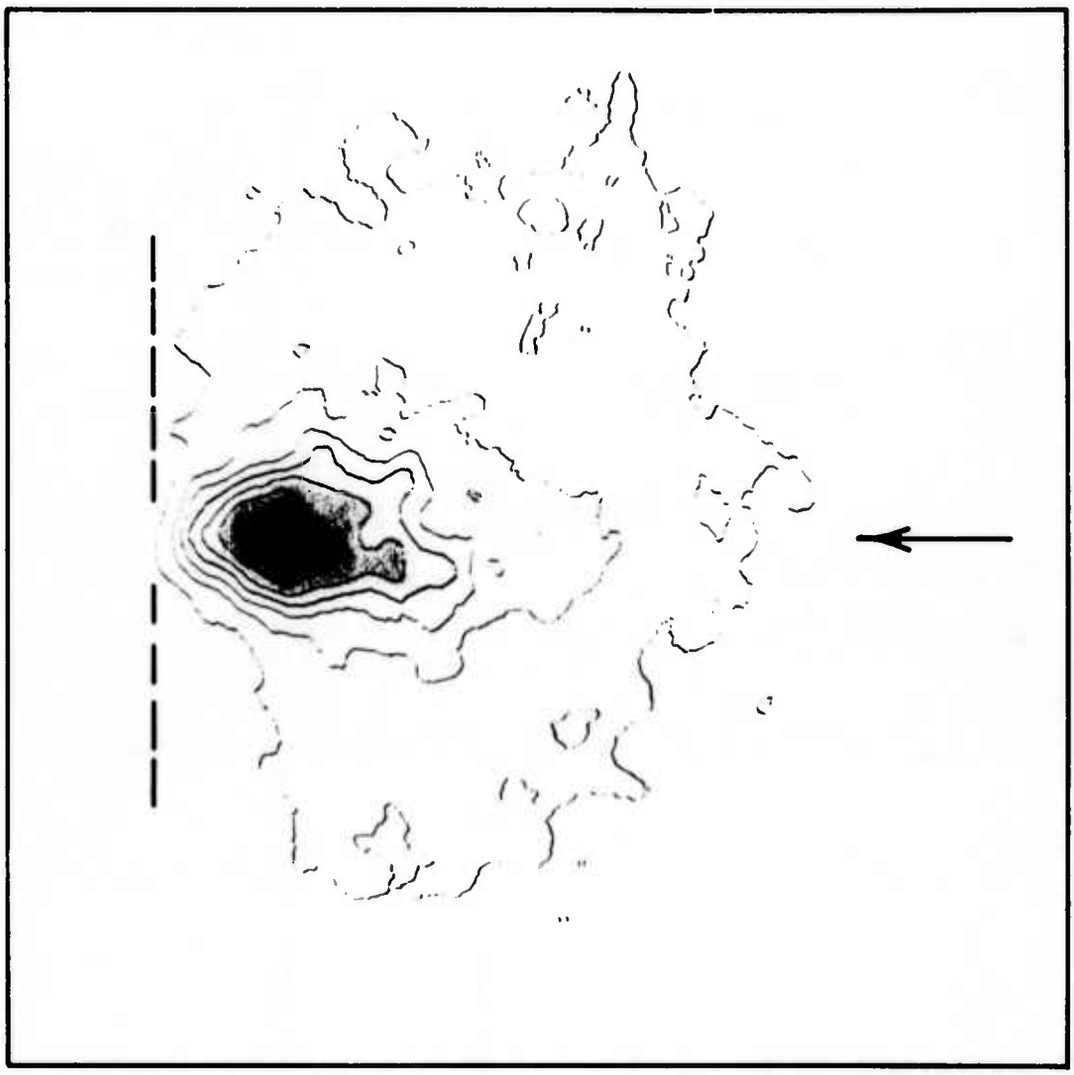

Figure 16 Densitometer scan of x-ray photograph taken with 25 μm pinhole, showing density contours. Outer contour extends 0.8 mm from the target surface which is indicated by the dashed line. Arrow mark shows the direction of incident laser beam.

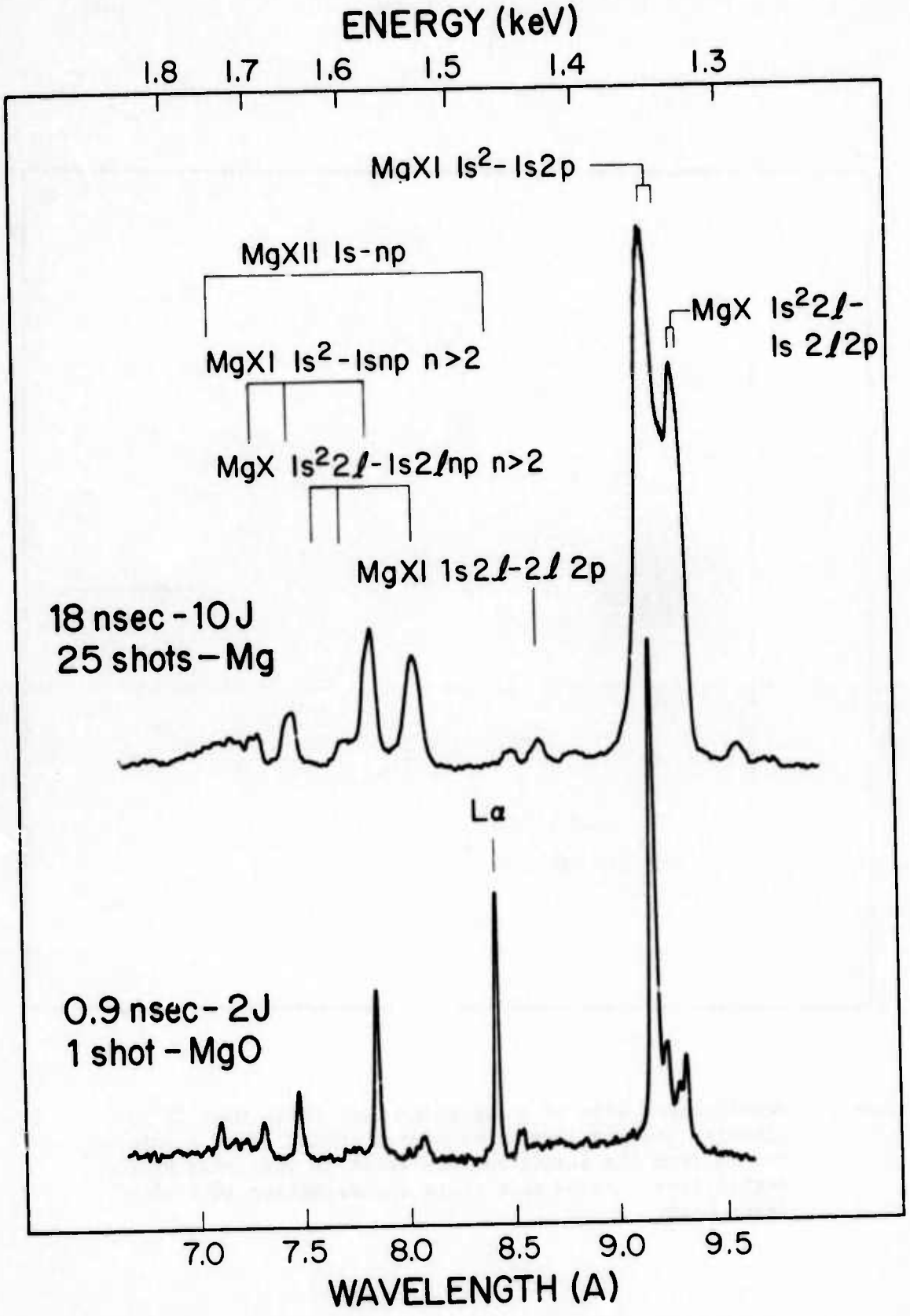

Figure 17 Mg spectrum taken with 0.5 GW ruby laser in 25 shots compared with spectrum produced by a single 2.2 GW shot of a Nd:glass laser.

plasma heating, and plasma diagnosis. In addition, reliable operation in terms of reproducibility of pulse energy, duration, and profile, and of interpulse synchronization are important for systematic study of appropriate interactions. Good beam quality is required for efficient use of optical power; and short pulse durations at extremely high intensity are required for plasma heating. Finally, knowledge of all these properties is necessary for meaningful comparison of experiments with theoretical models.

Such a laser system which is tailored to the needs of these experimental studies has been developed. A schematic diagram of the system is shown in Figure 18. The laser system produces multiple synchronized pulses on both nanosecond and picosecond time scales simultaneously. The picosecond pulses are generated in a mode-locked Nd:YAG laser that provides two 200 mJ output pulses of 30 psec duration with a time delay variable between 0 and 10 nsec. The nanosecond pulse is generated in a Q-switched laser and is variable in duration between 0.5 nsec and about 30 nsec with energy in the 1 to 10 J range. The two lasers are synchronized with a versatile switching technique which overcomes the jitter inherent in the production of either of the pulses separately and provides jitter times in the subnanosecond range. With this system plasmas can be generated with either the Q-switched pulse or one of the mode-locked pulses. The two output pulses of the mode-locked laser can be used for both pumping of existing plasmas and plasma diagnositics.

II. E. 1. MODE-LOCKED LASER

The mode-locked laser consists of a Nd:YAG oscillator, a Pockels cell shutter, five Nd:YAG amplifiers, beam expansion optics, beam splitter, and an optical delay track. The Pockels cell shutter transmits a single pulse from the train of mode-locked pulses generated in the oscillator. The pulse is amplified in the first three amplifiers and then split into two components. Each of the two resulting pulses passes through its own fourth amplifier. One pulse transverses a variable optical delay track. Beam expansion optics are required so the pulses will just fill each of the two final YAG amplifiers of ½ inch diameter.

The mode-locked laser oscillator-amplifier system was designed to provide sufficiently energetic pulses for plasma heating studies with the short pulse durations required by the lifetime of x-ray transitions being investigated. At the same time it is necessary to maintain diffraction limited beam quality and spectral purity by minimizing the effects of self focusing in the laser rods. Neodymium: YAG was chosen for this laser because of the ease with which it can be operated as a time-bandwidth limited mode-locked oscillator. Also this material offers advantages in amplifier use with higher efficiency and repetition rates than other available materials such as Nd:glass. This laser is capable of being fired once every 10 seconds where a Nd:glass amplifier could only be fired once a minute

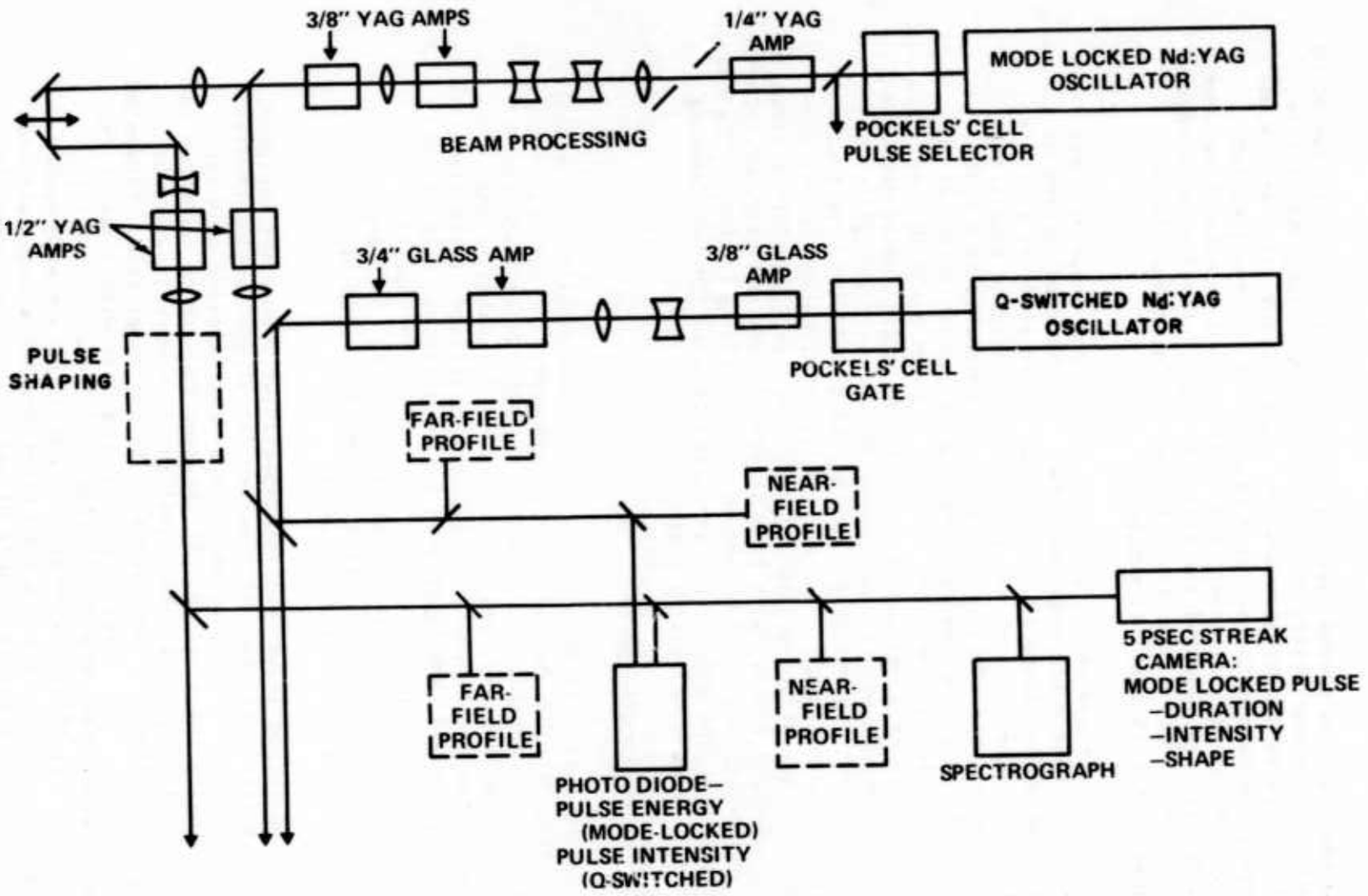

Figure 18 Schematic diagram of Short Pulse Laser Facility showing the coupled mode-locked and Q-switched laser system, and laser diagnostic measurements.

or slower. This is the first laser system of this type to use ½ inch diameter YAG rods, which is the largest size available commercially.

II. E. 1a DESIGN CONSIDERATIONS

The design parameters are the theoretical limit of the Nd:YAG laser material consistent with the performance requirements mentioned above. With a small signal gain of 7 as in the last amplifier rod, energy storage is .402 Joules per square cm of cross sectional area. We set as our design goal an output energy of half this value 0.2 J. Depleting the population inversion by such a large amount has the added advantage of stabilizing the output energy of the laser system.

With the short 30 psec pulse duration of mode-locked Nd:YAG, intensity will be high and nonlinear optical effects on beam propagation must be considered. Self focusing and self-phase modulation are caused by intensity dependent changes in the index of refraction. At these high intensities the index of refraction can be expressed by

$$n = n_o + n_2 \langle E \cdot E \rangle \quad ,$$

where $\langle E \cdot E \rangle$ is the average of the square of the electric field, n_o is the index for low intensity, and n_2 is a coefficient called the nonlinear index of refraction. The value of n_2 is known to be approximately $5 \times 10^{-22} m^2/V^2$ for YAG.

Self-phase modulation is caused by the delay of more intense temporal portions of a pulse and the resulting compression or expansion of the optical oscillation. Self focusing results when more intense spatial portions of a beam are delayed distorting the wavefront. With a slowly varying envelope approximation, the shift in wavelength $\Delta\lambda$ from the central wavelength λ due to self-phase modulation is given by

$$\Delta\lambda/\lambda = \frac{n_2 \ell}{C} \frac{d\langle E \cdot E \rangle}{dt} \quad ,$$

where ℓ is the length of the material and c the speed of light. Setting the maximum value of $\Delta\lambda = 1\text{Å}$, and using $\ell = 7.5$ cm, and assuming a Gaussian pulse shape 30 psec wide at the 1/e points, the maximum energy density would be approximately $0.9\ J/cm^2$.

The system is designed to avoid not only catastrophic self focusing in the laser material, but also slight self focusing which will cause distortion of the laser output. If a transverse intensity distribution $I = I_o \exp(-r^2/a^2)$ with an initial plane wavefront is transmitted through a slab of material of length ℓ, the central portion of the wavefront will be given a radius of curvature

$$R = \frac{a^2}{2\, n_2 \ell \langle E \cdot E \rangle} \quad .$$

Allowing only $R \geq 10m$, the maximum allowable energy density is $0.4\ J/cm^2$ for a pulse with a =0.5 cm and 30 psec wide at the 1/e points. This value is close to the design goal of 0.2 J through a ½ inch diameter rod. In performing the beam expansion through the amplifier chain, it is important to maintain a smoothly varying transverse intensity distribution to minimize self focusing. No diffraction fringes resulting from beam aperturing at the rod edges can be tolerated. Yet is it important to fill the final amplifiers as closely as possible for maximum gain and minimum self focusing.

In actual performance (Table I) the laser comes near to meeting the theoretical limits of operation. Output energies of 0.21 J in 30 psec pulses have been obtained in beams that diverge at only 1.5 times the diffraction limit. At these energies the effects of self focusing are just beginning. At this point it would not be advantageous to go to higher energy or add another YAG amplifier, because this would only increase the divergence due to self focusing and decrease the brightness on target.

II. E. 1b MODE-LOCKED OSCILLATOR

The mode-locked oscillator consists of a 1/4 inch diameter Nd:YAG rod pumped with a linear xenon flash lamp in a single elliptical reflector of the same design used in the NRL Glass Laser Facility (see Appendix B). The resonant cavity is formed by a 10 m radius 100% mirror and a flat 65% mirror (Figure 19). The laser is mode-locked with Kodak 9740 dye in a dichloroethane solution flowing in a cell contacted with the output mirror. An aperture inside the cavity gives transverse mode control. The laser output consists of a train of 25 psec duration pulses spaced by 6.7 nsec (Figure 20a). Peak energy is .25 mJ per pulse and there are approximately 10 pulses between the ½ intensity points of the pulse train. This operating point represents an acceptable compromise between the requirements of high power to drive the amplifier chain and long duration of the pulse train for ease of synchronizing with the Q-switched laser.

The output of the oscillator was analyzed spatially in the near and far fields, and temporally with a 5 psec resolution streak camera. The near field spatial profile (Figure 20b) was observed at a distance of 2.25m from the output mirror by scanning the beam with a 250 μ slit. It follows a Gaussian shape down to about the 10% intensity points, accounting for 90% of the energy. The beam parameter at this position agrees quite well with that predicted from an analysis of the cavity mode size. The fractional energy transmitted through an aperture in the far field was also measured to determine how well the beam propagated. For an aperture that would

TABLE I

PARAMETERS OF PICOSECOND LASER SYSTEM

● DESIGN GOALS

STAGE	PULSE ENERGY (mJ)	PULSE DURATION (PSEC)	POWER (W)	BEAM PROFILE	INTENSITY (W/CM^2)	AMPLIFIER GAIN
OSCILLATOR OUTPUT	.20	25	8×10^6	1 mm (CIRCULAR GAUSSIAN)	10^9	
AMPLIFIER OUTPUT (4 STAGE)	200	25	8×10^9	1.2 X .6 CM	1.4×10^{10}	10^3
TARGET	200	25	8×10^9	50 μ X 100 μ	2×10^{14}	

● MEASURED OUTPUT

OSCILLATOR	.20	25	8×10^6	1 mm (CIRCULAR GAUSSIAN)	10^9	
AMPLIFIER						
1st STAGE	4.8	25	1.9×10^8	2 mm	6×10^9	30 (30)
2nd STAGE	13.2	25	5×10^8	.6 X .3 CM (ELLIPTICAL AIRY DISC)	3.5×10^9	10.6 (12)
3rd STAGE	114.0	30	4×10^9	.5 X .9 CM	1.1×10^{10}	9.4 (12)
4th STAGE	210	30	7×10^9	.6 X 1.2 CM	1.25×10^{10}	4.1 (7)
TARGET	190	30	6.3×10^9	60 μ X 120 μ	1×10^{14}	

NOTE: The parameters of the picosecond laser system are tabulated at various stages. Large signal gain under actual operating conditions is given in the last column with small signal gain in parentheses. Total gain is reduced from the product of individual gains by power loss at the apertures and reflections.

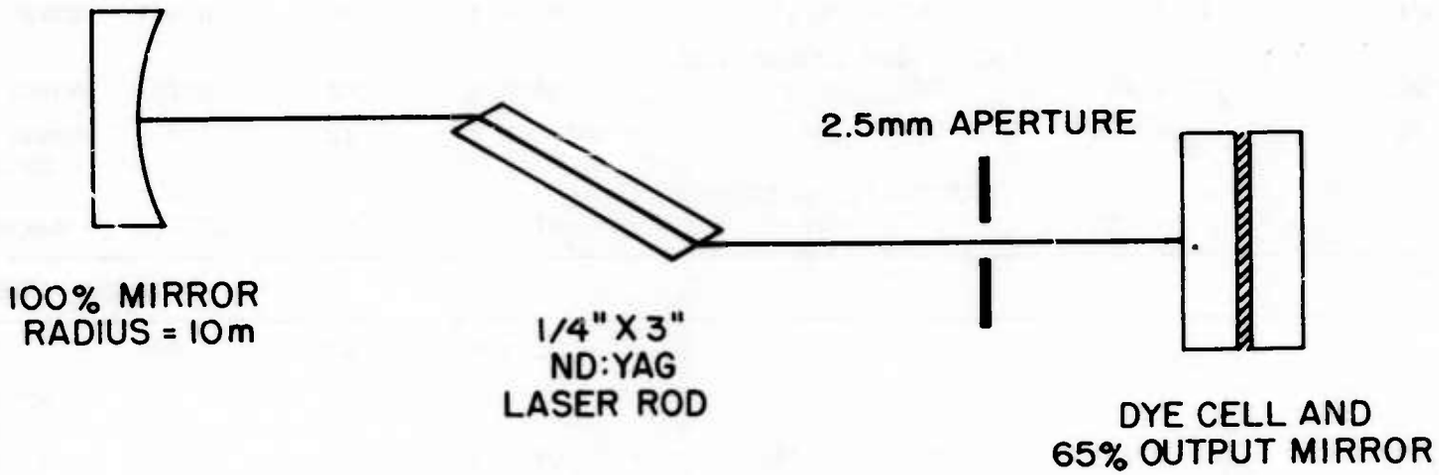

Figure 19 Mode-locked oscillator resonant cavity.

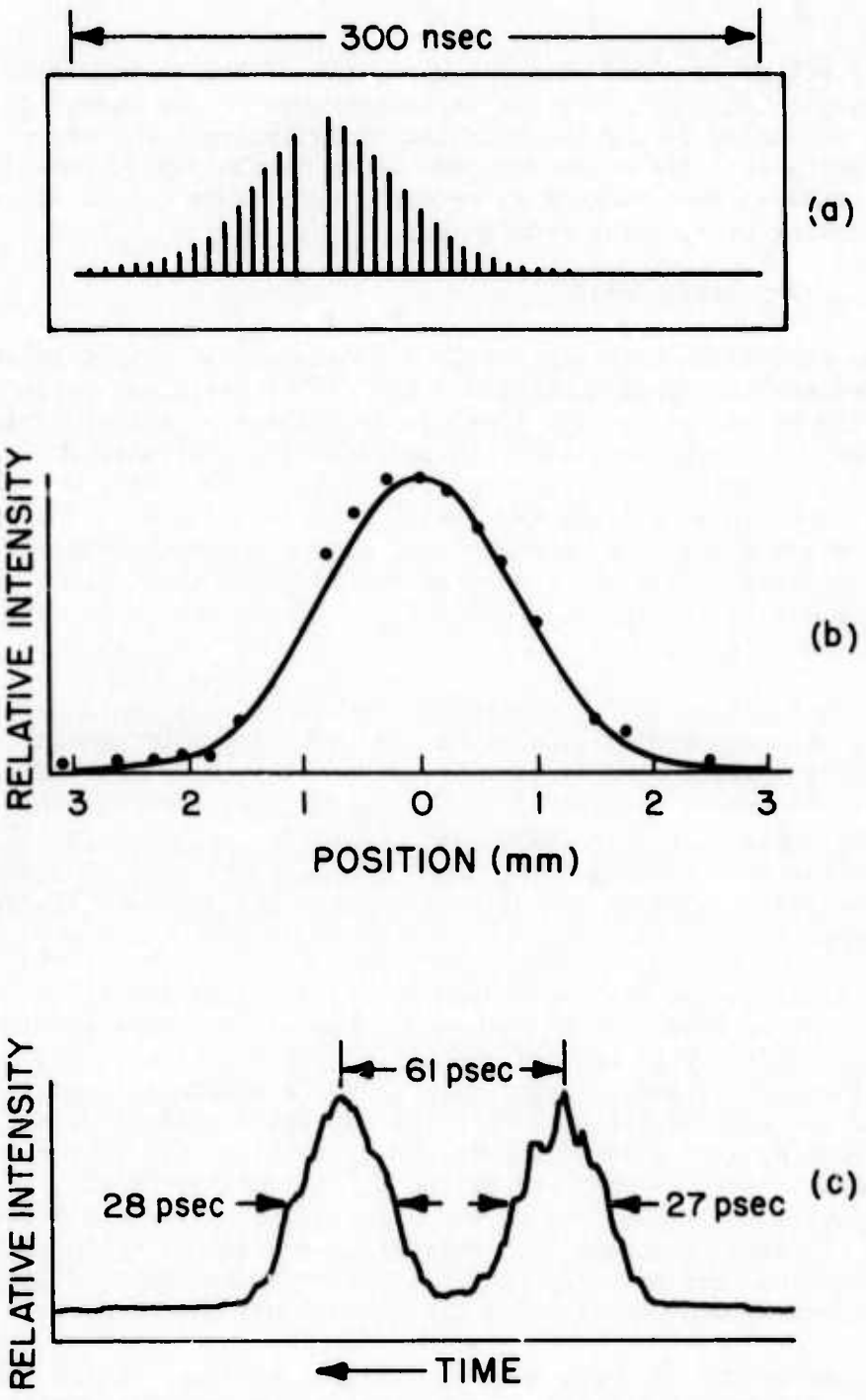

Figure 20 Measurements of mode-locked oscillator performance. (a) Oscillogram of pulse train with a single pulse switched out. (b) Spatial intensity profile of laser beam (data points) compared with a Gaussian curve with 1.14-mm radius at the 1/e point. (c) Fast streak camera record of two reflections of the same mode-locked pulse. A densitometer trace of the photographic record is shown.

transmit 66% of an ideal Gaussian beam, 60% of the actual laser beam was transmitted, confirming the fact that most of the energy in the beam is accounted for by the Gaussian distribution. The streak camera measurements show the pulse duration is approximately 30 psec (Figure 20c) and no temporal substructure is evident, indicating a lack of severe self focusing or spectral broadening.

II. E. 1c AMPLIFIER CHAIN

The amplifier chain was designed to provide an output pulse which would deplete the final amplifier stage without being distorted temporally or spatially by self-phase modulation or self focusing. The Nd:YAG amplifier rods are Brewster-Brewster configuration and 3 inches in length. The first rod is $\frac{1}{4}$ inch in diameter, followed by two 3/8 inch diameter rods, and finally a $\frac{1}{2}$ inch diameter rod in each of the output arms. The degree of population inversion depletion can be seen in comparing small and large signal gains (Table I) at the indicated energy levels; about 40% of the stored energy is extracted from the last stage.

In determining suitable operating points of the amplifiers, the small signal gain was measured as a function of pumping energy for each of the stages. The results are shown in Figure 21. The actual gain for each stage deviates from the theoretical curve at about the same pump energy. The limiting gains occur for an approximately constant value of $\alpha d \approx 0.45$ (gain coeff. X rod diameter), indicating that a parasitic mode is most likely responsible for the observed deviation.

In order to operate the system at these energy levels it is necessary to be able to take full advantage of the cross section of the larger rods. This requires that the gain be uniform across the full rod diameter, and that the beam fill the entire rod aperture. A study of the gain distribution produced by the single lamp, elliptical cavity pumping arrangement used in the oscillator indicates that it is too peaked to provide gain across the whole rod (Figure 22a). Consequently, it was decided to use a four lamp cloverleaf geometry, (Figure 23) with each lamp in a reflecting section of cylindical cross section. The gain distribution for this geometry (Figure 22b) is sufficiently uniform to allow use of the full rod aperture.

In increasing the beam size to fill the aperture of the larger rods, it is not sufficient to simply expand the Gaussion profile. Such expansion will result in Fresnel diffraction caused by aperturing of the wings of the beam at the rod edges leading to small scale self focusing and damage to optical components. The expansion scheme shown in Figure 24 solves this problem by converting the beam into an elliptical Airy pattern between the second and third amplifiers. A circular aperture tilted at 60° to the beam propagation direction provides an elliptical profile matched to the projection of the Brewster rods. Use of elliptical geometry instead of circular means

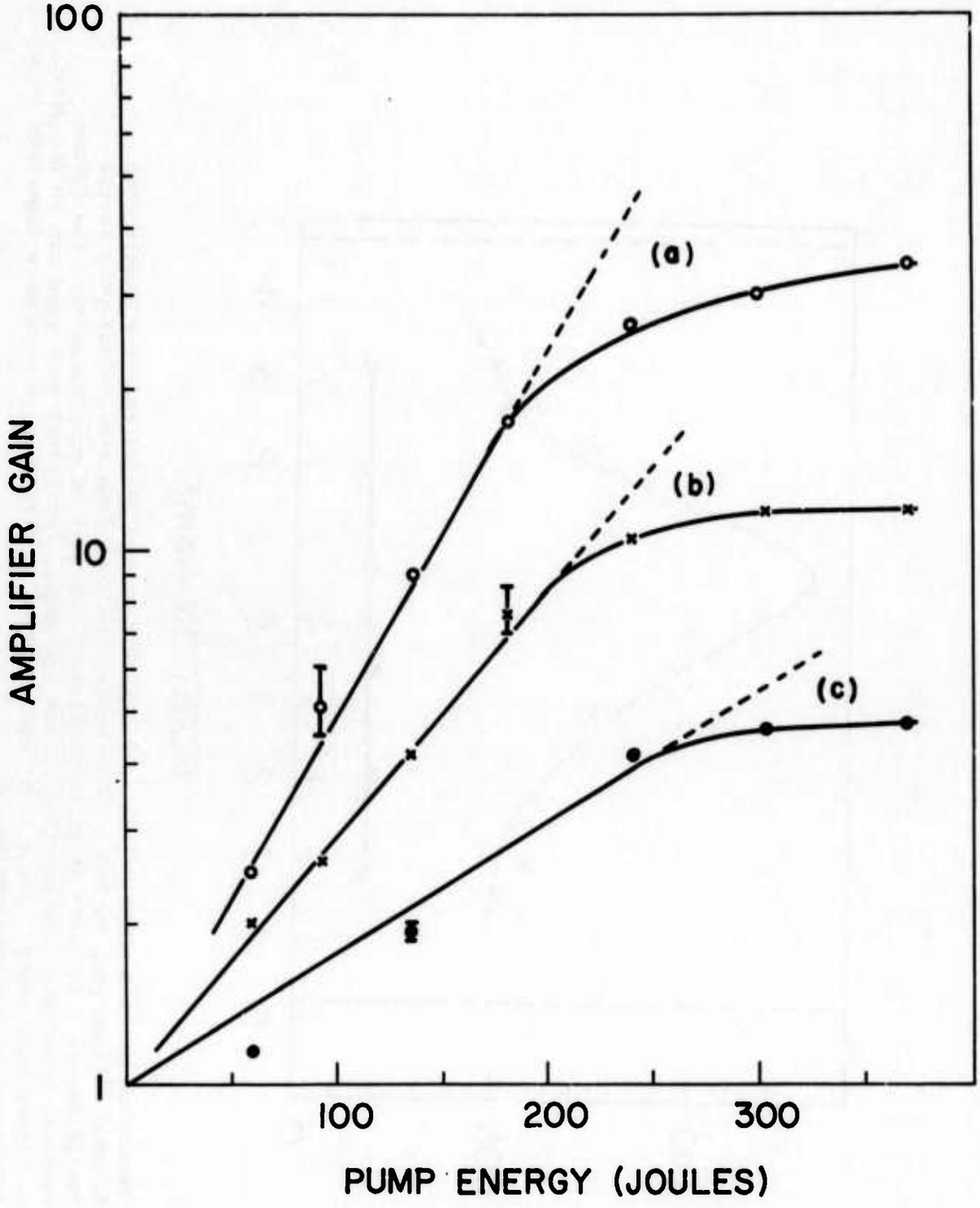

Figure 21 Small signal gain of Nd:YAG amplifiers using 4 lamp pumping geometry as a Function of pump energy. Curve (a) is for $\frac{1}{4}$ inch diameter rod, (b) for 3/8 inch diameter, (c) for $\frac{1}{2}$ inch diameter. The dashed portions of the curves are linear extrapolations of the low level gain.

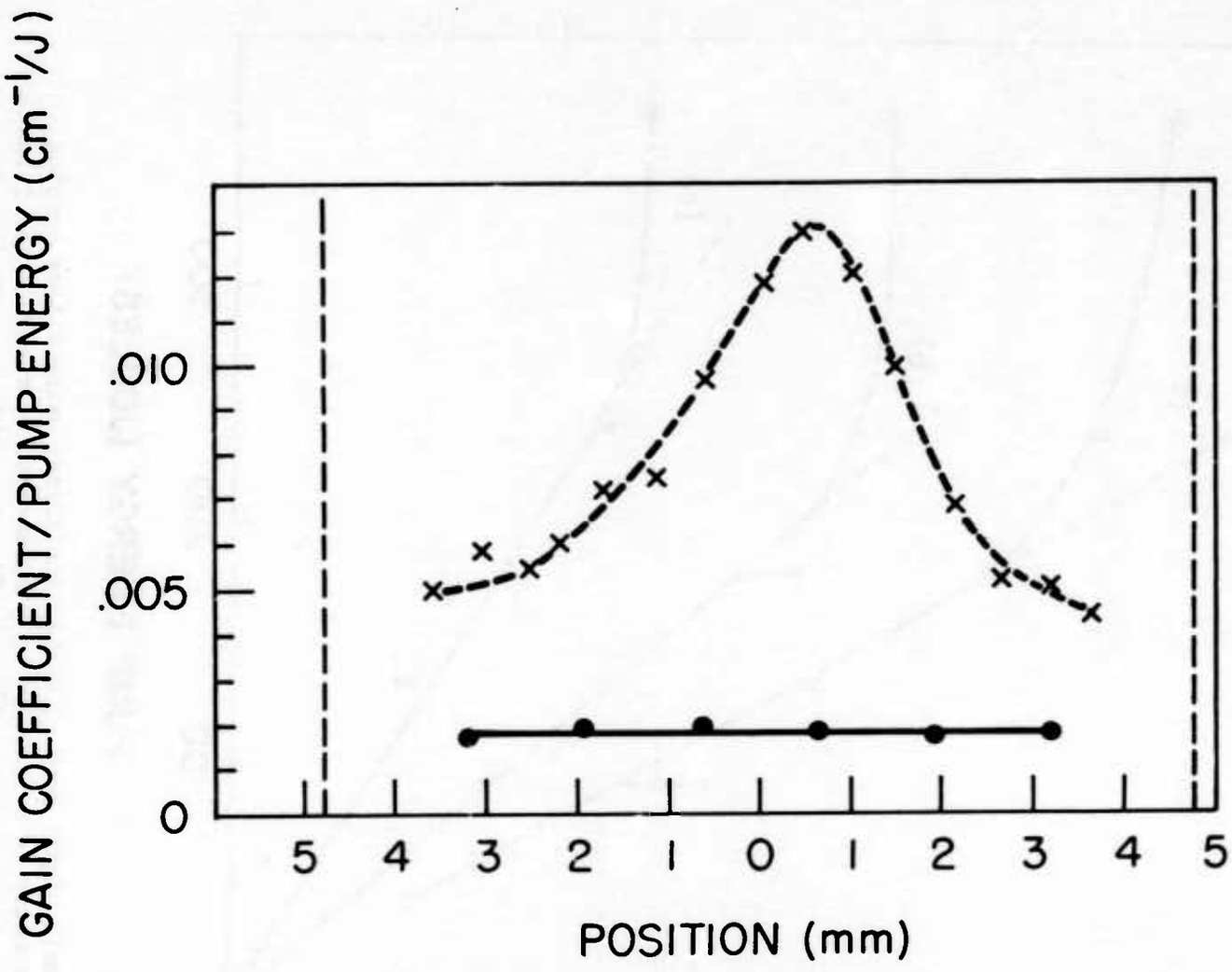

Figure 22 Comparison of gain distribution in 3/8 inch diameter Nd:YAG rods for single lamp focused ellipse pump cavity (dashed curve) and four lamp clover-leaf pump cavity (solid curve) in units of gain coefficient per unit of pumping energy. The dotted vertical lines show the position of the rod edges. Equivalent peak gain can be obtained at higher pump energy in the four lamp cavity. Uniform gain is much more important than efficiency in our application.

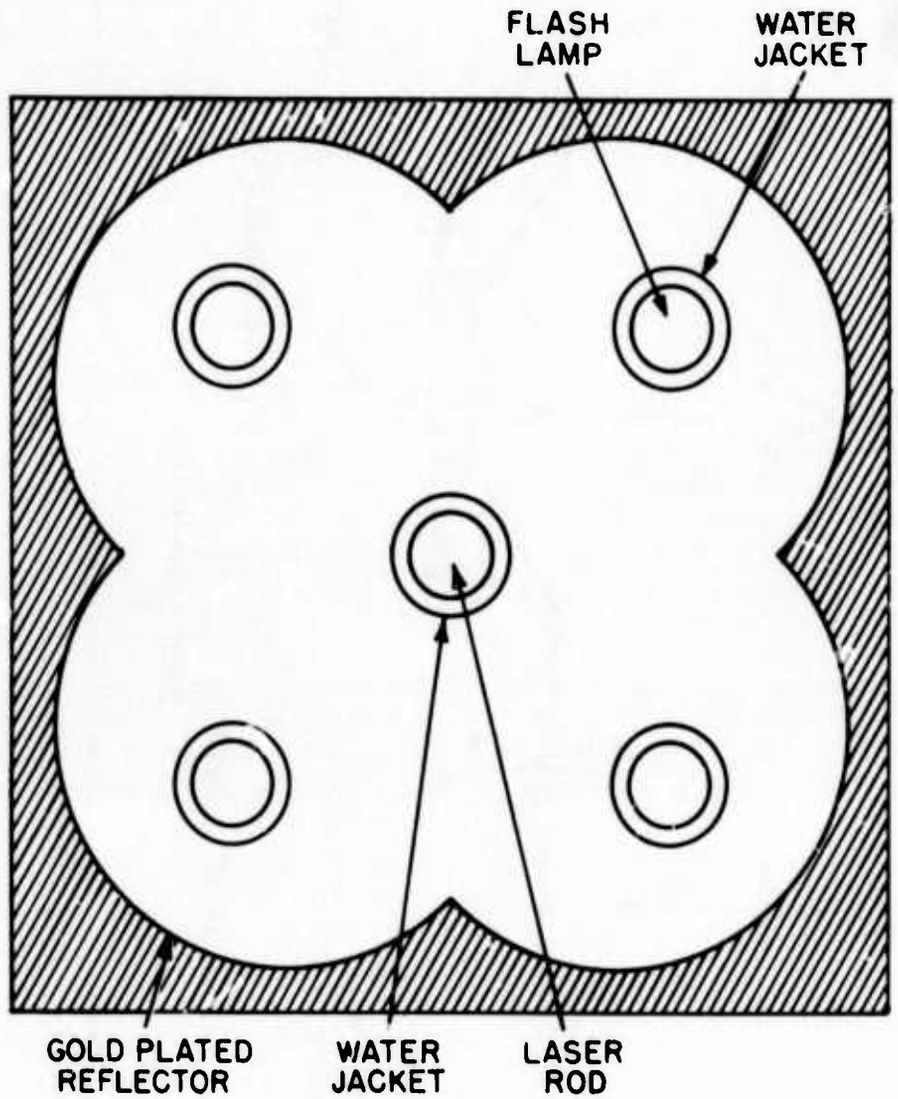

Figure 23 Cross section of four lamp cloverleaf pump cavity assembly.

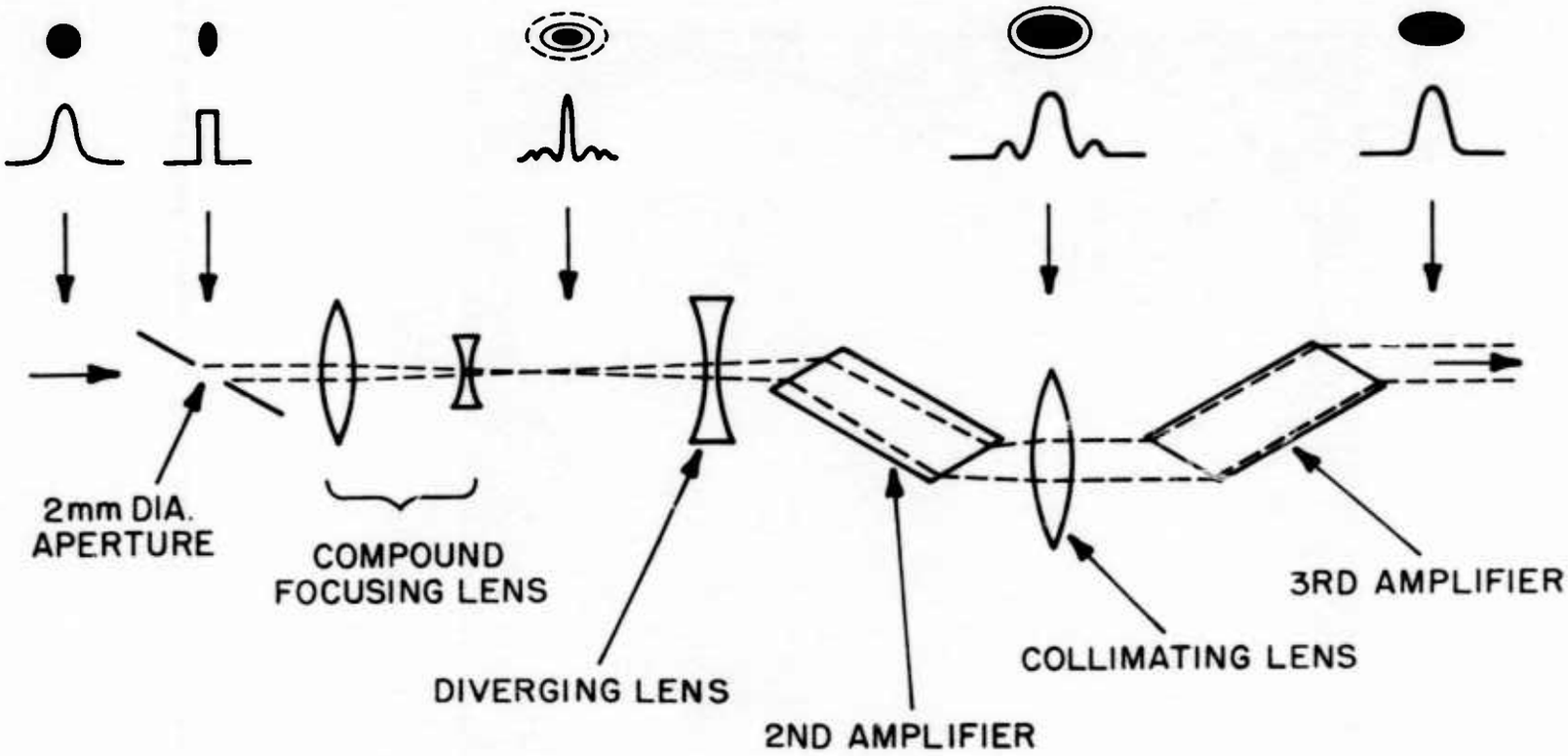

Figure 24 Beam expansion optics in mode-locked system amplifier chain. The intensity distribution at various points is indicated above.

that after refraction inside the rods, the beam will fill in the full rod volume. The beam is then brought to its Fraunhoffer pattern by a 50 cm compound lens. It is then expanded so that between the second and third amplifiers the major diameter of the first diffraction minimum is 3/8 inch.

It is then approximately collimated, and the third amplifier rod apertures the beam at the first Airy minima. The central Airy disc, still expanding slowly, fills the third and fourth rods, after which it is collimated by another lens. Aperturing the beam at the minima in the Airy pattern provides a sufficiently smooth beam to avoid small scale self focusing, and allowing the beam to expand as it propagates through the amplifiers also tends to reduce the nonlinear effects.

II. E. 1d PULSE SHAPING

The lifetimes associated with x-ray transitions are still extremely short compared to the duration of mode-locked pulses. It is desirable to make the durations of the laser pulse, or at least the risetimes, as close as possible to the lifetimes of the pumped x-ray transitions. Several schemes are being investigated to produce pulses shorter than those generated in the pulse system. These schemes involve either generation of shorter pulses at the source, or processing the longer pulses once they have been generated.

As a possible source of shorter pulses the properties of Nd:CaLaSOAP as an active medium for the oscillator have been studied. Its homogeneously broadened line of 45 cm^{-1} width indicated that it might provide bandwidth limited pulses of 5 psec duration. More careful study, however, indicated that spectral broadening of the pulses was significant and bandwidth limited operation was limited to pulse duration of about 10 psec. It does appear, however, that it might provide a source of pulses with a controlled chirp for subsequent compression.

Other possibilities for producing shorter pulses lie in processing the pulses from the YAG oscillator. A single pass through a saturable dye cell can result in significant shortening of the pulses. This technique was observed to reduce pulse duration from 28 psec to 14 psec (Figure 25). This process is currently being analyzed to determine optimum dye concentrations and minimum possible pulse duration. Combinations of pulse chirping followed by dispersive delay lines either to sharpen the leading edge of the pulse or to compress it are being investigated. This latter technique has received a careful analysis. The ideas involved are outlined in Appendix A.

II. E. 2. Q-SWITCHED LASER

The main purpose of the Q-switched laser is to provide a pulse for generating a plasma which can subsequently be heated/pumped with the mode-locked laser. Good spatial beam quality is again important

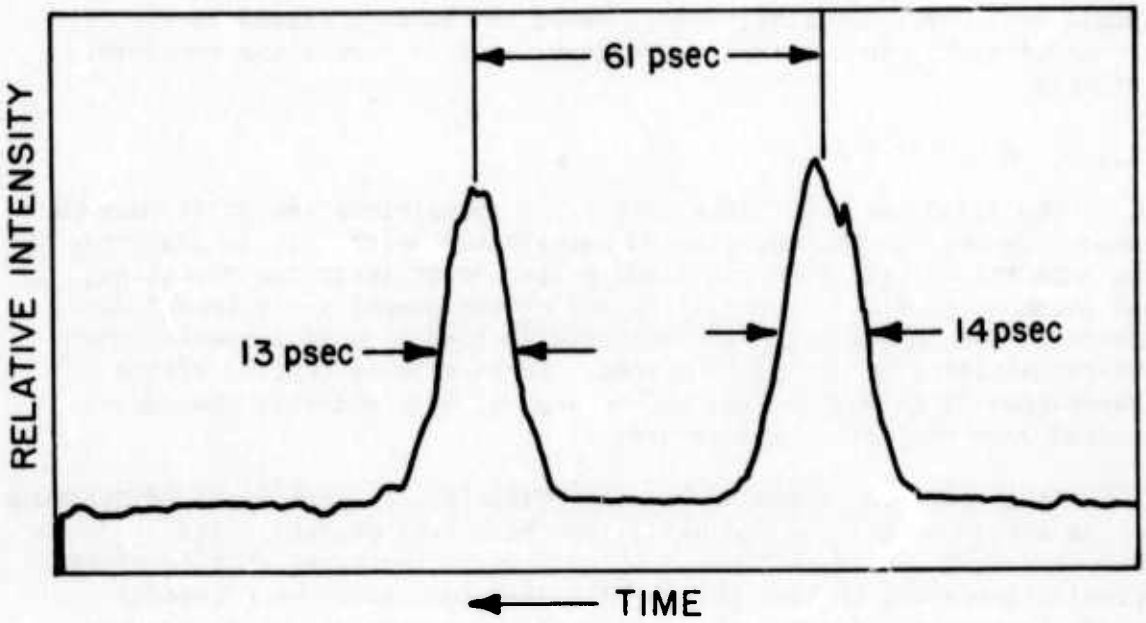

Figure 25 Fast streak camera record of two reflections of the same mode-locked pulse after transmission through a saturable absorber with linear transmission 10^{-10}.

for avoiding self focusing in the amplifier chain and to provide high brightness on target. Single longitudinal mode operation of the oscillator is required to avoid self-phase modulation in the amplifier and to provide reproducible pulses with no mode beating for plasma generation. It is also desirable to have adjustable pulse duration in the range from 0.5 nsec to 30 nsec with energies between 1 to 10 J. The Q-switched laser system is currently under evaluation and characterization and it will be operational soon. It will consist of a single transverse and longitudinal mode Q-switched Nd:YAG oscillator with the output shuttered by an external Pockels cell to switch out a portion of the laser pulse of the required duration. The energy of the output would cause severe depletion in Nd:YAG amplifiers except for the case of very short pulses in the first amplifier. Therefore Nd:glass amplifiers are used. The first amplifier has a 3/8 inch by 6 inch rod followed by two 3/4 inch by 12 inch amplifiers. Gains in excess of 2000 will easily be obtained from the three amplifiers to provide the required output pulse energy.

The nonlinear index of Nd:glass, $n_2 \approx 2 \times 10^{-22}$ M^2/V^2, is lower than that of YAG. The longer pulse length and larger diameter of the glass amplifier reduce the problems introduced by the nonlinear index of refraction even through the rod length is greater. Calculations similar to those done for the mode-locked system show that intensities on the order of 2×10^{10} Watts/cm^2 can be reached in the final amplifier before self focusing will cause significant distortion in the output. For pulse durations of 5 nsec energy density would be 100 J/cm^2 before self focusing becomes a problem (well in excess of the planned output of 10 J). It does remain critically important, however, to preserve a smoothly varying transverse intensity distribution. If this is not done, small scale self focusing will occur in the amplifier rod at lower pulse energies and cause damage.

The Q-switched oscillator shown in Figure 26 has a 3/8 inch by 3 inch Nd:YAG laser rod pumped with the same geometry used in the mode-locked oscillator. The narrow 7 Å fluorescence bandwidth of Nd:YAG makes the problem of longitudinal mode section less difficult, and for this reason it is used in preference to Nd:glass which has a 260 Å bandwidth. The resonant cavity is formed by a 10 m radius 100% reflector and a resonant reflector formed by uncoated sapphire optical flats with parallel surfaces. Currently two sapphire elements are used, but it appears it will be necessary to use three elements to obtain the desired longitudinal mode control. The sapphire elements are aligned interferometrically to be parallel. Using the cavity as an interferometer also allows accurate alignment of the 99% mirror. Transverse mode selection is obtained with an aperture inside the cavity. A polarizing prism and a Pockels cell operated at the $\frac{1}{4}$ wave voltage serve as the Q-switch. The Pockels cell is triggered from the mode-locked laser in a manner which will be described in the next sub-section to provide synchronization between the two lasers.

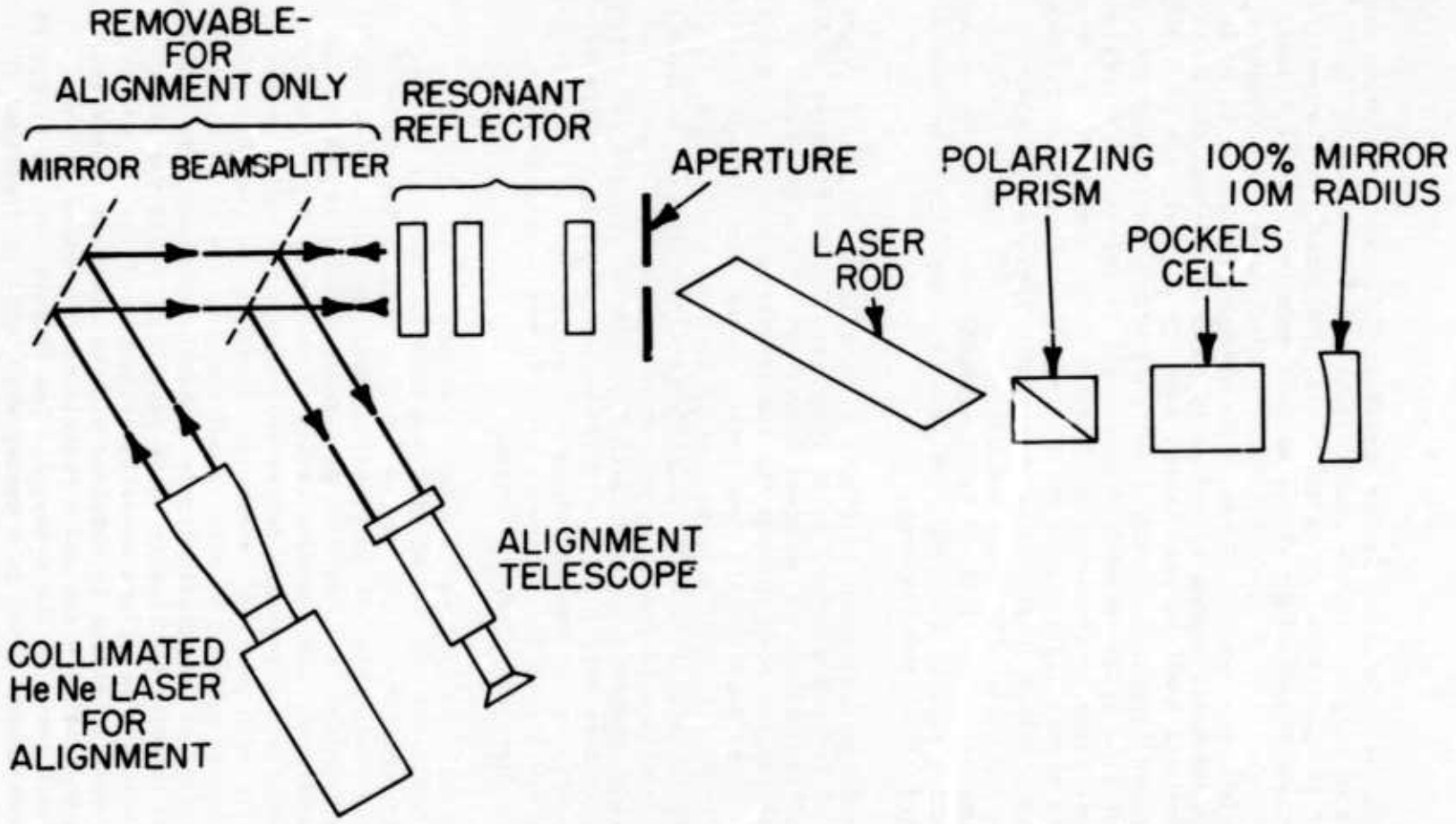

Figure 26 Q-switched oscillator and alignment optics.

The output of the Q-switched laser appears with a delay from the Pockels cell trigger of 100 nsec as shown in Figure 27. The jitter in the appearance of the pulse is approximately 30 nsec. It is expected that this value will be improved with further development of the oscillator. The output energy of the oscillator is approximately 15 mJ in a 30 nsec pulse. The duration of the Q-switched pulse at this point must be long enough to overlap with several of the mode-locked pulses, so that reliable synchronization of the two lasers can be obtained.

Currently, investigations of additional longitudinal mode control provided by operating the Pockels cell in a "simmer mode" with the voltage somewhat below exact $\frac{1}{4}$ wave voltage are underway. The presence of low level free running oscillations with long buildup times reduces secondary lonitudinal modes and mode beating in the Q-switched output (Figure 28). The intensity of the low level free running oscillations is down by more than a factor of 100 from that of the Q-switched oscillation. The amount of this pre-lasing which reaches the target will be further reduced by the Pockels cell that shutters the output.

II. E. 3. SYCHRONIZATION

The major problems in synchronizing the outputs of two independent pulsed lasers lie in the jitter inherent in the build up of the optical pulse from noise and the short time scales involved once the pulses are generated. The jitter in the time of appearance of the mode-locked pulse train relative to the ignition of the flash lamps is about $\pm$ 10 μsec. Since the pulse train lasts for only about 50 to 100 nsec, all subsequent events must be timed from the appearance of the pulse train, rather than the electrical trigger pulse. Similar problems occur in the Q-switched laser where delay times of the order of 100 nsec are expected in the build up time of the Q-switched pulse relative to the time the Pockels cell is triggered. Again, it is impossible to synchronize pulses to less than 10 nsec by using the electrical trigger pulse to the Q-switching cell as a reference.

Figure 29 illustrates the synchronizing scheme being used. It overcomes these problems by timing events from the time of appearance of each of the optical signals. The various switching steps are summarized in Figure 30, along with the jitter expected relative to the previous step. The sequence is initiated with the firing of the oscillator lamps of both lasers, synchronized to about $\pm$ 10 μsec. The mode locked pulse train appears with a time jitter of about $\pm$ 10 μsec relative to the flashlamps. The Q-switching of the second laser is synchronized to the leading edge of the mode-locked pulse train. A photodiode monitors the rejected pulse train, the output of the photodiode is used as a trigger signal for an electronically triggered spark gap with 35 nsec internal delay, and the spark gap is used to remove the voltage on the Pockels cell Q-switch. This synchronization has already been accomplished with a Q-switched glass laser using a krytron switch instead of the spark gap (Figure 31). The delay in buildup of the oscillation in the glass laser was longer

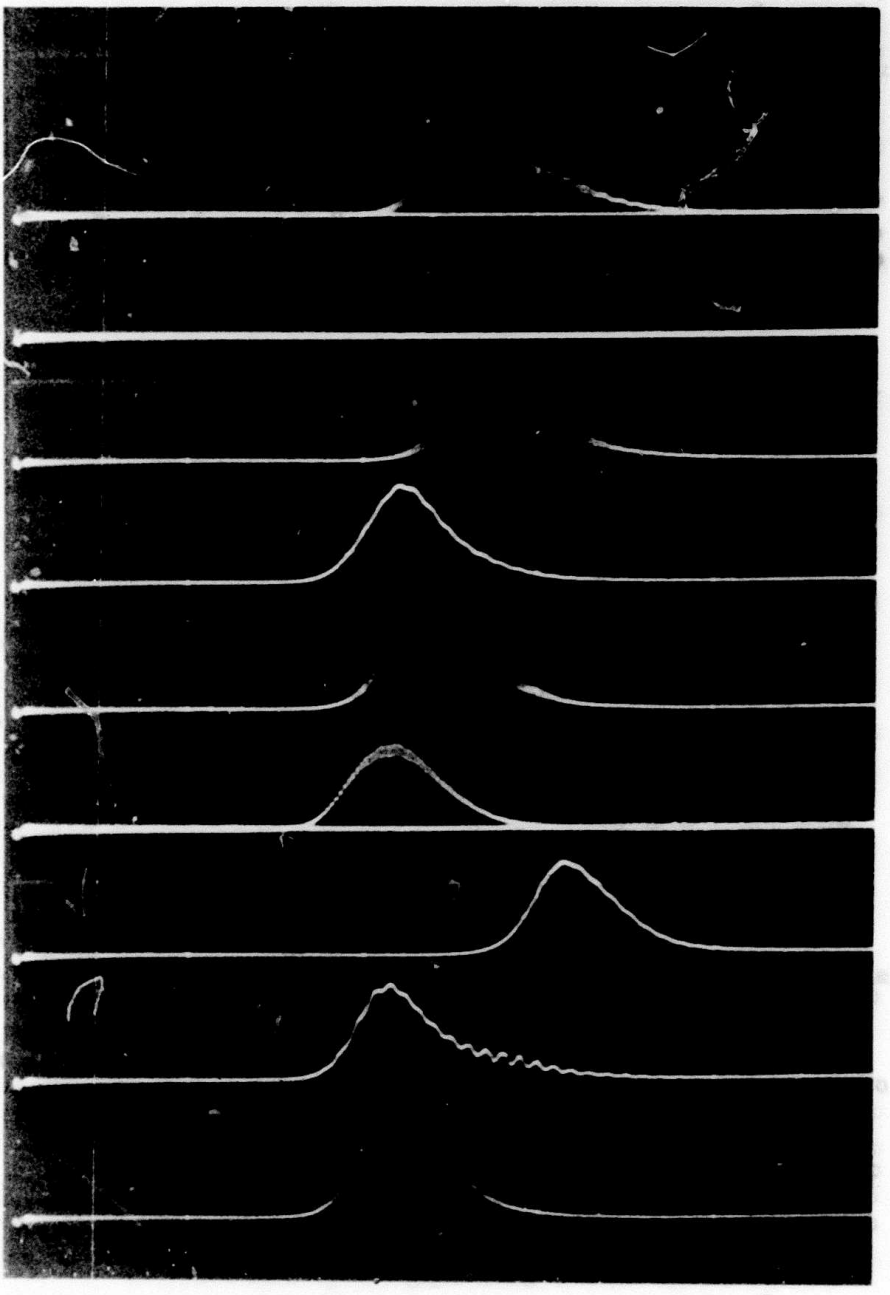

Figure 27 Oscillograms of several Q-switched oscillator pulses showing jitter in time between Pockels cell trigger and appearance of pulse. Time scale is 50 nsec/cm. Some mode beating is present in laser output.

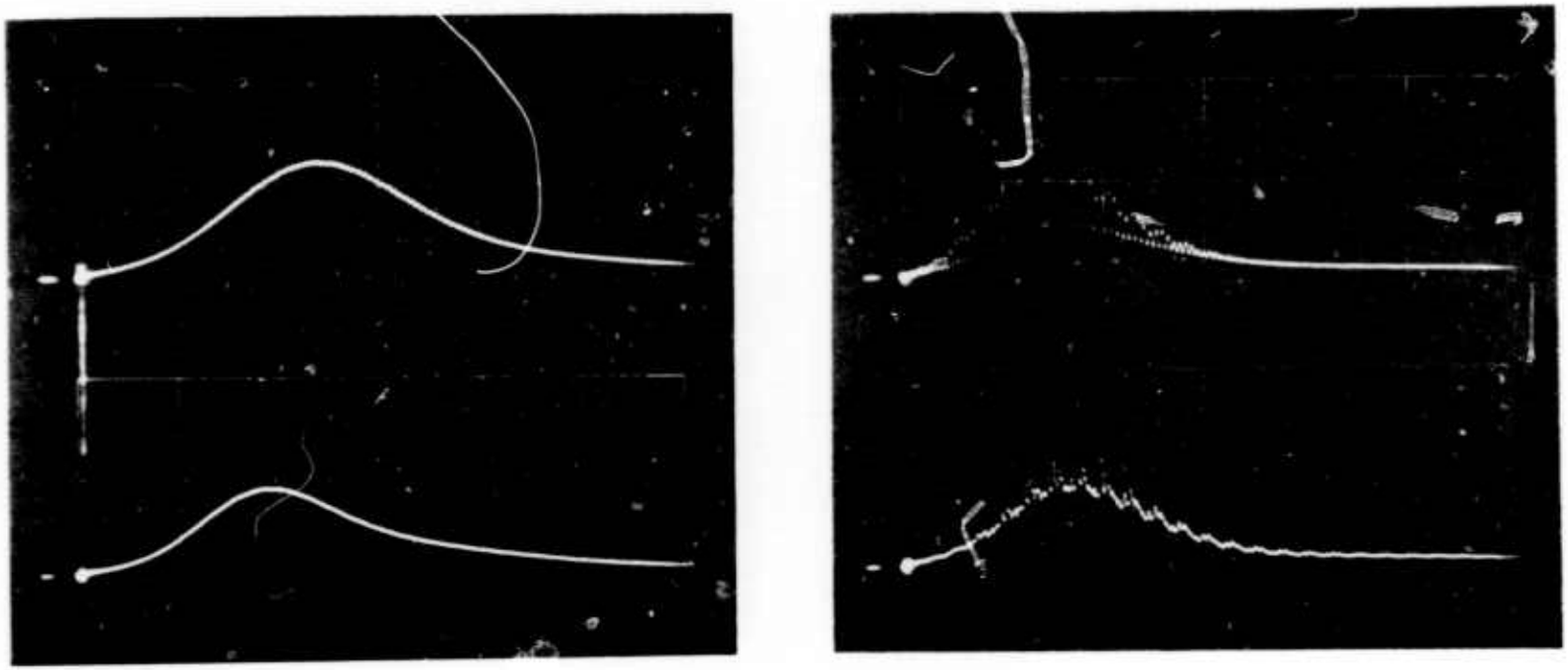

(a) (b)

Figure 28 Effect of running Q-switched oscillator is a "simmer mode" with Pockels cell voltage reduced below $\frac{1}{4}$ wave voltage. (a) Reduced Pockels cell voltage. (b) Full $\frac{1}{4}$ wave Pockels cell voltage.

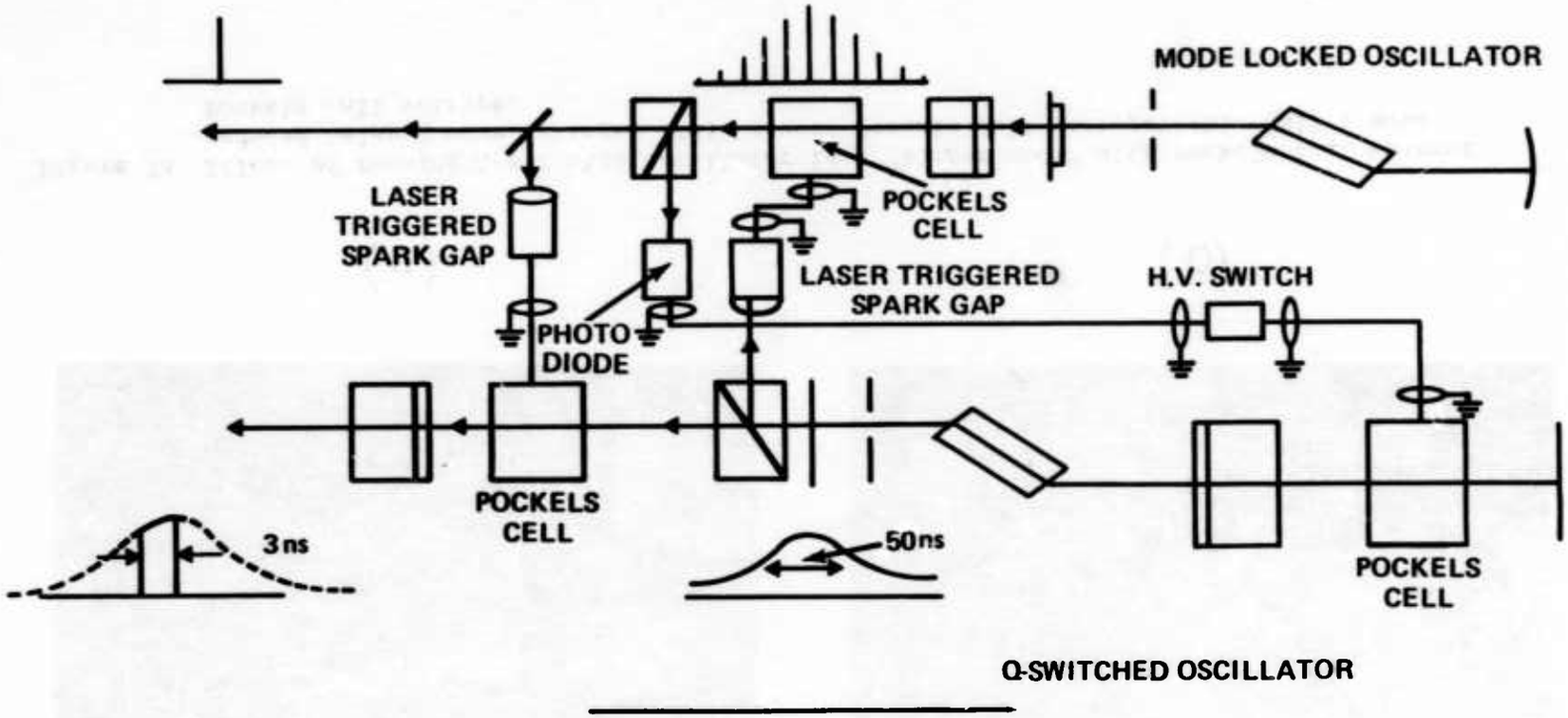

SEQUENCE OF EVENTS:

1. START OF MODE LOCKED LASER PULSE TRAIN
2. Q-SWITCHED LASER TRIGGERED ON EARLY PULSE FROM MODE LOCKED TRAIN
   ($\Delta t \sim$ 10-20ns
3. MODE LOCKED PULSE SELECTED AFTER START OF Q-SWITCHED PULSE
   ($\Delta t \sim$ 6-7ns
4. SECTION OF Q-SWITCHED PULSE GATED OUT BY SELECTED MODE LOCKED PULSE
   ($\Delta t <$ 1ns

Figure 29 Synchronization of mode-locked and Q-switched lasers. Sequence of events: (1) tart of mode-locked laser pulse train, (2) Q-switched laser triggered on early pulse from mode-locked train ($\Delta t \approx$10-20 nsec), (3) mode-locked pulse selected after start of Q-switched pulse ($\Delta t \approx$6-7 nsec), (4) section of Q-switched pulse gated out by selected mode-locked pulse ($\Delta t <$1 nsec).

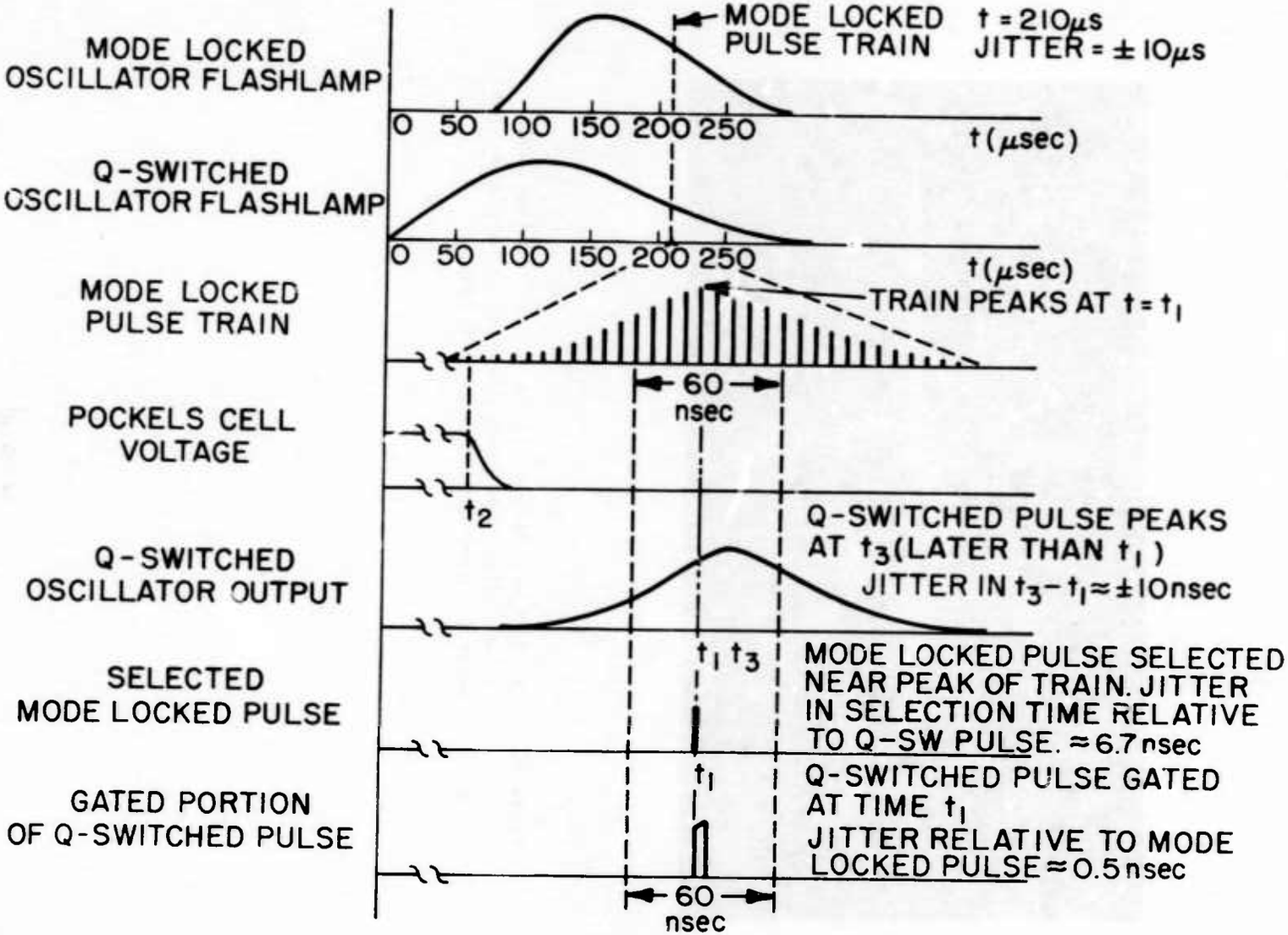

Figure 30 Synchronizing sequence for mode-locked and Q-switched lasers.

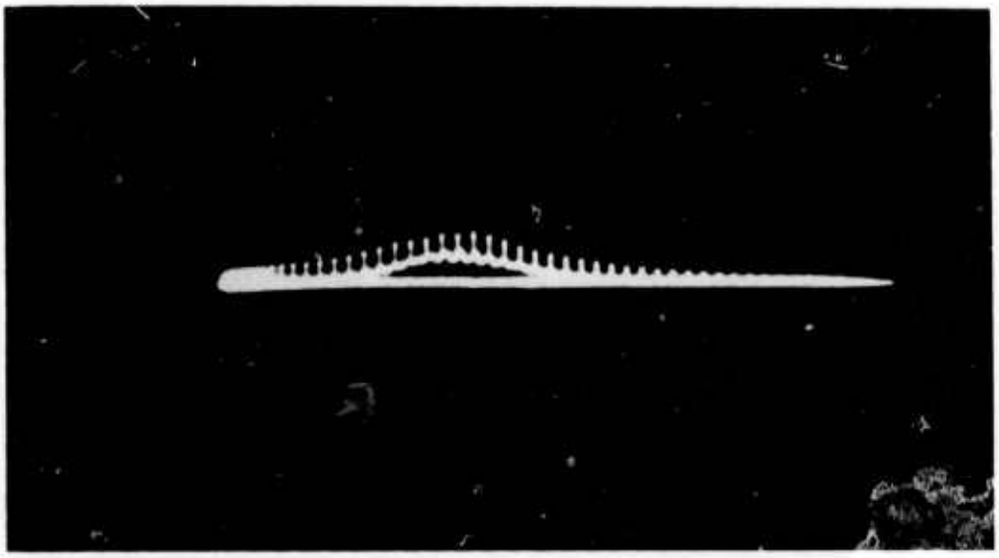

Figure 31 Oscillogram displaying both synchronized mode-locked pulse train and Q-switched Nd:glass laser pulse. Sweep duration is 300 nsec.

and the krytron had longer delay than the spark gap causing a jitter problem. Longitudinal mode selection was more difficult with the broader spectrum of glass, and it was decided to use the Q-switched YAG oscillator.

Once the Q-switched pulse has appeared, part of it is used to fire the pulse selector in the mode-locked laser, selecting a pulse near the peak of the train. The jitter in timing of the selected pulse relative to the peak of the Q-switched pulse is expected to be of the order of the interpulse spacing of 6-7 nsec. Finally the selected mode-locked pulse is used to gate out the desired portion of the Q-switched pulse near its maximum. Use of a laser triggered spark gap in this last stage will provide risetimes of the order of several hundred psec. Because the spark gap can be severely over-driven by the mode-locked pulse, the final jitter is expected to be in the subnanosecond range.

II. E. 4. LASER DIAGNOSTICS

A complete set of laser diagnostic measurements on a shot-by-shot basis is necessary for controlled investigation of the laser-plasma interaction as well as monitoring overall laser performance. Provision for monitoring laser performance have been made as shown in Figure 18. The pulse energy in both beams is measured with a calibrated photodiode. Provision for periodic recalibration of the diode against a calorimeter is also present. The duration and shape of the mode-locked pulses are measured on a streaking camera with a 5 psec resolution. Such measurements are indispensable in monitoring shot to shot variations of the mode-locked output, jitter in the interpulse spacing, and pulse separations for times less than 1 ns. Finally, the far field pattern of the beam is recorded on every shot by using a focusing lens identical to the one used to focus the beam on to the target. This measurement determines the spot size and distribution of the laser at the focus, monitoring possible fluctuations in beam divergence due to self focusing or other disturbances as well as fluctuations in the beam direction, and the overlap of the two beams brought to the target collinearly.

III. RESONANT CHARGE TRANSFER PUMPING

III. A. BACKGROUND

Binary collision processes have been the subject of an extensive literature[1]. In particular there is a substantial literature describing experimental and theoretical work on charge transfer processes during binary collisions. This type of process is of particular interest here since under appropriate conditions its cross-section can be extremely large and should dominate all other binary processes. If this is indeed the case in a parameter space pertinent to soft x-ray lasers, then this process can potentially be used to preferentially fill a specific electronic level in two colliding species. If this

level lies high enough then transitions to underpopulated lower lying levels can fall in the soft x-ray spectrum. Further, if the densities and rates are sufficient, an inversion and net gain should be possible. This scheme for pumping a soft x-ray laser with its anomolously large cross-section is described below.

Binary collisions can be described in terms of adiabatic potential energy curves for the two particle system before and after the collision. This is a valid approximation as long as the velocities of the particles are low enough that they are small compared to the velocity of the bound electrons ($\sim 10^8$ cm/sec), and large enough that the motion of the nuclei is classical. The general charge transfer process can be written as follows:

$$A^{z+} + B \rightarrow A^{(z-1)+} + B^{+} + \Delta E,$$

where B is a neutral atom and A is an ion and ΔE is the difference between the potential energy of the initial and final configurations at large internuclear separations, R. At infinite separation of A^{z+} and B the potential energy is assumed to be zero. The potential curves for both the (A^{z+}, B) and ($A^{(z-1)+}$, B^{+}) systems are shown in Figure 32. The latter curve represents the Coulomb repulsion between the two ions. In a precise quantum mechanical treatment these two curves do not cross but there is a mixing of states at the classical crossing point, R = X. Further, in any real situation there are several possible final states ($A^{+(z-1)}$) represented by the different electronic levels of the $A^{+(z-1)}$ ion. In Figure 32 these levels are represented by the hatched area. Note that for different levels the curve crossing points occur for different values of the internuclear separation, R, and the ΔE's are different. In fact, ΔE is in general a strong function of R. From the figure it can be seen that if ΔE is negative there is no classical crossing point and charge transfer is not very probable. Also if $\Delta E = 0$ the crossing point is at $R = \infty$ and charge transfer is not very likely.

Several theories exist to describe the charge transfer process. Landau and Zener (LZ) developed a semiclassical approximation using time-dependent perturbation theory. This theory is applicable in the low velocity adiabatic approximation described above. A later more vigorous theory has been developed by Bates, Johnson, and Stewart (BJS). A discussion of these theories and others is presented in Ref. 2. The LZ theory predicts a large cross-section for a velocity such that maximum time is spent with the two particles at separation R = X. The most severe limit on this theory is that it is strictly valid only for s-state initial and final states.

The BJS theory predicts the same large cross-section for low velocities as the LZ theory but also predicts a second maximum in the cross-section at higher energy due to interference terms in the

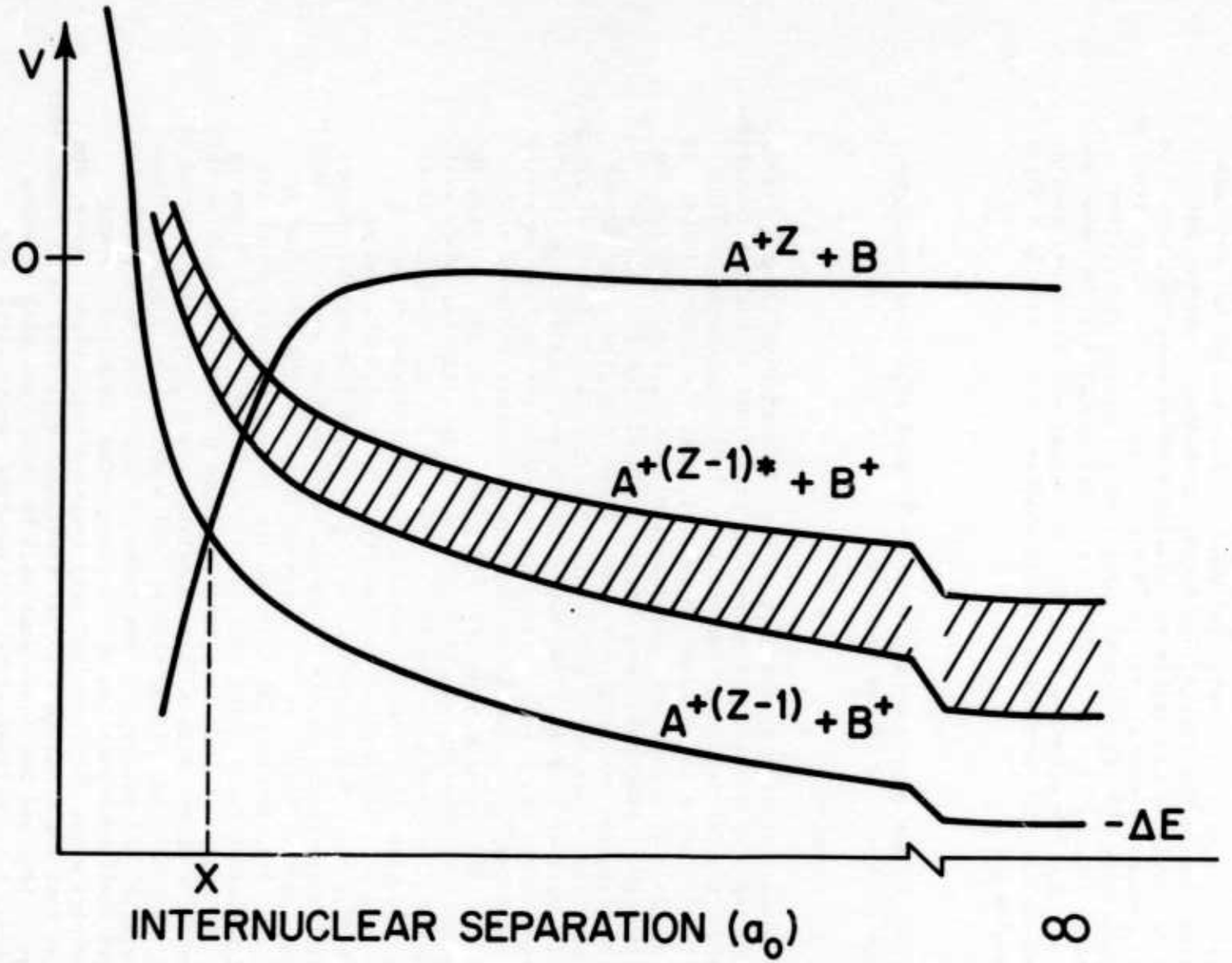

Figure 32 Potential energy curves for the systems (A^{+z},B) and ($A^{+(z-1)}$, B^{+}) used in the adiabatic (Landau-Zener) approximation for resonant charge transfer. The hatched area represents the collection of excited states.

quantum mechanical calculation. This second maximum in cross-section is the one studied experimentally using multi-kilovolt ion beams[3]. The very low energy maximum in cross-section has not been observed due to the lack of low energy ion beams. However, this process should be accessible to detailed studies with cold ions from laser produced plasmas. Figure 33 gives a plot of the charge transfer cross-section σ^{LZ}, from the LZ theory, as a function of relative velocity for the case Z=2. It is seen that as $\Delta E/(Z-1)$ becomes smaller, R_x, the crossing point, becomes larger and the cross-section increases with the maximum moving to smaller velocities. As a first approximation

$$\sigma_{max}^{LZ} \approx \pi a_o^2 Z^2$$

where a_o is the Bohr radius. Hence it is seen that cross-sections on the order of 100 Å^2 are possible.

III. B. EXPERIMENT

Several considerations must be born in mind when using a resonant charge transfer process for generating very short wavelength radiation. First, the potential laser ion has many electronic energy levels. The level spacing is maximum, in general, near the ground state. As one proceeds to higher and higher excited states, the level spacing and density of states becomes larger. Further, for the shortest wavelengths, one uses higher Z ions. These ions have their ground states at lower and lower potential. This is illustrated in Figure 34 for the case of hydrogen-like ions. The second consideration is that ion-ion charge exchange is not possible due to the Coulomb repulsion, and hence deep lying levels in ions are not accessible with this process. Only ion-atom processes will work. Hence, the question is which atom has the maximum ionization potential (IP) and hence will reach furthest down into the level structure of the potential laser ion. The best candidate is helium as shown in Figure 34 with an IP = 24.6 eV. Other possibilities are H (IP = 13.6 eV) and Ne (IP = 21.6 eV). Helium remains the best choice from another point of view however; the second IP should be as high as possible to avoid photoionization losses at the laser wavelength. The IP of He^+ is 54.5 eV. Also levels must exist on the ion and the atom which are near resonance for a large cross-section. A final consideration is that the source of ions is a laser produced plasma. One must be able to create a plasma with a large population of a <u>particular</u> species of ions. Recent laser plasma studies have shown that a given laser pulse width and energy, one tends to "burn" down to a particular closed shell configuration with a given target material. Energy thresholds exist for "burning" away deeper lying shells. Hence, the target ions for a charge transfer experiment will tend to be closed-skill -type ions and the laser ions will be these ions with an extra electron, i.e., hydrogen-like, lithium-like, sodium-like, etc.

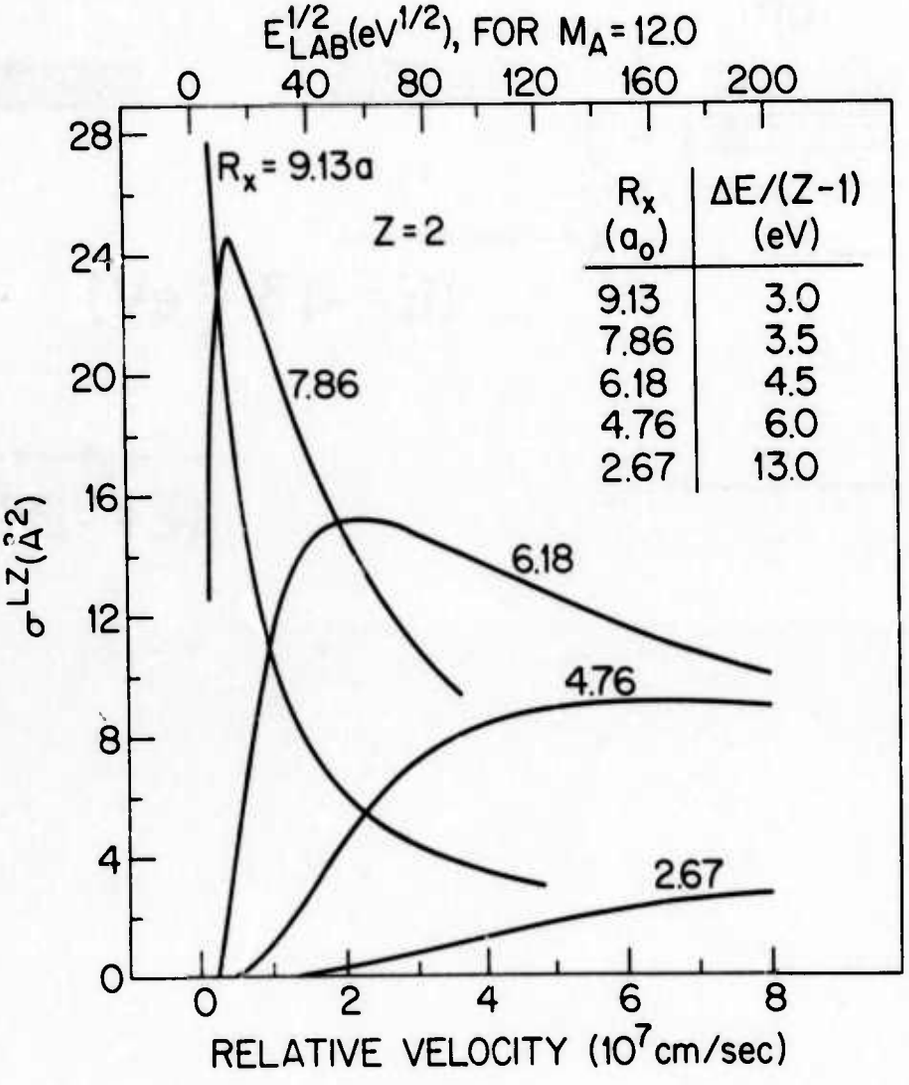

(FROM ZWALLY AND KOOPMAN, PHYS REV A, 2, 1851 (1970))

Figure 33 Charge transfer cross-section, σ^{LZ}, as a function of relative velocity of the two particles for the case Z=2.

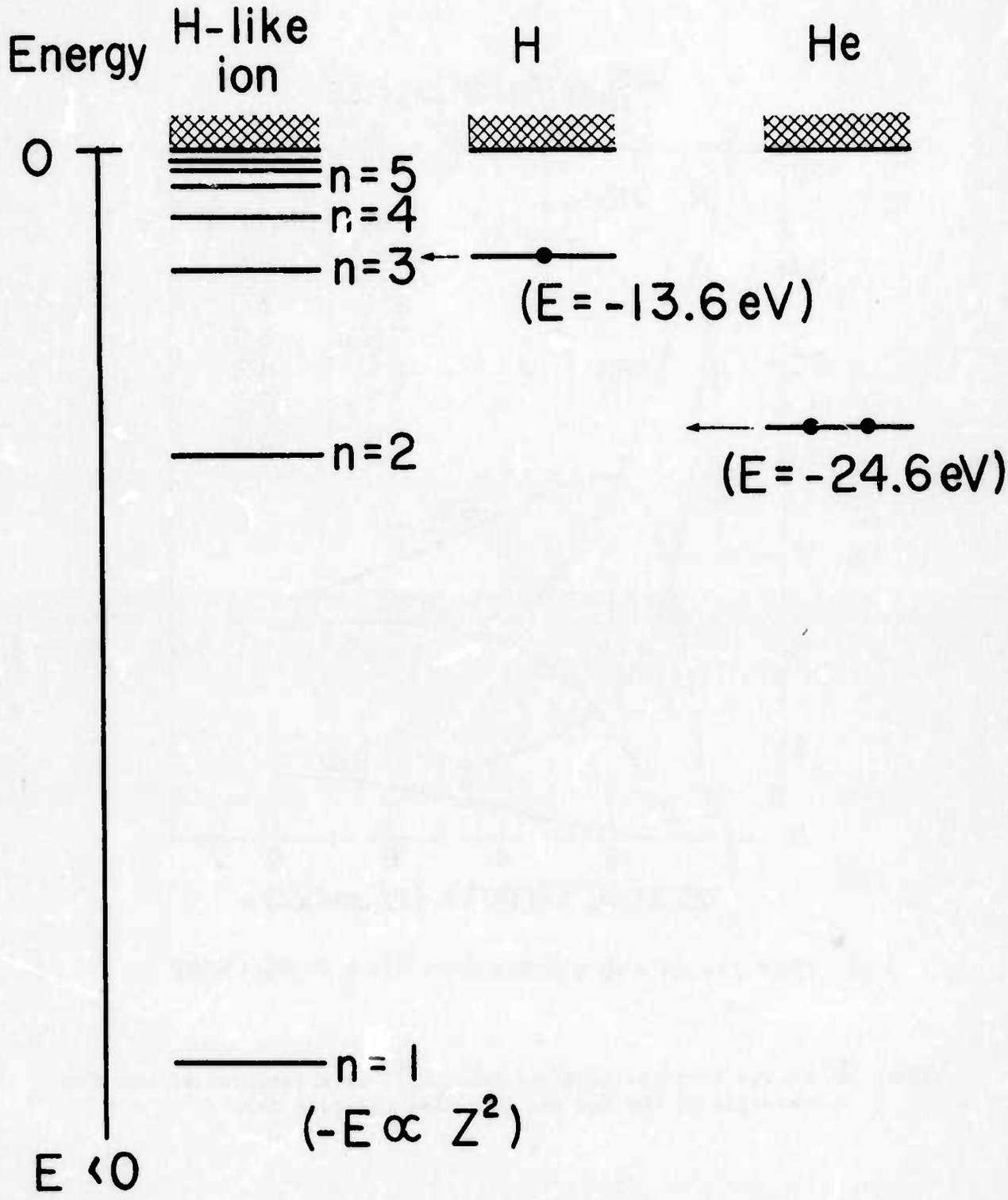

Figure 34 Potential energy diagram for an arbitrary hydrogen-like ion along with the first ionization potential of hydrogen and helium.

Given the above considerations, carbon appears to be a prime candidate for a charge transfer laser scheme. The energy level diagrams for Carbon IV and Carbon VI are given in Figures 35 and 36, respectively. The resonant charge transfer possibilities are as follows:

$$C^{4+}\ (^1S_o) + He\ (^1S_o) \rightarrow He^+ + C^{3+}\ (3s, {}^2S_{\frac{1}{2}}) \qquad \text{(i)}$$

$$C^{4+}\ (^1S_o) + He\ (^1S_o) \rightarrow He^+ + C^{3+}\ (3p, {}^2P_{\frac{1}{2}},\ 3/2) \qquad \text{(ii)}$$

$$C^{6+} + He\ (^1S_o) \rightarrow He^+ + C^{5+}\ (m=4) \qquad \text{(iii)}$$

TABLE II- RESONANT CHARGE TRANSFER REACTIONS

REACTION	$\Delta E/(z-1)$	TYPE TRANSITION	σ^{LZ}	LASER
$C^{4+}, He \rightarrow He^+, C^{3+}(3s)$	.78eV	s → s	> 100 Å^2	3s→2p (420 Å)
$C^{4+}, He \rightarrow He^+, C^{3+}(3p)$	.07eV	s → p	> 100 Å^2	3p→2s (312 Å)
$C^{6+}, He \rightarrow He^+, C^{5+}(4)$	1.16eV	s → s	> 100 Å^2	4 → 1 (27 Å)
				4 → 2 (135 Å)
				4 → 3 (521 Å)

The potential laser wavelengths, ΔE's, etc. for these reactions are listed in Table II. All of them represent very favorable situations.

The experiment to investigate this scheme using the (He,C) combination is under construction. It consists of the NRL Glass Laser Facility as a source of 10 Joule, 30 psec pulses, a plane carbon slab target in a vacuum chamber, and a grazing incidence spectrograph. The laser is line focused onto the target with one edge of the focus adjacent to the slit of the spectrograph. A pulsed solenoid is available to produce a 50 kG magnetic field orthogonal to the line focus. This magnetic field reduces the solid angle into which the plasma expands and thereby maintains a higher ion density. The helium gas is allowed to fill the vacuum chamber and surround the target just prior to the arrival of the laser pulse. This technique permits the use of the vacuum spectrograph without the need for differential pumping. The helium gas pressure is ~100 torr. A 10^{14} W/cm^2 laser pulse can propagate through this amount of helium without causing gas breakdown.

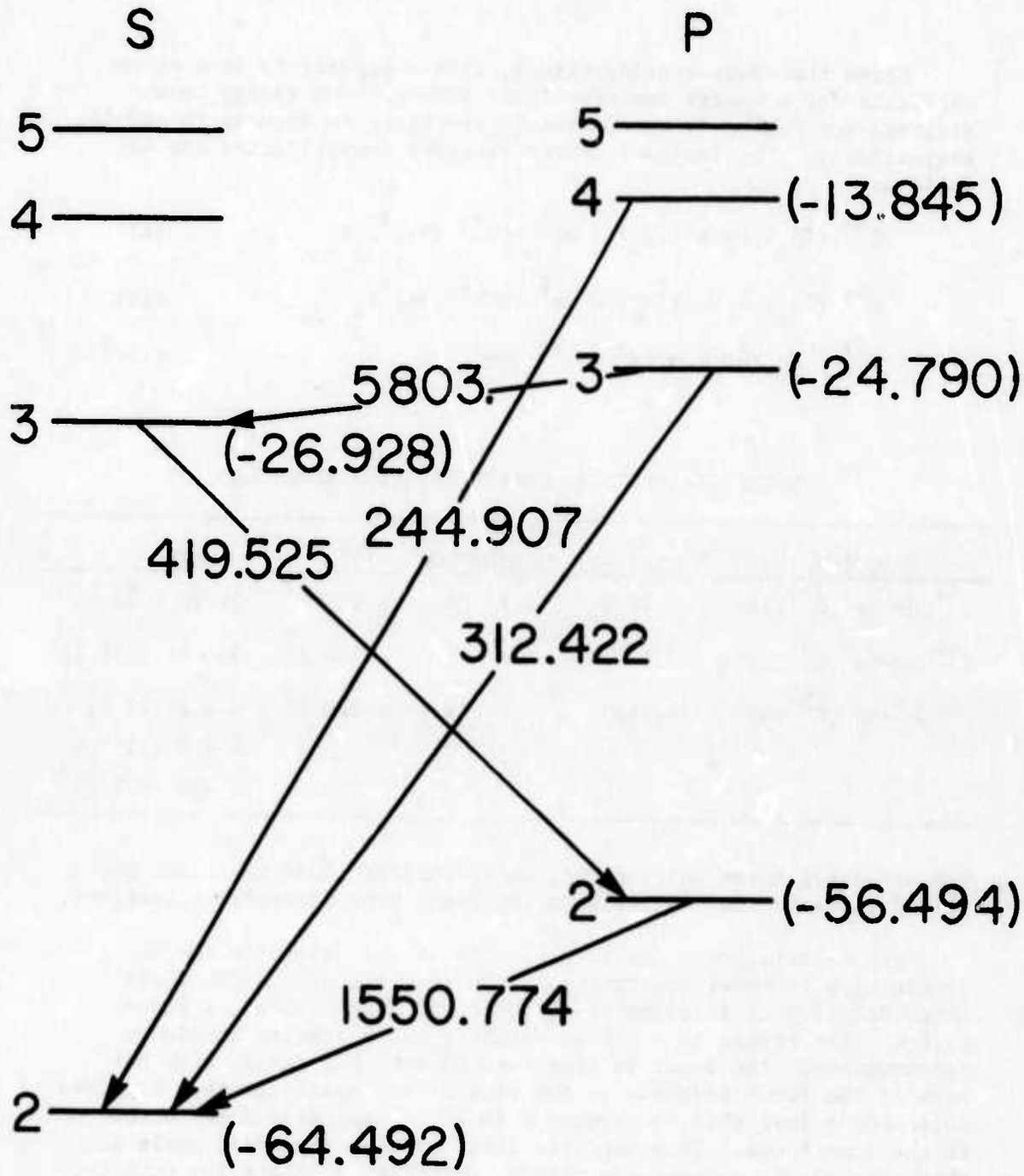

C IV (Lithium-like)

IP = 64.5 eV

Figure 35 Energy level diagram for Carbon IV.

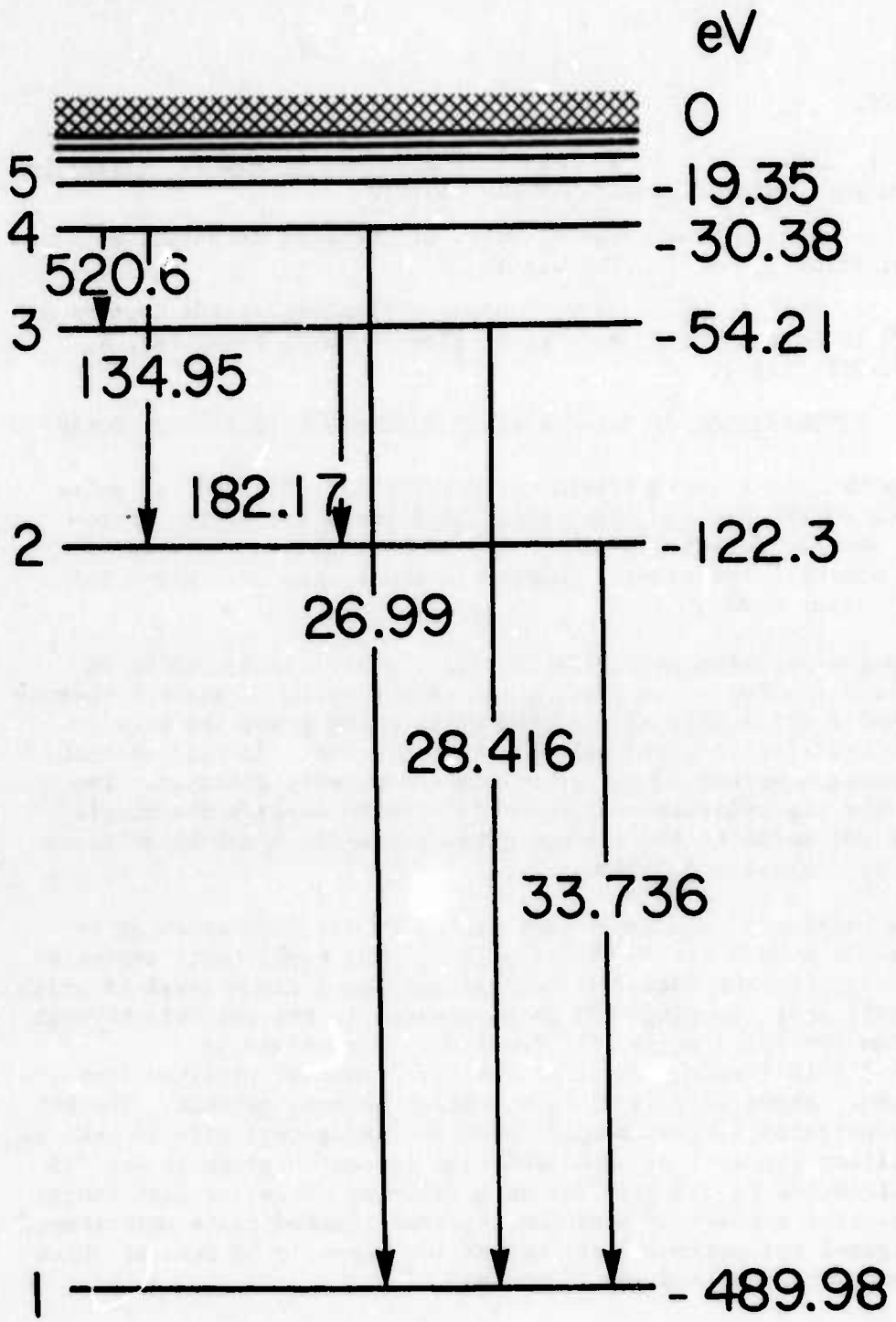

Figure 36 Energy level diagram for Carbon VI

C VI (Hydrogen - like)

IP = 490 eV

REFERENCES

1. N. F. Mott and H. S. W. Massey, The Theory of Atomic Collisions 3rd ed., Oxford Clarendan Press (1965).

2. H. Jay Zwally, PhD. thesis, Univ. of Maryland Technical Note No. BN-582, 1968 (unpublished).

3. H, Jay Zwally and David W. Koopman, "Single-Electron Capture by C^{4+} in Helium, Neon, and Argon below 40 keV", Phys. Rev. A, 2, 1851 (1970).

III. C. OPTIMIZATION OF THE NRL LASER SYSTEM FOR ULTRASHORT PULSES

The NRL glass laser system was originally optimized for pulse durations of 250 psec to 1000 psec. Reoptimization of the system for the shorter pulses (20 psec - 100 psec) required for x-ray laser studies necessitated several changes in the system to achieve the maximum output level.

The transmission mode selectors in the oscillator had to be removed and the dye concentration and gain reduced to achieve shorter pulses while still keeping the peak circulating power the same to minimize self-focusing and self phase modulation. In this fashion, clean Gaussian pulses 42 $\pm$ 4 psec long (FWHM) were obtained. The gain of the preamplifiers was then adjusted to amplify the single switched out pulse to the maximum intensity which could be obtained without self-phase modulation.

The staging of the amplifiers had to be modified somewhat to optimize the output for the short pulses. Our experiments indicated that the significant factor in determining the maximum level at which small scale self focusing will be suppressed is the net gain through the system for small scale self focusing. For values of $\int Idz < 4.5 \times 10^{11}$ W/cm, very high quality beams are obtained from the NRL system. Above this level beam breakup becomes evident. The NRL system configured for nanosecond operation had excess gain to make up for amplifier saturation. The isolation system in place in Dec '73 also contributed to the gain for self focusing since the high energy densities at a nanosecond duration required stacked plate polarizers. As configured the maximum level out of the laser in 40 psec at which good beams were obtained was 16 Joules.

During the last six months several changes have been instituted which have boosted the safe level from 0.4 TW to 0.55-0.6 TW:

(1) The new disc amplifier module has demonstrated a 20% higher gain coefficient than the prototype due to design improvements. When the laser discs of ED-8 glass are delivered by Owens-Illinois (1st quarter FY75) this margin should increase to 40%.

(2) Sufficient large aperture dielectric polarizers have been delivered to replace the stacked plate polarizer and reduce the contribution of the final isolator to the self focusing growth by a factor of 4.5.

(3) Parasitic suppressing liquid rod claddings have been synthesized and tested at NRL and result in a 40% increase in the gain coefficient of the French amplifiers and a consequent decrease in the self-focusing growth rate in these amplifiers.

By the end of FY'75, planned improvements to the system should increase these levels to between 0.75 and 0.9 TW, dependent largely on available funding. In appendix B, the laser system configuration is detailed at greater length and the track record over the past year is given for all programs (AEC, ARPA, and DNA).

IV. GENERATION OF COHERENT VUV/SOFT X-RAY PULSES BY NONLINEAR MIXING

IV. A. BACKGROUND

The Generation of short wavelength coherent radiation through harmonic generation and nonlinear mixing of laser pulses has been shown to be effective in producing light at wavelengths down to 1000 Å[1]. Extension of these techniques to shorter wavelengths is an attractive method of producing coherent soft x-radiation because the generated radiation maintains the spatial and temporal coherence of the pumping radiation. With the conversion efficiencies reported to date, however, pulses generated in the VUV range as harmonics of a Nd:YAG laser at 1.06 μ are too weak to use as sources for driving higher order nonlinear interactions.

There have also become available molecular lasers operating in the spectral range between 1100 and 1800 Å (e.g., H_2, Xe, CO). When operated as travelling wave oscillators, these lasers produce powers in the range of 10^6 W, which is again too low to serve as a source for pumping high order nonlinear processes. However, when used as an amplifier for picosecond pulses generated externally in the VUV range, they hold promise for providing the needed additional energy for driving the higher order nonlinear interactions.

This section describes an approach to the generation of intense mode-locked pulses in the VUV spectral range for use as pump radiation in third and higher order nonlinear optical mixing processes. The discussion emphasizes the production of pulses of high energy, short pulse duration, and high beam quality (temporal and spatial). In addition, since the pulses are to be amplified in molecular laser amplifiers which have narrow amplifying bandwidth, typically $\Delta\lambda = 0.1$ Å, it is impossible to use only successive stages of harmonic generation to produce VUV pulses and expect them to overlap spectrally with one of the amplifer gain lines. Consequently, in combining two or more

wavelengths to produce the VUV pulses, it is necessary that at least one of sources be tunable with accuracy sufficient to insure overlap between the generated radiation and the gain distribution of the laser amplifier.

The basic technique is outlined in Figure 37. Light from a Nd laser at 1.06 μm is converted into ultraviolet radiation at either the third or fourth harmonic in each of two parallel arms. The ultraviolet radiation in each arm is used to pump a mode-locked tunable laser with an output wavelength in the range of 4800 Å. The outputs of the two tunable sources are combined as shown, and mixed in a vapor cell to give a mode-locked pulse at a frequency $\omega_3 = 2\omega_1 + \omega_2$. By using two tunable sources, we gain the ability to tune one of them, ω_1, into coincidence with a two photon resonance in the mixing vapor, enhancing the efficiency of the mixing process. By tuning ω_2 the frequency of the generated light, ω_3, can be made to coincide with the desired gain line of the VUV amplifier.

IV. B. HARMONIC GENERATION

The first step is to generate the third or fourth harmonic of the laser output in order to provide a pumping source for the tunable laser. The primary consideration is to provide maximum conversion to the pumping wavelength radiation while maintaining the spatial quality of the input beam. The choice between the third or fourth harmonic depends on the type of tunable laser to be pumped. It is shown below that a single pass parametric down converter pumped with the fourth harmonic at 2660 Å is the best tunable laser for our application. Therefore, the remainder of this section will describe the results of two successive stages of second harmonic generation.

The conversion efficiency for second harmonic generation (SHG) from a plane wave at wavelength λ_1 propagating in a crystal of length L is given by

$$\frac{P_{2\omega}}{P_{\omega}} = \eta = \tanh^2 \frac{2\pi d}{cn\lambda_1} E_{\lambda_1} L \qquad (1)$$

where d is the effective SHG coefficient and $E_{\lambda 1}$ is the electric field amplitude of the fundamental beam. Whereas Eq. (1) predicts 100% conversion for sufficiently powerful beams, this value is seldom achieved in practice. Reasons for failure to achieve complete conversion include walk-off of the two beams due to birefringence in the nonlinear crystal, variation in fundamental beam intensity due to diffraction, and lack of perfect phase matching due to beam divergence or imperfect beam quality. These effects limit the interaction length over which efficient conversion can be obtained and lower the net conversion when the effective interaction length is less than the crystal

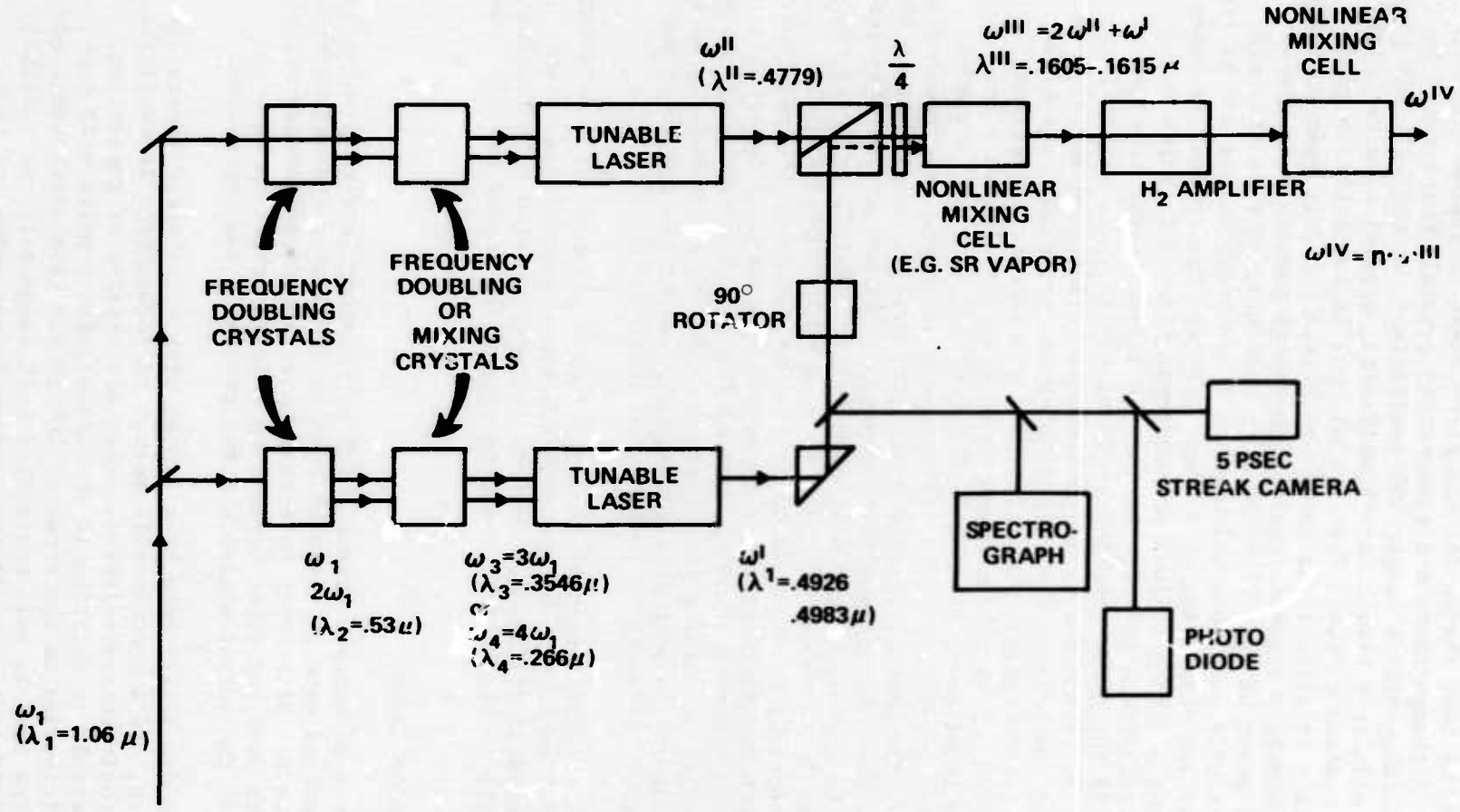

Figure 37 Schematic diagram for production and amplification of intense picosecond pulses in the VUV from fundamental radiation at 1.06μ.

length. KDP has been chosen for the first stage of second harmonic generation. Although there are alternative crystals which could be used (e.g., $LiNbO_3$ with a larger SHG coefficient, or CDA with 90° phase matching to eliminate birefringence walk-off), several considerations make KDP an optimum choice. The crystal must be available in good optical quality in sizes large enough to accept the full beam aperture of 1.25 cm, and have a sufficiently high damage threshold to withstand output power of 10^{10} W/cm^2 at this aperture. KDP is the only material currently available which meets these requirements and at the same time has low absorption at 1.06μm. Although the crystal is phase matched by angle tuning, no loss of performance is anticipated due either to birefringent walk-off or loss of intensity due to beam spreading. At the phase matching angle of 41° 12', the walk-off distance is 170 cm and the Rayleigh distance of the fundamental beam is 60 m. Consequently, for a crystal of 5 cm, the plane wave result in Eq. (1) should apply. In preliminary experiments conversion efficiencies of 56% have been observed in a KDP crystal of 5 cm length at an input power of about 3 X 10^9 W/cm^2. This is somewhat less than that predicted by Eq. (1) and the deviation may result from the fact that the beam divergence angle (125 μrad)is comparable to the width of the phase matching peak (150 μrad). The conversion efficiency is expected to improve if the beam diameter is doubled, reducing the divergence angle to about 60 μrad. For the next second harmonic generating section, temperature tuned ADP was chosen as the nonlinear element. Here 90° phase matching is possible between 5300 Å and 2660 Å at a temperature of 50°C. Use of ADP for this step is dictated primarily by its relatively low absorption as 2660 Å. In addition, it has approximately the same damage threshold as KDP and the 90° phase matching allows for extended interaction lengths.

We have observed generation of the fourth harmonic of the Nd:YAG laser in a 2.5 cm crystal of ADP with 57% conversion of the output of the KDP crystal at 5300 Å. Both of these conversion efficiencies are comparable to the highest reported values for lasers in this power regime.

IV. C. TUNABLE LASERS

Two types of tunable lasers which are compatible with pumping by picosecond pulses were considered: tunable dye lasers and parametric down converters. Both types have advantages and disadvantages and the choice of one over the other depends to a large extent on the requirements of the output signal and the available pumping source.

Tunable dye lasers have been pumped with mode-locked lasers for several years, and a considerable amount of information is available concerning their characteristics. They are capable of generating pulses comparable in duration to the laser pumping pulse with conversion efficiencies on the order of 10% in the wavelength range of interest. The beam is well controlled both temporally and spatially and can be filtered spectrally to produce pulses which are time-

bandwidth limited. However, the nature of the device requires that the tunable laser operate in the form of a cavity, in which the generated pulse is recirculated for amplification in the dye by successive pulses from the mode-locked train. This restricts the operation of the dye laser to relatively low pulse energies, since the entire pulse train cannot be amplified in existing amplifier systems.

Parametric down converters have also been studied in great detail for use in frequency conversion of Q-switched and CW lasers. Most of the work has involved resonators to provide extended build up time for the signal. Parametric conversion has also been observed on a single pass using both Q-switched[2] and mode-locked[3] pulses, with conversion effeciencies for the mode-locked pulses in excess of 1%. This technique appears to be attractive for use in the present system to generate tunable visible radiation from the fourth harmonic of the Nd:YAG laser. The proposed system is shown in Figure 38. By using temperature tuned ADP for the parametric down conversion, light can be generated across the entire visible region of the spectrum as shown by the tuning curve in Figure 39. The first crystal is used to generate a single pass parametric amplifier, providing most of the conversion. In the space between the crystals, the beam is to be cleaned up both spatially and spectrally.

The projected performance of the two types of tunable lasers are compared in Table III. The parametric down conversion scheme is seen to have two distinct advantages over the tunable dye lasers. First, since it is effectively a stimulated process in the high gain limit significant pulse shortening is predicted. This aspect is most important in the present application since the subsequent high order nonlinear processes to be driven with these signals will depend strongly on the available laser intensity. Secondly, since it is a single pass device, a larger starting energy is available off setting the expected lower conversion efficiency. These two effects combine to give pulses which are about 8 times more intense with the parametric converter then with the dye laser.

The outputs of the two tunable lasers that are to be combined as shown in Figure 37. The path lengths can be adjusted in the geometry shown so that the combined pulses overlap in time. The 90° rotator is used so that the two beams can be combined with minimum loss with a polarizing prism. The quarter wave plate circularly polarizes the two beams with opposite sense, for use in the mixing process.

The VUV radiation is generated by combining the two beams in a cell containing an appropriate nonlinear medium in a three wave mixing interaction. As a specific example, light at 1610 Å, appropriate for amplification in a H_2 laser, can be generated in Sr vapor as shown in Figure 40. Two photons with frequency ω_2 to generate a third frequency $\omega_3 = 2\omega_1 + \omega_2$. The interaction is described by the third order susceptibility

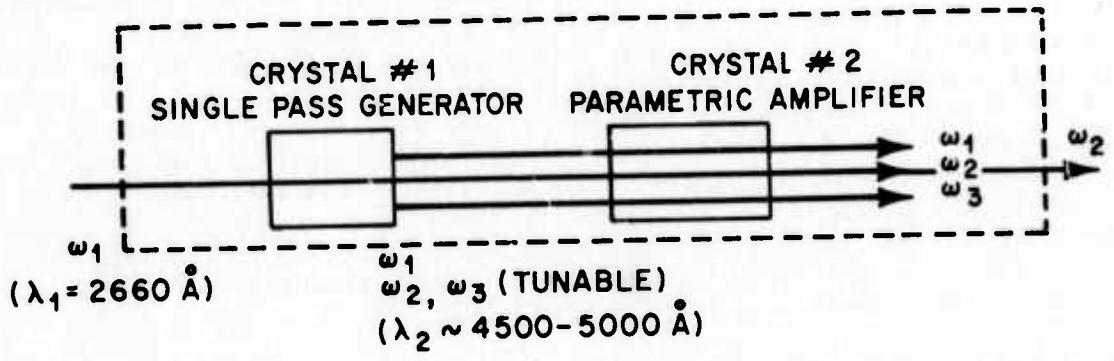

Figure 38 Schematic diagram of single pass tunable parametric generator. Crystal #1 provides high gain with relatively low spectral and spatial discrimination. Crystal #2 provides some what lower gain with high spectral and spatial discrimination.

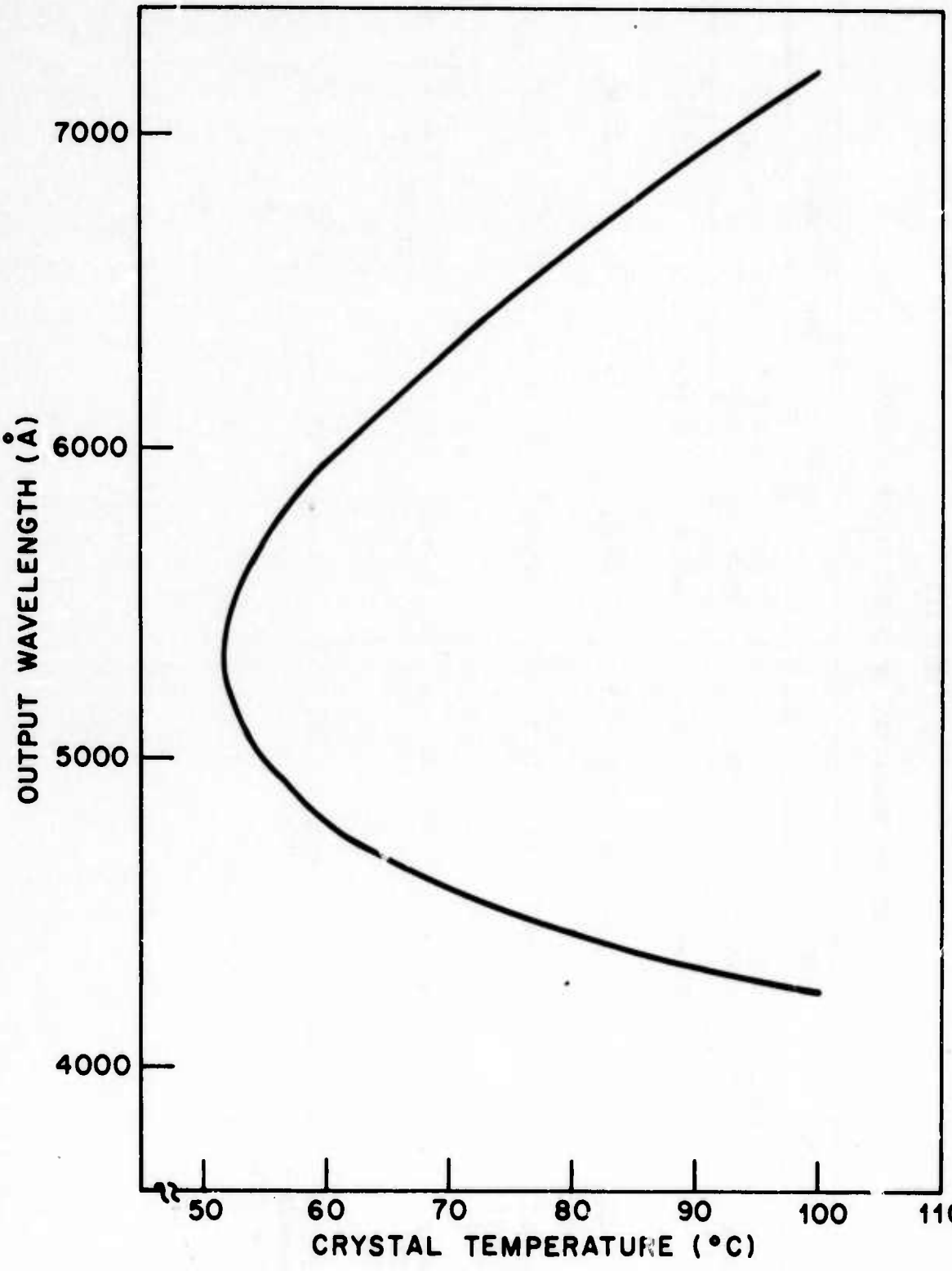

Figure 39 Temperature tuned phase matching curve for parametric down conversion in ADP for pump radiation as λ = 2660 Å.

TABLE III

DESIGN PARAMETERS OF 1600 Å TUNABLE SOURCE

TUNABLE DYE LASER					PARAMETRIC DOWN CONVERTER			
STAGE	PULSE ENERGY	PULSE DURATION	η	P(W)	PULSE ENERGY	PULSE DURATION	η	P(W)
INPUT	10 mj	25 psec		4×10^8	180 mj	30 psec		6×10^9
1st SH CRYSTAL	5 mj	25 psec	50%	2×10^8	90 mj	30 psec	50%	3×10^9
2nd HARMONIC (Mixing) CRYSTAL	0.5 mj	25 psec	5%	2×10^7	9 mj	30 psec	5%	3×10^8
TUNABLE LASER OUTPUT	0.05 mj	40 psec	0.5%	1.25×10^6	0.09 mj	10 psec (EST.)	0.05% (EST.)	9×10^6
OUTPUT OF NONLINEAR MIXING CELL	0.002 mj	40 psec	0.2% (EST.)	5×10^4	0.03 mj	10 psec	0.018% (EST.)	3×10^6

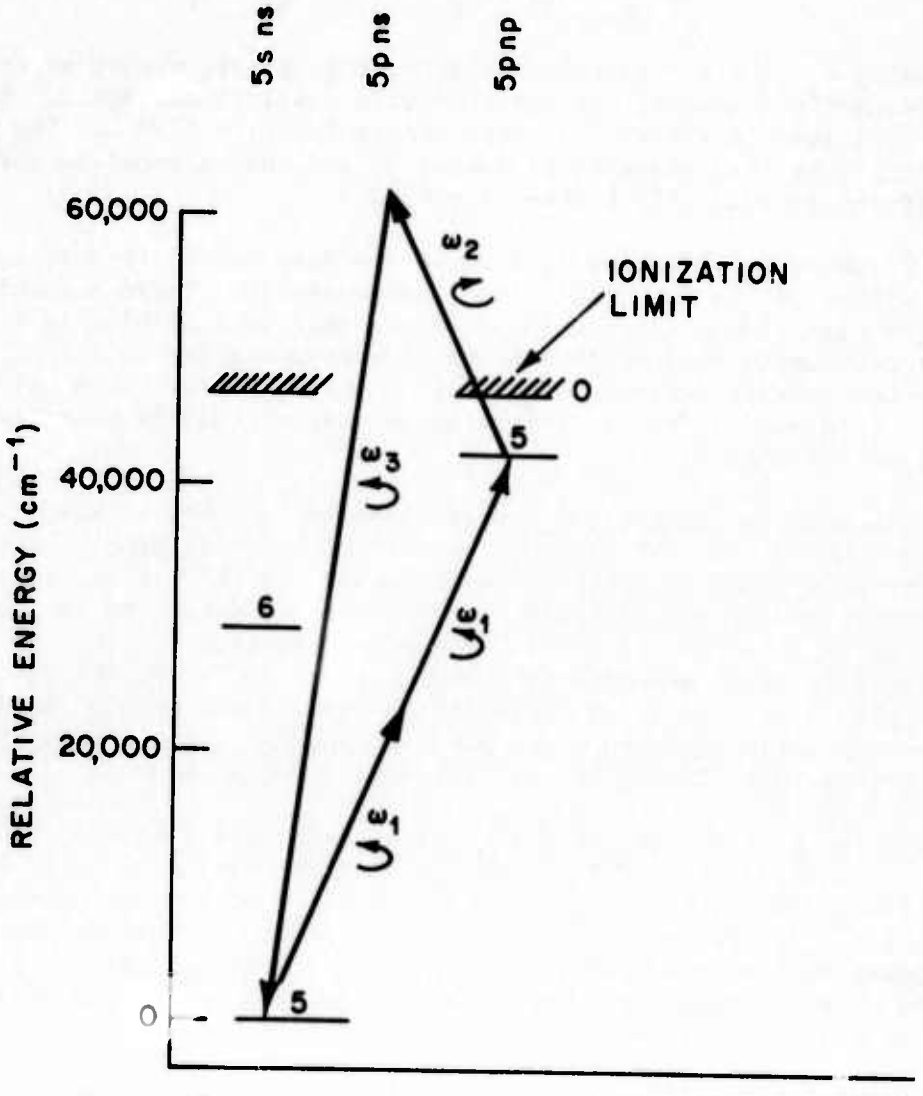

Figure 40 Partial energy level diagram of Sr showing two photon resonantly enhanced sum frequency generation as $\omega_3 = 2\omega_1 + \omega_2$. ω_3 is tuned by tuning ω_2.

$$\chi^{(3)} = \Sigma N_g \frac{\langle g|u_i(3)|o\rangle\langle o|u_j(2)|n\rangle\langle n|u_k(1)|m\rangle\langle m|u_l|g}{(\nu_{og} - \nu_3)\ (\nu_{ng} - 2\nu_1)\ (\nu_{ng} - \nu_1)} .$$

By tuning ω_1 to a two photon resonance, the optical mixing process will be resonantly enhanced, but the absorption will remain small. For the case indicated in Figure 4, this occurs for $\lambda_1 = 4779$ Å. The output wavelength is then adjusted by tuning ω_2 and can be tuned to the H_2 amplifying line at 1610 Å when $\lambda_2 = 4900$ Å.

Circular polarization is used to suppress third harmonic generation from either of the two input beams independently. Third harmonic polarization from a circularly polarized beam is forbidden in an isotropic medium because it does not conserve angular momentum. The three wave mixing process is allowed, however, if the beams are polarized in opposite senses and the generated wave is circularly polarized in the same sense as ω_1.

The process indicated has been observed by other workers[4] using pulses from tunable dye lasers. By scaling their results to the present experimental situation, an estimate for the overall conversion efficiency and generated pulse energy at 1610 Å radiation can be made and is shown in Table III. The signal is then fed into a H_2 laser for amplification. Because of the high gains involved, the picosecond pulse should be capable of depleting the stored energy and result in pulses containing between 1 and 5 mJ lasting for approximately 10 psec and corresponding to a power of between 1 and 5 X 10^8 W.

The gain line width of 0.1 Å corresponds to a frequency width of 4 cm^{-1}. This width should be capable of supporting a pulse of 6 psec duration so that the mode-locked pulse should not be lengthened in the amplifier. By tuning the parametric converters to other wavelengths and using appropriate mixing vapors, it should be possible to produce pulses at other wavelength in the VUV range that can be amplified with H_2, CO, and Xe amplifiers.

Following amplification, the pulses can be used as pumping radiation for third harmonic generation is a manner analagcus to the mixing process shown in Figure 40. Neutral He gas can be used as a nonlinear medium for generating wavelengths down to about 480 Å. For shorter wavelengths, ionized species of alkali metals (e.g., Li) can be used for successive stages of third harmonic generation or higher order odd harmonic generation directly from the amplifier output.

REFERENCES

1. S. E. Harris, Phys Rev. Lett. 31, 341 (1973).

2. J. M. Yarborough and G. A. Massey, Appl. Phys. Lett. 18, 438 (1971).

3. A. Laubereau, L. Greeter and W. Kaiser, Appl. Phys. Lett. 25, 87 (1974).

4. R. T. Hodgson, P. P. Sorokin and J. J. Wynne, Phys Rev. Lett. 32, 343 (1974).

IV. D. HYDROGEN AMPLIFIER

The essential ingredient in any nonlinear optical mixing approach to the generation of short wavelength radiation is a means to maintain high peak intensities. By definition nonlinear mixing processes are more efficient at high intensities. However, to go from the visible or near IR as in the case of 1.06μm radiation to the soft x-ray region requires a cascade of several processes each of which has associated losses. Hence, a gain medium at as short a wavelength as possible is required if significant powers are to be generated in the far VUV or soft x-ray region. The shortest wavelength laser demonstrated to date is the hydrogen laser at $\sim$ 1160 Å and $\sim$ 1600 Å. This laser was developed simultaneously by groups at IBM[1] and NRL[2]. It is a resonatorless, single pass ASE device and hence does not offer the possibility of a coherent intense source to use for nonlinear mixing processes. It is a high gain medium in the 1600 Å region, however, and as such offers potential for an amplifier of coherent radiation in this region. Other possibilities are the rare gas (Xe_2, Kr_2 etc) at similar wavelengths.

The hydrogen laser is a TW discharge ASE configuration was developed at NRL. As such, this technology offers a convenient starting point for developing a H_2 amplifier at 1600 Å. The NRL H_2 lasers has characteristics as given in Table IV. This system, as presently configured, could be used as an amplifier. Because of the high gain, the incoming pulse would saturate the system. For a 25 psec pulse the output would be on the order of 10^8 Watts/cm^2. There is reason to believe that this can be significantly improved. It was recently reported in the Russian literature[3] that a H_2 laser can be made to operate at atmospheric pressure. The Russian device was a TW discharge system 0.006 cm X 1 cm X 35 cm. It produced 0.5 nsec, 0.5 mJ pulses. Because of the higher gas pressure the stored energy density is higher. The Russian device [ℓ = 35 cm] has an extraction energy density of $\sim$ .08 J/cm^2 compared to .01 J/cm^2 for the NRL device [ℓ = 100 cm]. Operating the NRL device at 1 atm should raise the extraction energy density to $\sim$ 0.25 J/cm^2 or 10^{10} Watts/cm^2 for a 25 psec pulse. This is a power density comparable to the original signal at 1.06μm and it should make the nonlinear mixing approach to obtaining shorter wavelengths practical.

The problems that have to be overcome in the above approach are primarily twofold: 1) a 2 mm thick discharge channel under normal conditions will produce an arc discharge which will not pump the entire volume of hydrogen and 2) the hydrogen amplifier must be synchronized with the incoming 25 psec pulse. The problem of high pressure uniform

TABLE IV - CHARACTERISTICS OF THE NRL H_2 LASER

Configuration -	TW discharge device: Flat plate Blumlein circuit
Laser volume -	Discharge channel: 2 mm X 10 mm X 100 cm
Discharge voltage -	160 kV
Pressure -	30 Torr
Measured gain (1600 Å) -	200 db/m
Stored Energy -	$2\ 10^{-3}$ Joules
Pulse width -	1 nsec

discharges has received a lot of attention, primarily in connection CO_2 TEA lasers. The approaches used include e-beam controlled discharges and preionization. Due to the inherent design of the high voltage Blumlein circuit used in the NRL hydrogen laser device, it is not compatible with such things as high voltage e-beams, preionization trigger electrodes, and high voltage series-arcs for UV generation. Also, the Blumlein circuit has a nanosecond risetime and special cathodes for producing prebreakdown electron densities simply will not work. The technique that appears most promising is UV preionization of the laser medium in a manner similar to that of Javan and Levine[4] for CO_2 lasers. The concept here is to add a second gas to the lasing medium. This gas is photoionized by a UV discharge lamp in such a way that a uniform electron density is produced in the main discharge gap just prior to the arrival of the main HV pulse. This prevents arcing and ensures uniform pumping of the laser medium. This second gas must be transparent at the laser wavelength and have a penetration depth for the photoionizing radiation such that a uniform electron density is produced.

Experiments are underway to evaluate a possible photoionization scheme that will work with hydrogen at 1600 Å. The first strong absorption band in CO starts at around 1500 Å;hence it will pass 1600 Å hydrogen radiation. Two step photoionization is possible in

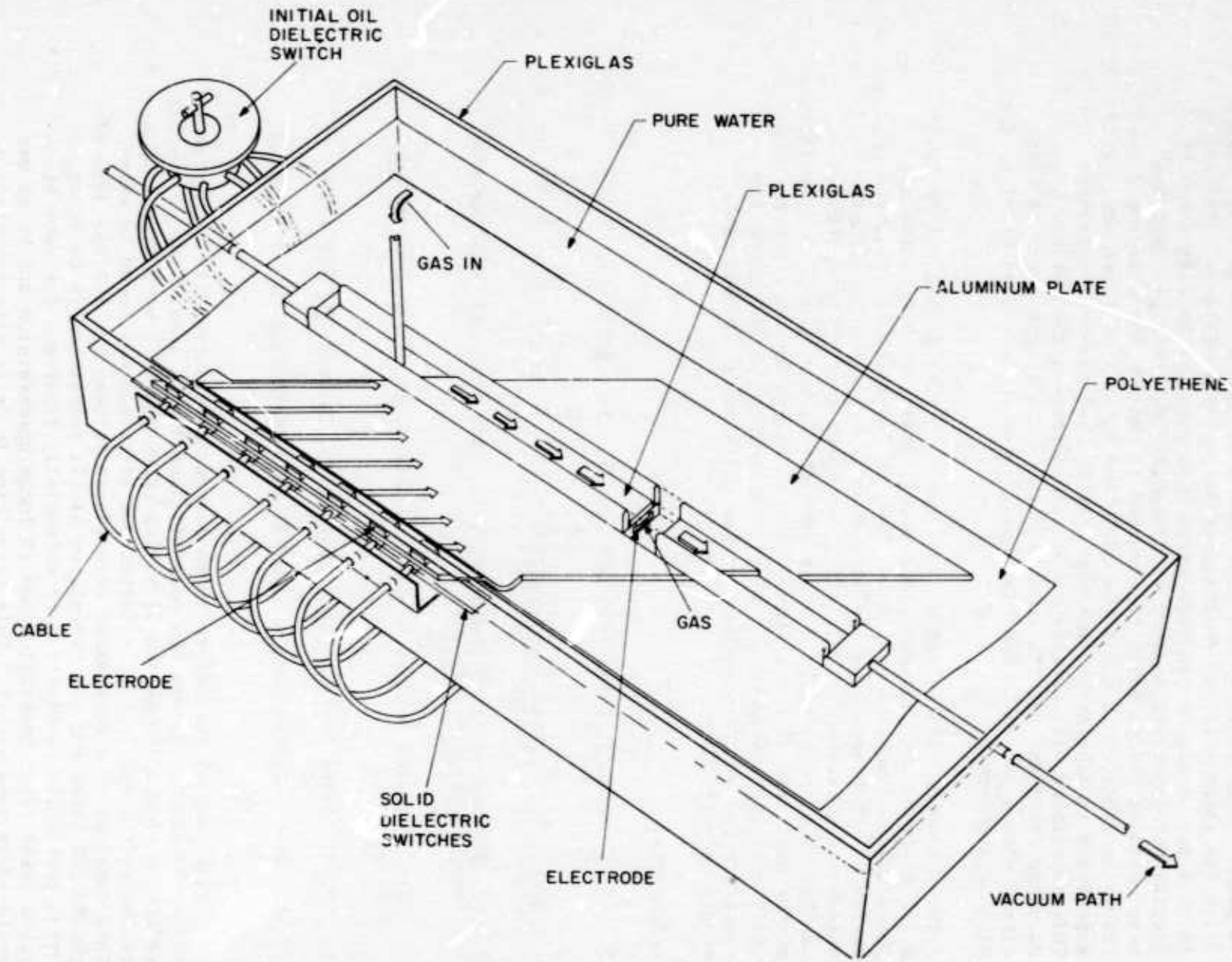

Figure 41 Schematic diagram for the TW electric discharge (Blumlein circuit) used for the NRL hydrogen laser.

CO using weakly allowed molecular states at 2000 Å, 1780 Å, and 1580 Å which lie about half way to the ionization limit of 14 eV. Radiation in this region can be produced using high pressure Xe flashlamps with special envelopes for maximum UV transmission. An experiment has been designed and is being constructed to measure the electron distribution produced in a mixture of CO and H_2 by a Xe flashlamp. This experiment is simular to that done for CO_2 and tri-n-propylamine[5]. This experiment will provide numbers to determine the optinum CO_2, H_2 concentrations. At the same time the NRL hydrogen laser is being fitted with a 100 cm Xe flashlamp positioned above and parallel to the discharge channel.

The second problem is synchronization. This problem has not received a lot of attention, however, conceptual ideas have been formulated. The Blumlein discharge device as shown in Figure 41 is triggered by a series of synchronized pulses at its outer edge. Each of these pulses was generated by triggering one spark gap. This spark gap can be laser triggered by a pulse from the 1.06μm mode-locked oscillator at the beginning of the system. Optical delays can be appropriately built into the system to ensure proper timing. Further, the laser spark gap can be overdriven to ensure a jitter of $\lesssim$1 nsec which should be sufficient.

REFERENCES

1. R. T. Hodgson, Phys. Rev. Letters 25, 494 (1970).

2. R. W. Waynant, I. D. Shipman, R. C. Elton, and A. W. Ali Appl. Phys. Letters 17, 383 (1970).

3. V. S. Antonov, I. N. Knyazev, V. S. Letokhov, and V. G. Movshev, JETP Letters 17, 545 (May 73).

4. Ali Javan and Jeffrey S. Levine, IEEE J. of Ouant. Electr. QE8 827 (1972).

5. J. S. Levine and A. Javan, Appl. Phys. Letters 24, 258 (1974).

IV. E. TWO PHOTON RESONATLY ENHANCED SELF-DEFOCUSING IN Cs VAPOR AT 1.06μm

As a part of the effort to understand nonlinear optical processes in vapors and to explore the possibilities for 1) generation of tunable radiation around 1600 Å, and 2) mixing processes that work from 1600 Å to the soft x-ray region, a fortuitous situation was found to exist. This consists of a near exact coincidence between the 1.079μm line of the Nd:YAG laser and the two photon 6s$\rightarrow$7s transition in Cs vapor. (This particular combination is potentially important for Navy blue-green laser light generation and IR image upconversion and hence was explored in some detail.) This transition in Cs is also important at 1.06μm.

It has also been shown theoretically that the nonlinear refractive index in Cs at 1.06μm should be negative, and should consist of two distinct contributions[1]. One arises from a two-photon resonance between the 6s ground and 7s metastable states, the other from intensity-dependent population at the first excited state 6p. For 1.06μm radiation both terms are negative, and at modest vapor densities they can be made comparable in magnitude to the n_2 of laser glass. Since they arise from electronic mechanisms, they respond on a subpicosecond time scale.

The self defocusing of 30 psec pulses from a mode locked Nd:YAG laser in a cell of Cs vapor of atomic density 0.5×10^{17} cm^{-3} has been observed[1]. For 0.2 mJ pulses, the beam diameter is essentially identical to that observed without Cs in the cell. With linearly polarized 8.0 mJ pulses (10^{10} W/cm^2 peak intensity), the diameter increased by a factor of about 5, in good agreement with the theoretically predicted increase of 4.4. Measurements at intermediate intensities showed that the diameter grows monotonically with input power, indicating that the change in beam size is actually due to self defocusing rather than self focusing. With circularly polarized pulses, the self defocusing is expected to be smaller, since in this case, the two-photon resonance term does not contribute. For 8 mJ, the theory predicts an increase in beam size by a factor of 2, in qualitative agreement with an observed increase of about 3.7. The discrepancy is probably due to the admixture of some linear polarization in the input beam due to the sapphire cell windows. An additional series of experiments is planned to measure these effects more accurately, and to attempt the compensation of self focusing in a glass rod.

This result is potentially of major importance to the development of high energy pulsed Nd:Glass lasers for such things as laser fusion and laser x-ray generators. The useful output power that can be generated in pulsed Nd:glass lasers is limited by self focusing due to the positive nonlinear refractive index ($n_2 \approx 1.7 \times 10^{-13}$ ESU) of the glass. It may be possible to raise this power by compensating for the self focusing; i.e., by first sending the pulse through a material with a comparable negative n_2, which would tend to defocus it. The negative nonlinear refractive indices observed previously have arisen either in restricted wavelength ranges attainable only by the use of tunable lasers, or from thermal effects too slow to be useful for compensating pulses of nanosecond or subnanosecond duration.

REFERENCE

1. R. H. Lehmberg, J. Reintjes, and R. C. Eckardt, "Two Photon Resonantly Enhanced Self-defocusing in Cs Vapor at 1.06μ", Appl. Phys. Lett. 25 (1 Oct. 1974); expanded version published in NRL Memorandum Report (in preparation).

V. TRAVELING WAVE PUMPED UV AND VUV LASERS

V. A. BACKGROUND

The Naval Research Laboratory was among the first to develop a vacuum ultraviolet laser.[1,2] In the past four years molecules have lased with wavelengths as short as 1100 Å[3,4] and a multiply charged ion has been evidenced to lase in the 1550 Å region[5]. A technological breakthrough that assisted these advances was the development of a traveling-wave transverse excitation system.

The traveling-wave principal is fundamental to short wavelength ASE laser development for two reasons: (1) it is nearly impossible to build resonators below 1050 Å since no material transmits and few materials have high reflectivity and; (2) the lifetime of the inverted medium usually allows only a single pass through the amplifying medium. Since the length of gain available is given by $L_a = c\Delta t$, where Δt is the lifetime, the inversion density, n, must be sufficient to make $\alpha L \geq 1$. This equation defines the critical length (or threshold length) for amplified spontaneous emission (ASE). Table V shows the inversion density required for reaching threshold ($L_c = L$) during the length afford by the gain lifetime and the intensity, P/A, (where the diameter $a = L_a/100$) in watts/cm^2 required to produce it.

TABLE V. MINIMUM LASER PARAMETERS WITHOUT TRAVELING-WAVE PUMPING

λ(Å)	Δτ(Sec)	Δν(Hz)	L_a(cm)	n (cm^{-3})	P/A (Pump) (watts/cm^2)
1000	10^{-9}	10^{12}	30	8.3×10^{12}	10^3
100	10^{-11}	10^{12}	3×10^{-1}	8.3×10^{15}	10^8
10	10^{-13}	10^{14}	3×10^{-3}	8.3×10^{18}	10^{13}
1	10^{-15}	10^{15}	3×10^{-5}	8.3×10^{21}	10^{18}

When traveling wave excitation is used, however, it is not possible to exceed the critical length in L_a. Since the excitation travels at the group velocity of the pulse, the length of the amplifier, in principle always can be made longer than the critical length. The longer length reduces the intensity of pumping radiation and allows the total energy to be spread over a longer time, since only a length on the order of L_a need be pumped at any one time. Table VI shows the parameters important to ASE when a fixed length of 100 cm is pumped by a traveling-wave and the critical length is set equal to

100 cm. The diameter, a, of the cylindrical gain region is set at 1 cm.

TABLE VI. LASER PARAMETERS WITH TRAVELING WAVE PUMPING (L = 100 cm)

λ(Å)	$\Delta\tau$(sec)	$\Delta\nu$(Hz)	L_a(cm)	n(cm^{-3})	P/A (Pump) (watts/cm^2)
1000	10^{-9}	10^{12}	30	2.5×10^{12}	15
100	10^{-11}	10^{13}	3×10^{-1}	2.5×10^{13}	1.5×10^{3}
10	10^{-13}	10^{14}	3×10^{-3}	2.5×10^{14}	1.5×10^{5}
1	10^{-15}	10^{15}	3×10^{-5}	2.5×10^{15}	1.5×10^{7}

Table VI gives the minimum intensity and inversion density required for ASE, since 100 % efficiency is assumed (as was done in Table V); for a practical laser the length would need to be several critical lengths for reasonable output.

V. B. TRAVELING WAVE ELECTRON BEAM EXCITATION

The development of rare gas molecular VUV lasers utilizing high pressures (eximer lasers) has been carried out primarily with high voltage electron beams. The use of high voltage electron beams for pumping the laser media is required because of the high pressures needed for eximer formation. However conventional high voltage electron beams have several difficulties. Best used in transverse pumping modes for obtaining uniform inversion densities, they are limited in length and cannot offer traveling-wave excitation. Also, because of the short gain length, a resonator is usually required. Use of a resonant cavity is not possible below 1050 Å and the intense beam generated can cause damage in the 1050-2000 Å region. To improve operation for wavelengths longer than 1050 Å and to try to achieve lasing a wavelengths shorter than 1050 Å, a new traveling-wave transverse electron beam system was conceived and built.

Based largely on the design of the original traveling-wave electric discharge system, an electron emitting diode and a high pressure gas chamber were incorporated into a flat-plate Blumlein circuit. This diode section is shown in Figure 42 and the design parameters are given in Table VII.

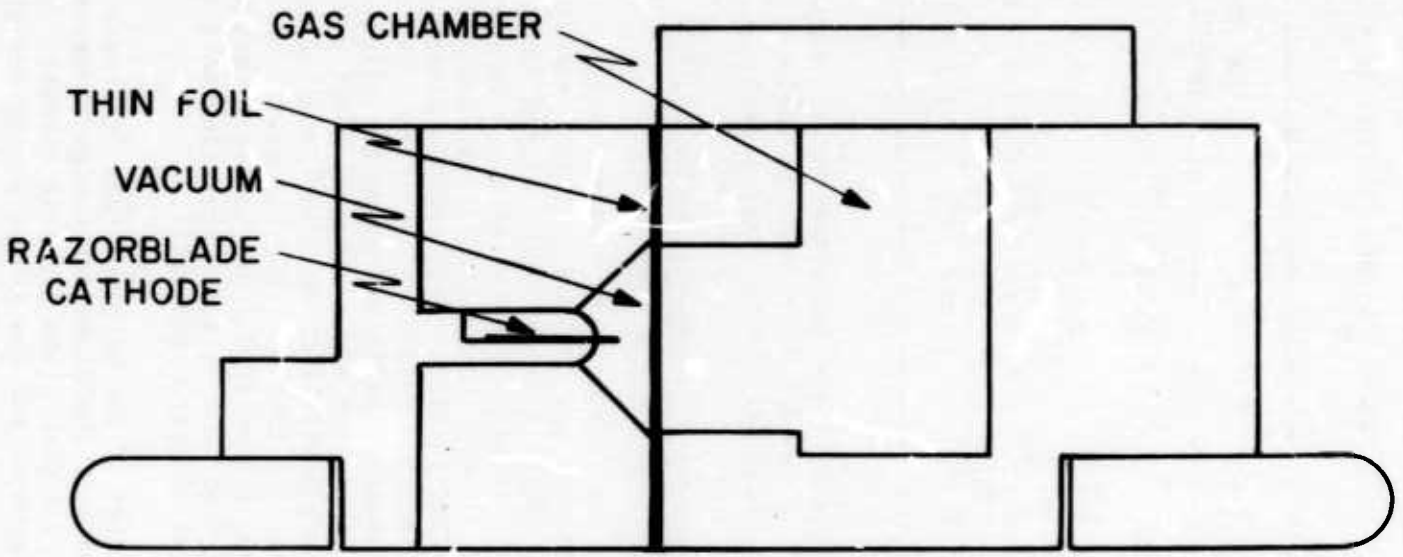

Figure 42 Cross section of traveling-wave electron beam excitation system and high pressure gas laser chamber.

TABLE VII - DESIGN PARAMETERS FOR DIODE SECTION

Inductance -	L = 0.5 nH
Capacitance -	C = 26nF, Energy Stored - 520 Joules
Voltage -	200 KV
Impedance -	0.145 Ω
Current Density -	8.5 kA/cm^2
Pressure -	1 - 10 atmospheres

The system was assembled during the fall of 1973 and became operational in December 1973. Since this configuration is a departure from conventional technology, a sizeable amount of development has been carried out in the area of foil supports, cathode materials and shapes, and diode insulation. Improvements in this system are still going on while at the same time experiments are being done investigating the emission from the system. Some of the experiments under evaluation or consideration will be discussed.

V. B. 1. RARE GAS MOLECULAR LASERS

Since the initial reports of the possibility of a xenon laser by Basov[10] and the successes with xenon in this country[6-9], the rare gas molecules have been attractive for extending laser wavelengths below 1000 Å. Projections of inversion densities of 10^{16} cm^{-3} and powers in the gigawatt range in the 600-900 Å region with high efficiency (1-10%) and with tunability are attractive. With gain linewidths of 150 cm^{-1} such devices could operate as amplifiers for tunable picosecond pulses of high directionality and enable far shorter wavelengths (200-300 Å or less) to be attained by frequency tripling. Amplifier experiments with existing VUV lasers are discussed elsewhere in this section.

Results to date with xenon and argon at pressures to 45 psia show spontaneous emission without measureable amplification in the 1700 Å and 1250 Å regions, respectively. These experiments were conducted with acceleration voltages less than 200 kV and scattering losses were high. In addition, the coupling losses in the present system between the foil anode and the optical cavity could be appreciable and it is possible that the region of maximum excitation and gain is not being

viewed. Both of these difficulties can be overcome and new methods of fabrication have been conceptualized already. The voltage will be raised by improving the coupling with the energy storage capacitor through a change in the dielectric or by employing a Marx generator. The gas chamber will be redesigned to move the foil surface to the edge of the laser axis as shown in Figure 43. This redesign will also allow an improved diode to be built.

V. B. 2. HIGH PRESSURE H_2 LASER

The possibility of a very efficient hydrogen laser has been predicted by the Russian scientists Letokhov, Knyazev, et. al.[11] This idea, which works best at pressures of 1-10 atmospheres, utilizes a transition from the $B\ ^1\Sigma_n^+$ (v=11, J=3) to $X\ ^1\Sigma_g^+$ (v=14, J=4) level of the hydrogen molecule. The lower level of this transition is just <u>above</u> the dissociation energy level of the molecule so that rapid molecular dissociation takes place, emptying the lower laser level and preventing self-termination. This is somewhat similar to the rare gas molecular systems. Efficiency as high as 13% is predicted on the ~ 1550 Å Lyman band line.

This experiment seems ideally suited to the traveling-wave electron beam system since the risetime has already proven sufficient for Lyman and Werner band lasing and since the device can operate at high pressures. Preliminary tests at 150 kV and 1-3 atmospheres pressure during the last months indicate faint spectra from the Lyman band. Optimization of the device as discussed to increase voltage, current density, and output coupling should enable gain to be detected, if it is present. Additionally, the P(4) transition in ordinary hydrogen is possible only in the 25% of the molecules which are para-hydrogen. Enrichment of the parahydrogen component can be accomplished by collecting boil-off from liquid hydrogen and would increase the chances of a successful experiment. It is hoped to do this in the near future.

V. B. 3. DISSOCIATION AND RECOMBINATION LASERS

These types of lasers are mentioned here because of their suitability to traveling-wave electron beam excitation. Ideas have already been put forward for dissociative and dissociative-ionization lasers which are initiated by electron impact with molecules:[12]

$$e + NO \rightarrow N^* + O + e \qquad (1)$$

$$e + NO \rightarrow (O^+)^* + N^* + e \qquad (2)$$

In these reactions the molecules dissociate to produce highly excited atoms and molecules. The wavelength of the transition in (1) is 1200 Å and the wavelength of the ion transition in (2) is 800 Å. Both of

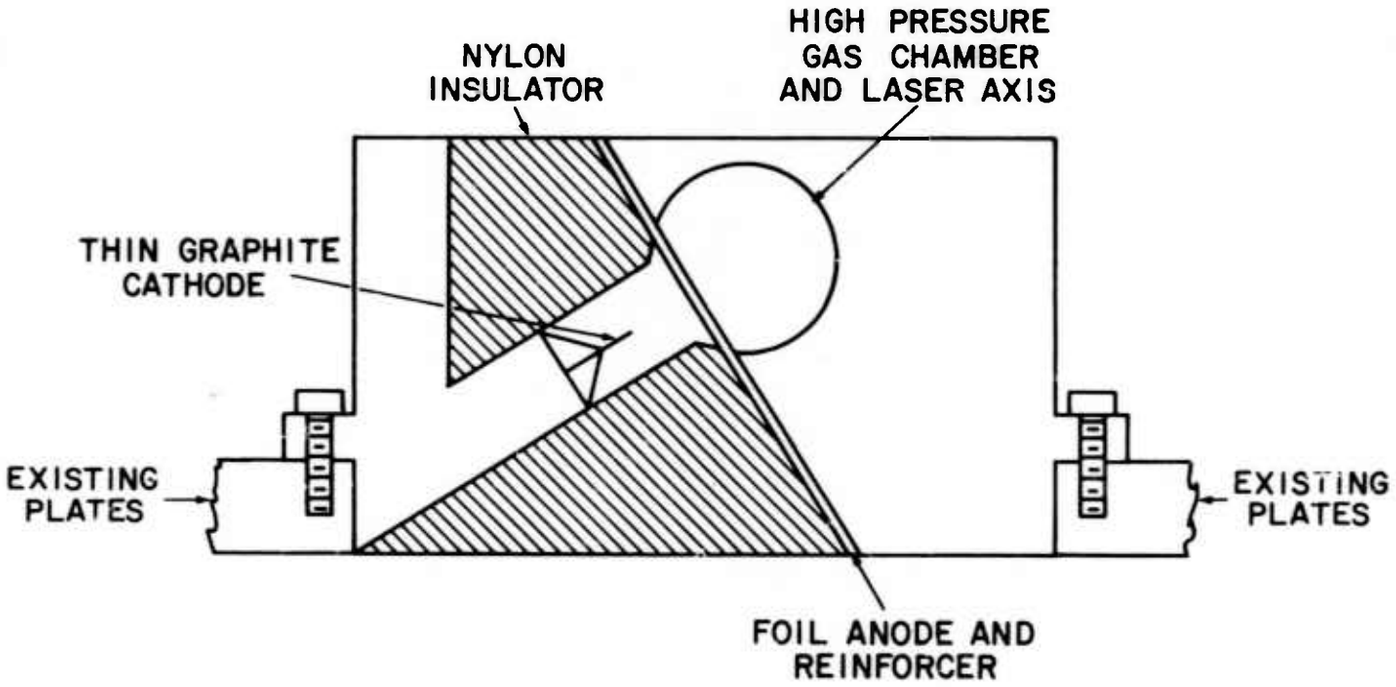

Figure 43 Conception of improved diode and gas chamber with closer coupling between electron beam and laser axis.

these reactions give rise to population inversions and, if the inversion density is large, can lead to useable gain. The traveling-wave electron beam system has fast enough risetime for exciting such reactions on a time scale suitable for lasing.

In a somewhat different manner the recombination laser works to produce excited states by combining the ions generated by electron impact with the plasma electrons[13]. This capture leads to excitation of higher states and subsequent cascading to other states producing an inverted population at some stage in the cascade process. As an example of the recombination process in helium, consider the example below after Collins et. al[13]:

$$He^{+} + e \rightarrow H_e^{*}(p) + h\nu \qquad (3)$$

$$He^{*}(p) \rightarrow He^{*}(q) + h\nu (p > q) \qquad (4)$$

Similar processes can occur in other gases. While the traveling-wave system could produce the ionization for this type of laser, the reaction rates for visible transitions may negate the traveling-wave virtues. Recombination at higher stages of ionization could lead to faster reaction rates where traveling-wave virtues could be applied and where shorter wavelength lasers would result.

Some very tentative experimental data obtained our laboratory recently perhaps falls into this category of laser. The system was filled with nearly two atmospheres of N_2 and the electron-beam was fired with voltages calculated at 180 kV on the diode. A single emission line has been observed at about 3650 Å and no other emission is seen in the 1000 - 6000 Å region. End-on and side-on photomultipliers seem to show different time signals. The side-on multiplier shows a double pulse——a broad ($\sim$ 50 ns) pulse followed by a narrower one. The end-on detector shows only a pulse comparable to the narrower one. No mirrors are used to form a resonant cavity. Tests for amplified spontaneous emission (ASE) have not yet been made, but early speculation of a recombination laser in N_2 is developing. The transition is from atomic N so that first the electron in the beam must cause dissociation of N_2 and then ionization and it is in the recombination that lasing will occur.

V. C. TRAVELING-WAVE DISCHARGE EXCITATION

The traveling-wave transverse discharge excitation of gas lasers, developed at NRL, is well known. Early versions were used by Shipman[14] to produce two megawatt peak power pulses from nitrogen. Later versions were used by Waynant, Shipman, Elton, and Ali[2] to produce megawatt pulses in the Lyman band of hydrogen and deuterium[15] at 1600 Å. Further development led to the observation of lasing in the Werner band

of hydrogen[3] at 1160 Å, to the discovery of the importance of matching excitation velocity with pulse velocity[3], to the realization of the utility of length variation for verification and quantitative measurement of gain, and to the ability to obtain very high temperatures at low pressures[5].

V. C. 1. CO VACUUM ULTRAVIOLET LASER

Because of the success of this system over non-traveling-wave, lower energy systems it seemed reasonable to investigate the CO molecule which was previously made to lase in the 1800 - 2000 Å region, but with only a few watts of peak power. In the traveling-wave excitation system the peak power from CO was found to be nearly a megawatt[16]. This may have a number of interesting implications.

V. C. 2. ION LASERS

The fast risetime of the traveling-wave discharge system (< 2.5 ns) represents a unique excitation source for ion lasers. When operated in the low pressure (milliTorr) region it can produce transient electron temperatures of at least several hundred electron volts in the time of a hundred picoseconds[17]. When produced in a traveling-wave fashion, multiply-charged excited ions can be generated and gain can exist for a brief period of time such that a pulse can travel from one end to the other and be amplified. This type of laser emission has been observed on a C^{+3} (CIV) impurity at 1550 Å and gain has been measured[5] by the length variation method to be about 5db/m. The transition involves a resonant level, suggesting excitation from a lower stage of ionization (or the ground state) directly into the excited state of the CIV ion as shown in the level diagram of Figure 44. Such transitions have been well documented in the case of the Ar II 4765 Å line. Other explanations are also possible. It is quite likely that a large number of vacuum ultraviolet laser lines can be generated in this manner.

REFERENCES

1. R. T. Hodgson, "Vacuum-Ultraviolet Laser Action Observed in the Lyman Band of Molecular Hydrogen", Phys. Rev. Lett., vol. 25, pp 494-497, 24 August 1970.

2. R. W. Waynant, J. D. Shipman, Jr., R. C. Elton, and A. W. Ali, "Vacuum Ultraviolet Laser Emission From Molecular Hydrogen", Appl. Phys. Lett., vol. 17, pp. 383-384, 1 November 1970; and "Laser Emission in the Vacuum Ultraviolet from Molecular Hydrogen", Proc. IEEE, vol. 59, pp. 679-684, April 1974.

3. R. W. Waynant, "Observations of Gain by Stimulated Emission in the Werner Band of Molecular Hydrogen", Phys. Rev. Lett., vol. 28, pp. 533-535, 28 February 1972.

4. P. T. Hodgson and R. W. Dreyfus, "Vacuum UV Laser Action in D_2 Werner Bands: 1161 - 1240 Å", Phys. Rev. Lett., vol. 28, pp. 536-539, 28 February 1972.

5. R. W. Waynant, "Vacuum Ultraviolet Laser Emission from C IV", Appl. Phys. Lett., vol. 22, pp. 419-420, 15 April 1973.

6. H. A. Koehler, L. J. Ferderber, D. L. Redhead, and P. J. Ebert, "Stimulated VUV Emission in High Pressure Xenon Excited by High Current Relativistic Electron Beams", Appl. Phys. Lett., vol. 21, pp. 198-200, 1 September 1972.

7. J. B. Gerardo and A. W. Johnson, "High Pressure Xenon Laser at 1730 Å", IEEE JQE, vol. QE-9, pp. 748-755, July 1973.

8. P. W. Hoff, J. C. Swingle, and C. K. Rhodes, "Demonstration of Temporal Coherence, Spatial Coherence, and Threshold Effects in the Molecular Xenon Laser", Opt. Comm., vol. 8, pp. 128-131, June 1973.

9. E. R. Ault, M. L. Bhaumik, W. M. Hughes, R. J. Jensen, C. P. Robinson, A. C. Kolb, and J. Shannon, "Xenon Molecular Laser in the Vacuum Ultraviolet", IEEE JQE, vol. QE-9, pp. 1031-1032, October 1973.

10. N. G. Basov, E. M. Balashov, O. V. Bogdankevitch, V. A. Danilychev, G. N. Kashnikov, N. P. Lantzov, and D. D. Khodkevitch, "Luminescence of Condensed Xe, Kr, Ar and Their Mixtures in Vacuum Region of Spectrum Under Excitation by Fast Electrons", J. Luminescence, vol. 1, 2, pp. 834-841, 1970.

11. I. N. Knyazev, V. S. Letokhov, and V. G. Movshev, "On the Collisional Four-Level H_z VUV Laser", Opt. Comm., vol. 6, pp. 424-426, December 1972.

12. A. W. Ali, "Towards Snorter Wavelength Lasers and Breaking the 1000 Å Barrier", (to be published).

13. C. B. Collins, A. J. Cunningham and B. W. Johnson, "Investigation of the Feasibility of the Electron Beam-Excited, High Pressure Recombinatior Laser", UIDP Report #A003-1, 1973.

14. J. D. Shipman, Jr., "Traveling Wave Excitation of High Power Gas Lasers, Appl. Phys. Lett., vol. 10, pp. 3-4, 1 January 1967.

15. R. W. Waynant, A. W. Ali, and P. S. Julienne, "Experimental Observations and Calculated Band Strengths for the D_2 Lyman Band Laser", J. Appl. Phys., vol. 42, pp. 3406-3408, August 1971.

16. R. W. Waynant, "Increased Power From CO Laser Lines in the Vacuum Ultraviolet", submitted for publication.

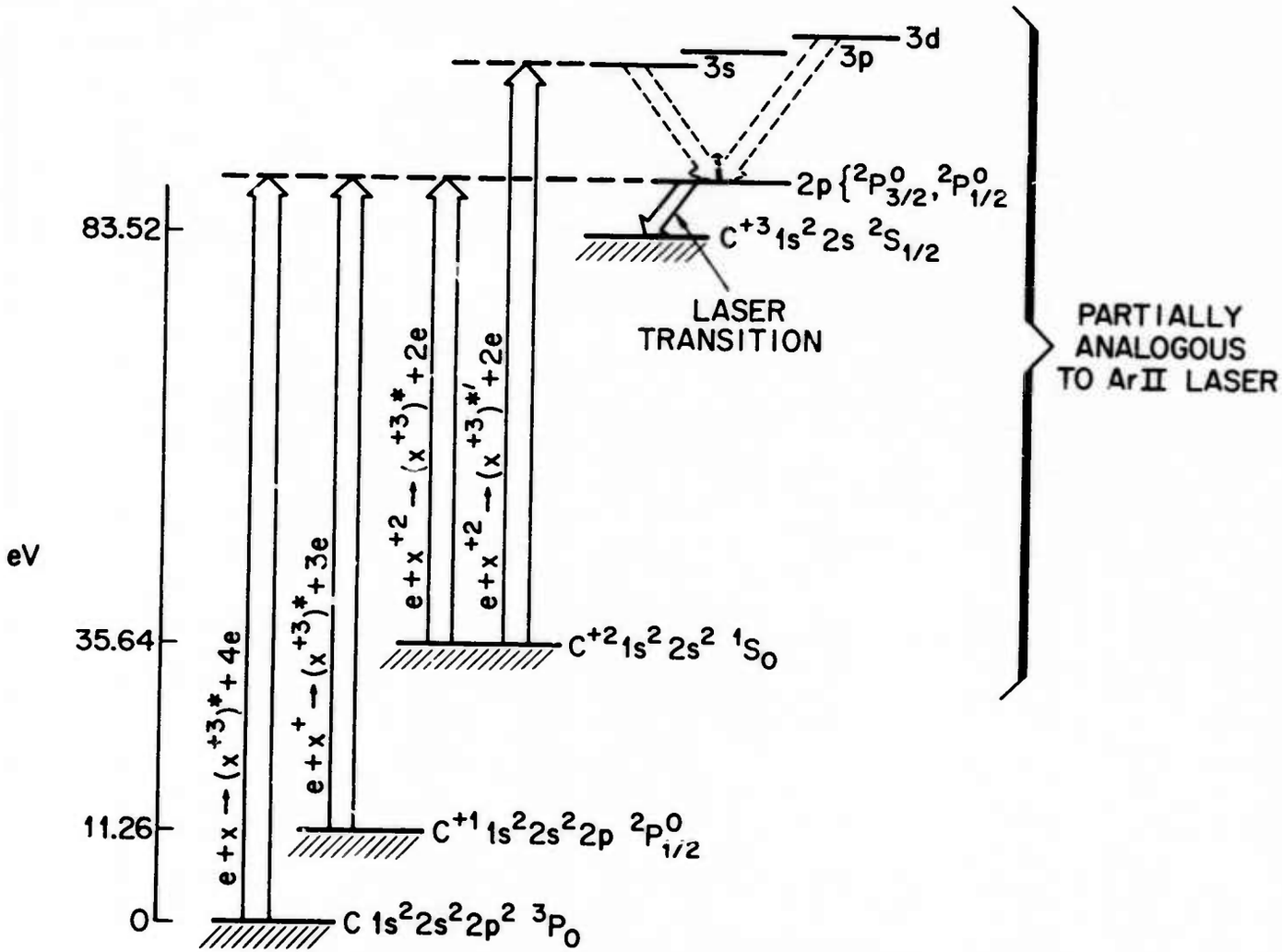

Figure 44 Some of the many possible mechanisms for exciting C^{+3} involve direct excitation from the ground state of the atom or ion to an excited level of the next or nearby ionic state. This type of transition appears to be important during rapid pulsed excitation as in the 4765 Å transition of ArII.

17. A. W. Ali, private communication.

VI. THEORY, ANALYSIS, AND NUMERICAL MODELING

VI. A. ANALYSIS OF VUV ION LASERS

Lasers in the vacuum-UV region below 1000 Å will likely be limited to superfluorescent devices of high brightness and collimation but with limited spatial coherence, due to a lack of efficient resonant cavities. However, a high degree of coherence can conceivably be achieved by progressive nonlinear mixing techniques which have been applied successfully[1] so far for reaching 887 Å. The decreasing efficiencies of such up-conversion steps can then be compensated-for with VUV amplifiers, maintaining the original coherence.

In developing such VUV amplifiers, large pumping fluxes are inevitably required because of a strong wavelength dependence of the gain coefficient. Thus, the production of a plasma laser medium will invariably occur. It is therefore natural to consider plasma ions as the amplifying vehicle, in a linear geometry such as created from a solid surface by a line-focused laser. The length of plasma that can presently be heated sufficiently to achieve multiple ionization is in the centimeter range. Thus, the question becomes whether such a medium can be used at a sufficiently high density to generate significant net gain while at the same time avoiding excessive collisional quenching of the inversion.

There exists a host of literature on near-UV and visible lasing from multiply-ionized atoms in plasmas, and it is reasonable to investigate some of these transitions for shorter wavelengths, using isoelectronic ions. An initial inspection of the collisional mechanisms involved shows that transitions between n=3 levels are most promising, based upon a general model of electron collisional $n=2 \rightarrow 3$ pumping through a non-dipole, slow-decaying transition and lasing into another n=3 level, which undergoes rapid $3 \rightarrow 2$ spontaneous dipole decay (See Figure 45). Pumping into higher quantum states (n=4, 5, etc.) could produce shorter wavelength laser emission; however these levels are much more susceptible to rapid collisional ionization and collisional mixing with dipole-decaying states. Helium-like ions with possible $3 \rightarrow 2$ lasing transitions require excessive $1s^2\text{-}1s3\ell$ pump energy. Therefore, transitions between 3p and 3s states in, for example, carbon-like ions seem to offer a reasonable initial compromise, and hold promise of achieving amplification in the 300 Å region with molybdenum ions.

A simple analysis[2-5] can be carried out assuming that $2p \rightarrow 3p$ monopole pumping by electron collisions proceeds at a rate comparable to $2p \rightarrow 3d$ dipole excitation, as evidenced by experimental and theoretical studies. For such $\Delta\ell=0$ transitions, the effective-Gaunt-factor approximate formula may be conveniently used to obtain the pumping rate[6]. The n=3 excited state densities are then estimated as

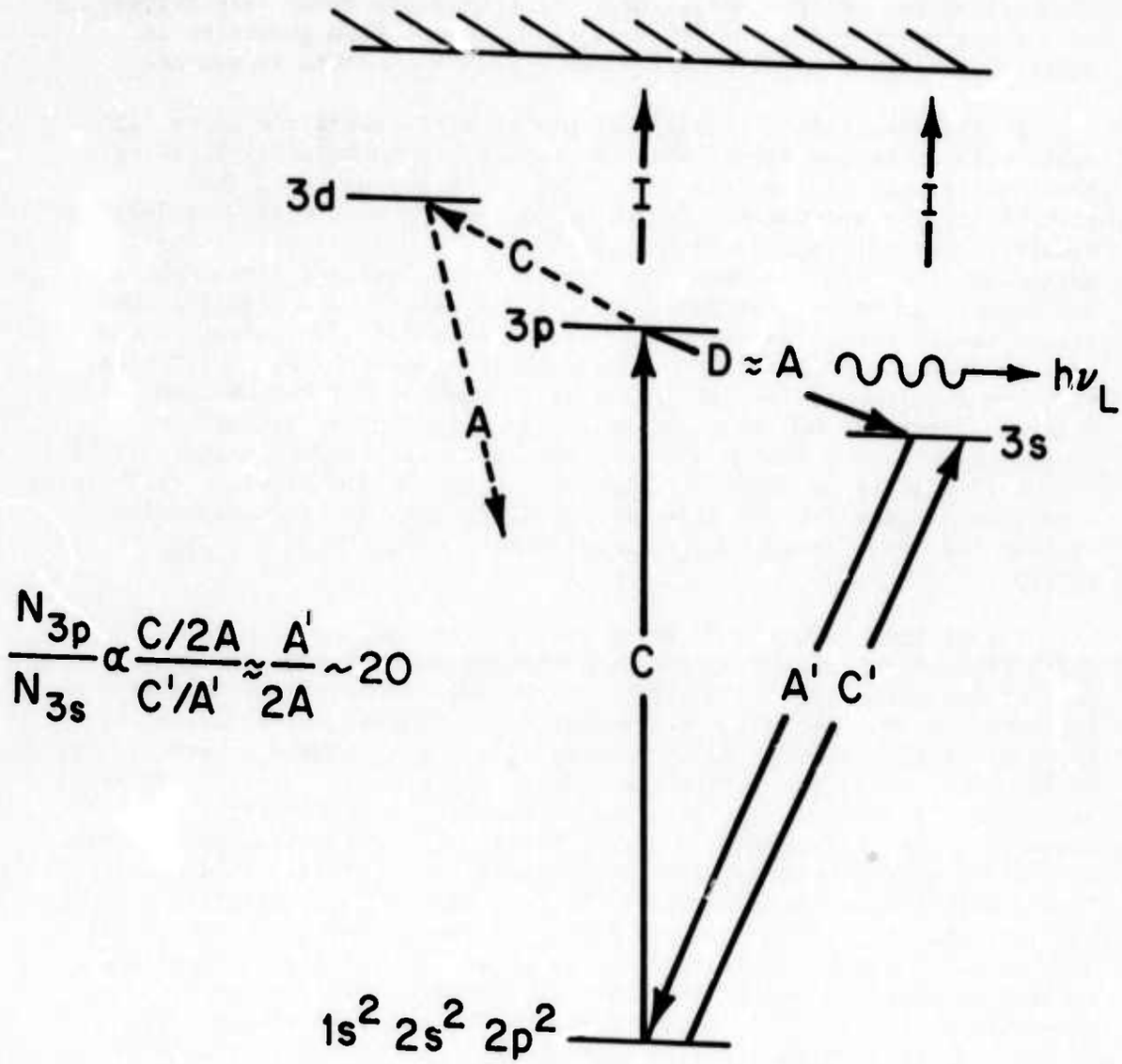

Figure 45 Schematic energy level diagram for carbon-like ion species. Collisional excitation is designated by C and C', radiative decay by A and A', ionization by I, and collisional depopulation by D. The relative 3p to 3s population densities are estimated from a modified corona model, where excitation is balanced by radiative decay and collisional deexcitation. Competing collisional depopulation to the 3d level is also indicated.

$N_3/N_2=N_eX/A_3$, where N_3 and N_2 are the excited and ground state population densities, respectively, N_e is the electron density, X is the excitation rate coefficient, and A_3 is the dominant decay mode of each n=3 state. With $A_u \ll A_\ell$, where the subscripts refer respectively to the n=3 upper and lower laser states, a population inversion is achieved, at least until some further equilibrium state is reached.

At high densities, collisional mixing will couple the upper laser state with other n=3 states which decay rapidly to n=2. By limiting this collisional mixing rate to a value of the laser transition probability for spontaneous decay, we can arrive at a maximum tolerable density. The collisional mixing rates of $\Delta\ell=0$ transitions can be estimated, assuming the rates are double the calculated linewidths[7]. Preliminary numerical estimates indicated a slight advantage for the carbon isoelectronic sequence. Therefore more detailed calculations have been completed for carbon-like ions from neon through molybdenum, with the results plotted in Figures 46 through 48 for various conditions (described below). For these elements and the estimated temperatures shown, the collisional mixing by electrons exceeds that by ions sufficiently to ignore the latter. Equating the electron collisional mixing rate N_eX_{33} for the laser transition to A_{33} (the corresponding spontaneous decay rate) gives the maximum electron density $(N_e)_{max}$ plotted.

The minimum length over which gain factors of $\alpha L=1$ (threshold) and 5 [in the relation $I/I_o=\exp(\alpha L)$] are achieved at the maximum permitted density are calculated from the gain formula[8] for Doppler broadened lines. The results are plotted in Figures 46-48 for the cases where the electron and ion temperatures are assumed, respectively, to be equal, to differ by a factor-of-10 (preferential electron heating) and for a fixed 100 eV electron temperature (also preferential heating). The preferential electron heating is expected to be achieved by rapid electron heating with, for example, an auxiliary axial laser beam and in a time period shorter than the electron-ion energy equipartition time. The results for equal temperatures are consistent with proven z-pinch ion lasers[9] operating in the visible and near-UV regions in cavities and at densities of approximately 10^{15} cm^{-3}. More encouraging for the vacuum-UV region are the high electron temperature results which indicate that lengths on the order of a centimeter are feasible for achieving gains greater than threshold.

The pump power density (required to overcome radiative decay) in the auxiliary laser beam is estimated for $\alpha L=5$ and $T_e=10\ T_i$ to be $\sim 2 \times 10^{12}$ W/cm^2 for all elements considered. This is encouraging when compared to state-of-the-art picosecond lasers that produce 10^{14} W/cm^2, even if a $\sim 1\%$ total pumping efficiency is assumed.

The laser action will be self-terminating in an equilibrium relaxation time to be determined by a detailed numerical analysis. In any case, it is not expected to be shorter than $\tau_u=A_{33}^{-1}/2$, the upper

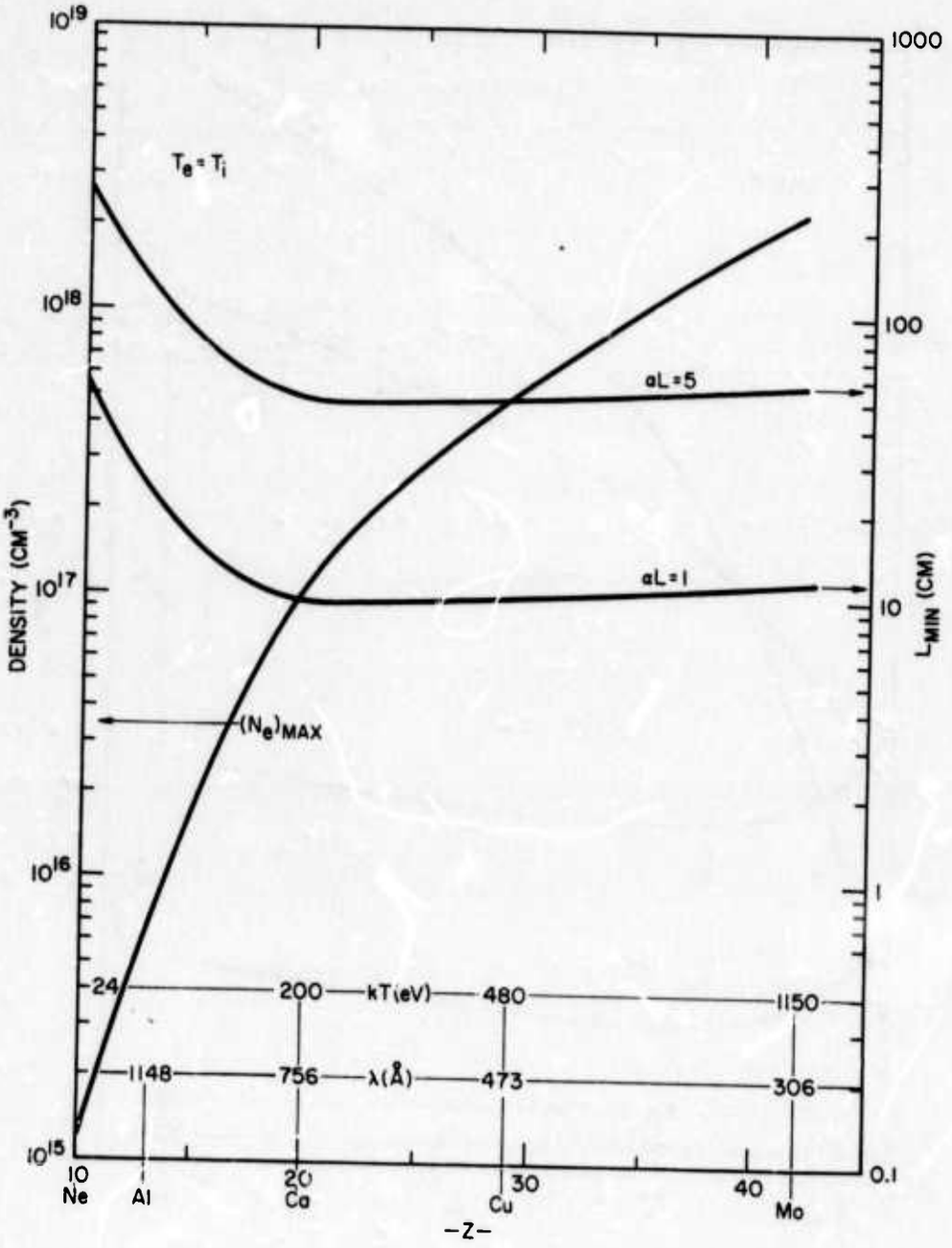

Figure 46 Minimum length L_{min} for amplification with gain exp (αL) versus atomic number Z, wavelength λ, and temperature, where the electron (kT_e) and ion (kT_i) temperatures are assumed equal. Maximum electrondensity $(N_e)_{max}$ is also shown.

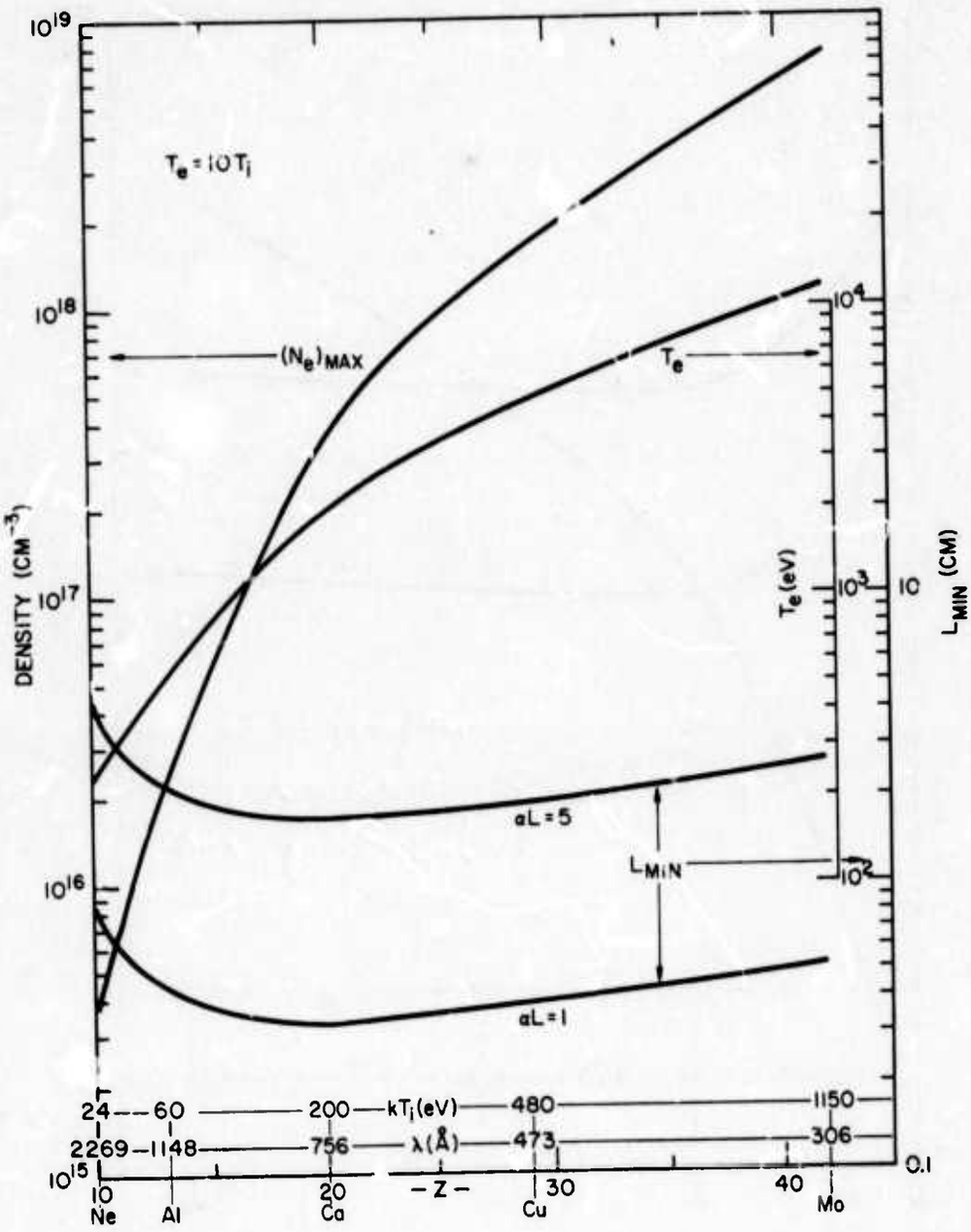

Figure 47 Minimum length L_{min} for amplification with gain exp (αL) versus atomic number Z, wavelength λ, and ion kinetic temperature kT_i. The electron kinetic temperature kT_e is assumed equal to 10 kT_i and is plotted. Maximum electron density $(N_e)_{max}$ is also shown.

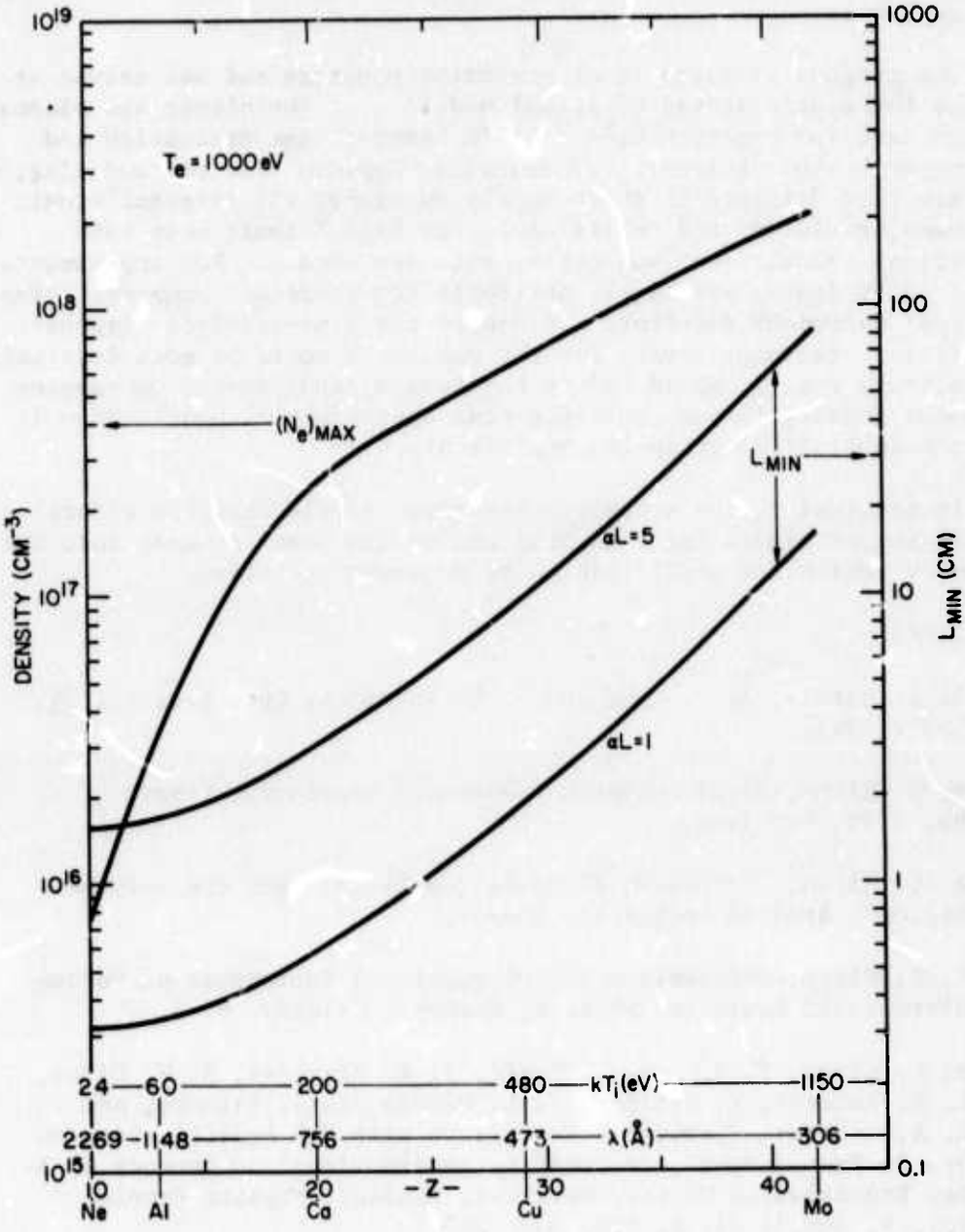

Figure 48 Minimum length L_{min} for amplification with gain exp (αL) versus atomic number Z, wavelength λ, and ion kinetic temperature kT_i. The electron kinetic temperature kT_e is assumed constant at 1000 eV. Maximum electron density $(N_e)_{max}$ is also shown.

laser state lifetime, which is sufficiently long[4] for present 10-25 ps pumping lasers.

The present analysis is of preliminary nature and has served as impetus for sophisticated numerical modeling of the atomic and plasma physics, and for experiments[5,10,11] in laser-plasma production and heating with short pulses (both described herein). For the modeling, it is clear that data are in short supply on almost all relevant atomic processes, radiative and collisional, for high-Z ions; here both theoretical calculations and experiments are needed. For experiments, higher power lasers are always desirable for increased pumping. Also, fast (ps) vacuum-UV detectors are needed for time-resolved diagnostics. An efficient resonant cavity for the vacuum-UV would be most desirable in the sense that it would reduce the severe requirements on pumping and media density through multiple-pass operation, although again it is not essential for achieving amplification.

In conclusion, the presently described simple analysis offers encouraging prospects for extending proven ion laser schemes into the vacuum-UV region for amplification of coherent radiation.

REFERENCES

1. S. E. Harris, A. H. Kung and J. F. Young, J. Opt. Soc. Am. 64, 556 (1974).

2. R. C. Elton, Naval Research Laboratory Memorandum Report No. 2799, May 1974.

3. R. C. Elton, "Extension of 3p-3s Ion Lasers Into the Vacuum-UV Region", Applied Optics (in press).

4. R. C. Elton, Proceedings IV International Conference on Vacuum Ultraviolet Radiation Physics, Hamburg, Germany, p. 6.

5. R. C. Elton, T. N. Lee, J. Davis, J. F. Reintjes, R. H. Dixon, R. C. Eckardt, K. Whitney, J. L. DeRosa, L. J. Palumbo, and R. A. Andrews, "Towards X-Ray Lasers with VUV Amplification on 3p→3s Transitions", Proceedings International Conference on X-Ray Processes in Matter, Helsinki, Finland, Physica Fennica Vol. 9, Suppl. S1, p. 400, July 1974.

6. R. C. Elton, "Atomic Processes", (in) Methods of Experimental Physics - Plasma Physics, Vol. 9A, eds. H. R. Griem and R. H. Lovberg, (Academic Press, New York, 1970).

7. H. R. Griem, "Broadening of Spectral Lines by Charged Particles in Plasmas", (Academic Press, New York, 1974).

8. R. C. Elton, R. W. Waynant, R. A. Andrews, and M. H. Reilly, "X-Ray and Vacuum-UV Lasers: Current Status and Prognosis",

NRL Report 7412, May 2, 1972.

9. Y.Hashino, Y. Katsuyama and K. Fukuda, Japan J. Appl. Phys. 11, 907 (1972); 12, 470 (1973).

10. T. N. Lee, J. Davis, J. F. Reintjes, R. H. Dixon, R. C. Eckardt, K. Whitney, J. L. DeRosa, R. A. Andrews, and R. C. Elton, Bull. Am. Phys. Soc. 19, 558 (1974).

11. T. N. Lee, J. Davis, J. F. Reintjes, R. H. Dixon, R. C. Eckardt, K. Whitney, J. L. DeRosa, R. A. Andrews, and R. C. Elton, "Towards VUV-Lasing in Plasmas Produced by a 25 ps Laser", Proceedings IEEE VIII International Conference Quantum Electronics, San Francisco, June 1974.

VI. B. NUMERICAL MODELING OF 3p→3s LASING SCHEME

VI. B. 1. INTRODUCTION

A cooperative effort has been established between the Optical Sciences and Plasma Physics Divisions for extending our continuing analysis of feasible x-ray laser schemes to encompass the numerical plasma/atomic models already in existence at NRL. The chief computer code used in this cooperative effort is a "Hot Spot" model[1] which solves rate equations for the atomic levels of interest on the assumption that the plasma is pumped by a sub-nanosecond laser pulse. This code was developed and thoroughly tested by the Plasma Physics Division under DNA sponsorship as part of the Laser-Matter Interaction (LMI) Program and has obtained excellent agreement with experiment when used to model K-line x-ray generation from laser produced plasmas.[2] This continues to be part of the LMI program and the work done with it is reported through that program. However, since the x-ray laser problem is so closely related to laser x-ray generation, an effort in this program has been devoted to attempting to use this code to evaluate possible x-ray laser schemes.

The Hot Spot code is used to provide guidance and rationale in choosing potential laser schemes to try experimentally with the short pulse laser system and to provide guidance in the choice of initial conditions. This model is particularly valid in the ultrashort pulse regime. It is a relatively simple code which uses relatively small amounts of computer time and can serve as a test bed for more elaborate codes by weeding out unpromising schemes. Modifications are inexpensive and quick, requiring mainly the writing of a short subroutine to supply atomic data for a particular scheme to the main code. The use of the code is approached from the philosophy of starting with a simple atomic level scheme and progressively adding more levels and more physics to ascertain the effect of the greater complexity actually encountered in the real world.

The more immediate goals sought through the use of the Hot Spot code are the demonstration of amplified spontaneous emission in laser heated plasmas of oxygen and neon by a parameter study of a 3p - 3s lasing scheme discussed in the preceding section and to extend this scheme isoelectronically into the vacuum UV region by studying more highly stripped ions. Such lasing schemes can be used as stand-alone ASE sources or as amplifiers for coherent VUV radiation produced by frequency up-conversion.

Although this approach uses a fairly simple code, it does provide the needed time-dependent numerical calculations to study the time evolution of population densities of the atomic levels involved which would be almost impossible to do analytically. The numerical solution can determine whether a steady state or a pulsed inversion exists.

VI. B. 2. THE MODEL

The Hot Spot code was originally designed to provide first-order comparisons of the capability of different Z plasmas to convert laser energy to K-line x-rays. The dynamic variables of this code are the ion population densities (the electron density depends on these through charge neutrality) and the electron and ion temperatures; the spontaneously generated magnetic field and the fluid velocity are assumed to remain zero. The validity of the model rests on the assumption that, when a cold plasma absorbs laser radiation in less than a nanosecond at intensity levels between 10^{11} and 10^{16} W/cm^2, only a weak, at first neglectable, magnetohydrodynamic plasma motion will be generated over 1 to 2 ns time intervals.

The atomic processes considered in solving the rate equations in this model are radiative decay, collisional excitation and deexcitation, collisional (3-body) recombination and ionization, and radiative recombination. The energy flow, as diagrammed in Figure 49, is from the laser photon energy into the electrons by inverse bremsstrahlung. The energy is then coupled into the ions by collisions or is carried away by conduction from the small heated volume ΔV (the "hot spot") to the surrounding cooler plasma. Further energy is lost by line and continuum radiation from the excited ions; radiation transport is neglected (the plasma is assumed to be optically thin). Details of the model including equations used to solve for rates of particular atomic processes appear in references 1 and 2.

The input parameters are the initial T_e and T_i, the densities of each relevant ion species, and atomic data on the energy levels to be considered for each ionization stage. Any of the dynamic variables including the populations of the excited and ground levels can be calculated as a function of time. Of particular interest in the study of lasing transitions is the gain coefficient α:

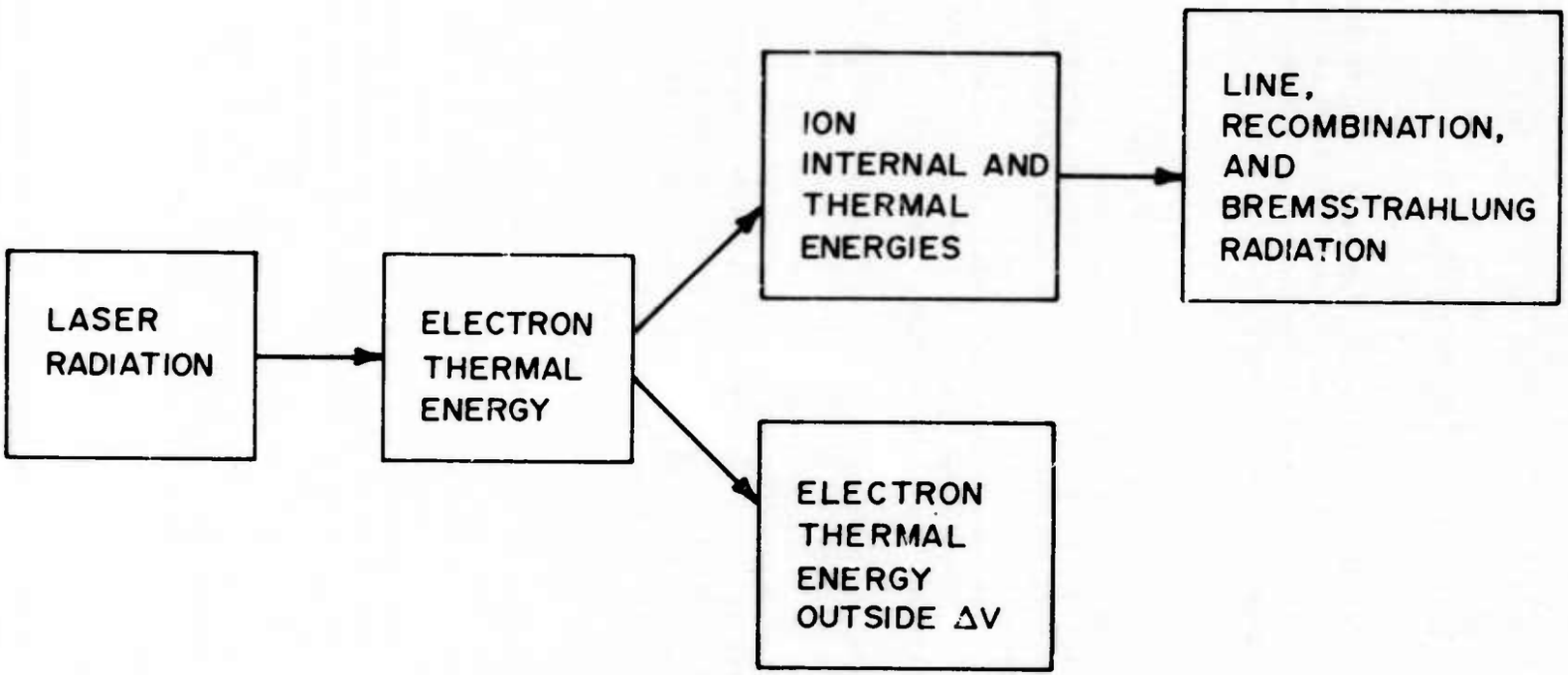

Figure 49 Hot-Spot model energy flow diagram.

$$\alpha = \frac{\lambda^2}{8\pi\Delta\nu} \; A_{u\ell} \left[N_u - \frac{g_u}{g_\ell} N_\ell \right] \qquad (1)$$

where λ is the wavelength, $\Delta\nu$ is the Doppler width, $A_{u\ell}$ is the spontaneous emission probability from the upper state u to the lower state ℓ, N_u and N_ℓ are the upper and lower state population densities, and g_u and g_ℓ are their statistical weights.

VI. B. 3. THE 3p - 3s LASING SCHEME

The initial use of the Hot Spot code was the simulation of a 3p - 3s lasing scheme as discussed by Elton.[3] Based on Elton's analytical estimates and on the existence of near UV ion data, it was decided to try this 3p -3s scheme numerically for the oxygen III ion in order to test the code on a species which has been proven to lase. If the code proves successful, this scheme will be further modeled for more highly-stripped ions with four to six electrons to study the possibility of lasing at shorter wavelengths.

A diagram showing the important energy levels for O III is shown in Figure 50. The mechanism for producing a population inversion is as follows. Both the upper laser level ($1s^2\ 2s^2\ 2p\ 3p\ ^3D$) and the lower laser level ($1s^2\ 2s^2\ 2p\ 3s\ ^3P^o$) are populated by electron collisional excitation from the $2p^2\ ^3P$ ground state of O III at comparable rates. However, the upper level is metastable whereas the lower level rapidly decays to the ground state by dipole emission, thus creating an inversion. The 3d ^3D level shown in Figure 50 is the level most expected to perturb the basic three-level lasing system; the effect of other levels is studied by including and removing them from the computations.

The main mechanism for destroying the inversion is by collisional mixing between the upper and lower laser levels; thus an upper limit of density is incurred as discussed in detail in reference 3 and above. This results in a limit on the population inversion obtained, thus limiting the gain obtainable in a plasma of reasonable length (say about 1 cm). However it is possible to compensate for this density induced gain limit by narrowing the Doppler width [see Eq. (1)] and increasing T_e to the point where the hotter electrons become relatively more effective in pumping the upper laser level from the ground state than in collisionally mixing the 3p and 3s levels. A small Doppler width implies a low ion temperature, thus a large ratio of T_e to T_i, which is not uncommon in transient laser produced plasmas is desired.

VI. B. 4. RESULTS

Based on the analytical estimates for 3p - 3s lasing, the pertinent atomic data were gathered for the O III levels discussed above, as well as for the ground terms of all stages of ionization of oxygen. These

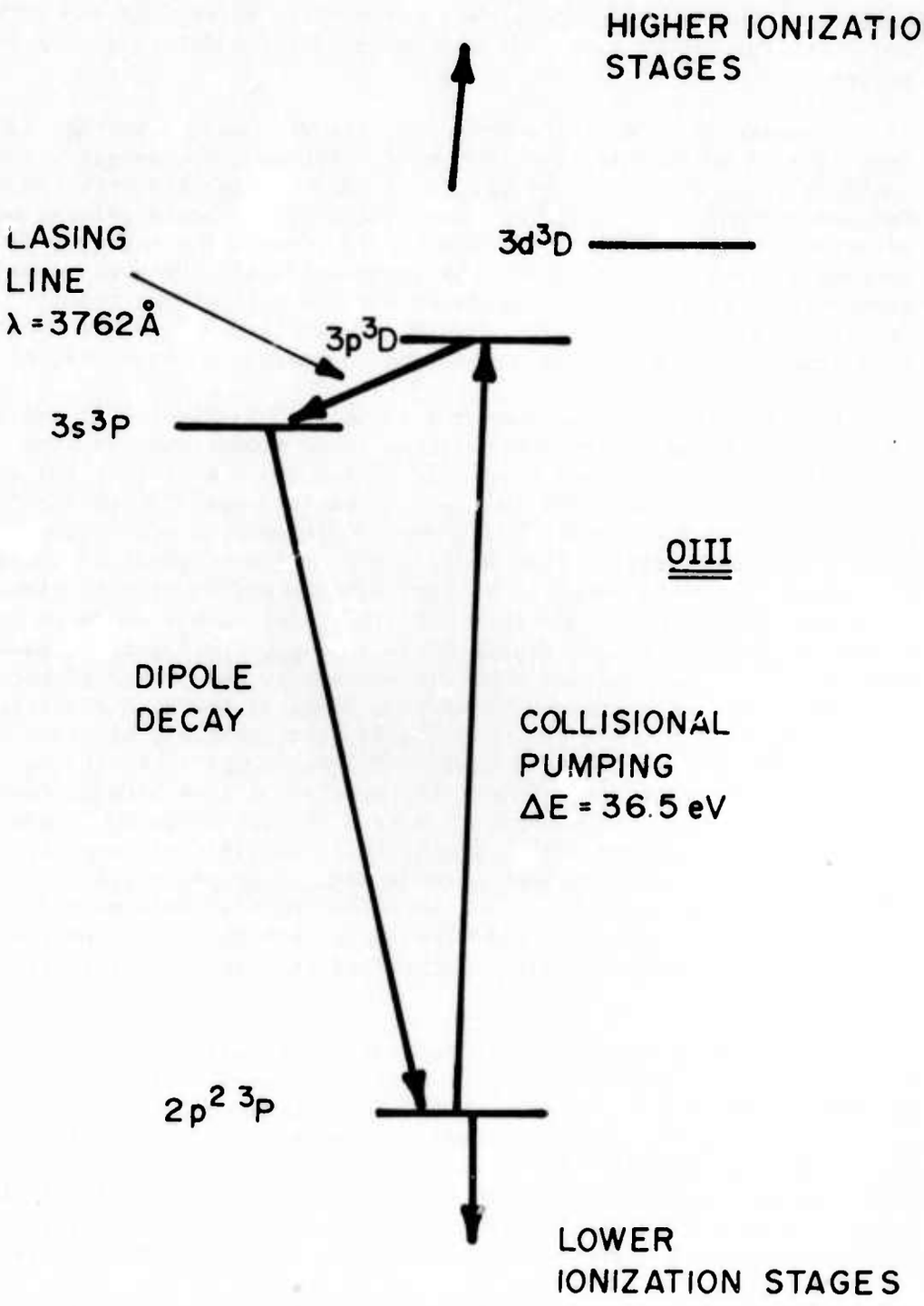

Figure 50 Oxygen III energy level scheme.

data were incorporated into a rate calculation subroutine and further modifications of the main code were made to accomodate the oxygen system.

A series of runs of the Hot Spot code was made at initial ion densities of 10^{13}, 10^{15}, and 10^{17} cm^{-3}. For each ion density, the incident laser intensity was varied to produce peak electron temperatures between 2 X 10^5 and 9 X 10^5°K. The radius of the heated plasma was adjusted for each value of ion density to prevent the energy loss by conduction from dominating, and the integration time step was chosen proportional to $1/N_i$ since the rates for the collisional atomic processes vary as N_e ($\propto N_i$). The rates used for collisional excitation were computed using the distorced wave approximation by Davis, et al.[4]

Some results of these runs are summarized in Figures 51 and 52. In Figure 51 plots of ion and electron temperatures and the gain coefficient (Eq. 1) for the 3p - 3s transition (see Figure 50) are shown for the run where the initial ion density was 10^{15} cm^{-3} and the peak T_e reached 9 X 10^5°K. For those conditions the model computes a gain coefficient greater than unity for a period of about 50 ns, thus indicating the achievement of a population inversion of sufficient magnitude to produce single-pass amplified spontaneous emission in a plasma of length $\sim$ 1 cm. Figure 52 is analogous to Figure 51 except that $N_i = 10^{17}$ and the time scale is reduced by two orders of magnitude to account for the faster equilibration times at the higher electron and ion densities. Here the gain coefficient peaks out at about 200 cm^{-1} but for a very short time ($\sim$ 0.5 ns) compared to the $N_i = 10^{15}$ case. At these higher densities, the population inversion is destroyed by electron collisional deexcitation from the 3p to the 3s levels (For T_e between 10^5 and 10^6°K, the 3p to 3s collisional deexcitation rate is equal to the spontaneous decay rate, A(3p-3s) = 1.07 X 10^8 sec^{-1}, for N_e equal to a few times 10^{14} cm^{-3}). Runs made for $N_i = 10^{13}$ cm^{-3} showed gain coefficients of less than 0.05 because of the low excited state population densities in this type of rarefied plasma.

In the future it is planned to modify and update the code to better suit our needs for studying short wavelength lasing. The effect of adding more atomic levels to the O III scheme and the effects of small changes in the rates of atomic processes populating these levels will be studied. It is intended to modify the code to output a more detailed description of the time-dependent populations and the rates of populations of the various atomic levels and to pinpoint which processes are most important in creating or destroying the inversion.

All atomic processes believed to be significant are included in the rate equations solved by the model. Better estimates for these rates and for cross sections are continually being persued and the code is constantly updated to include the best estimates available. Some specific physical processes to be incorporated into a more advanced

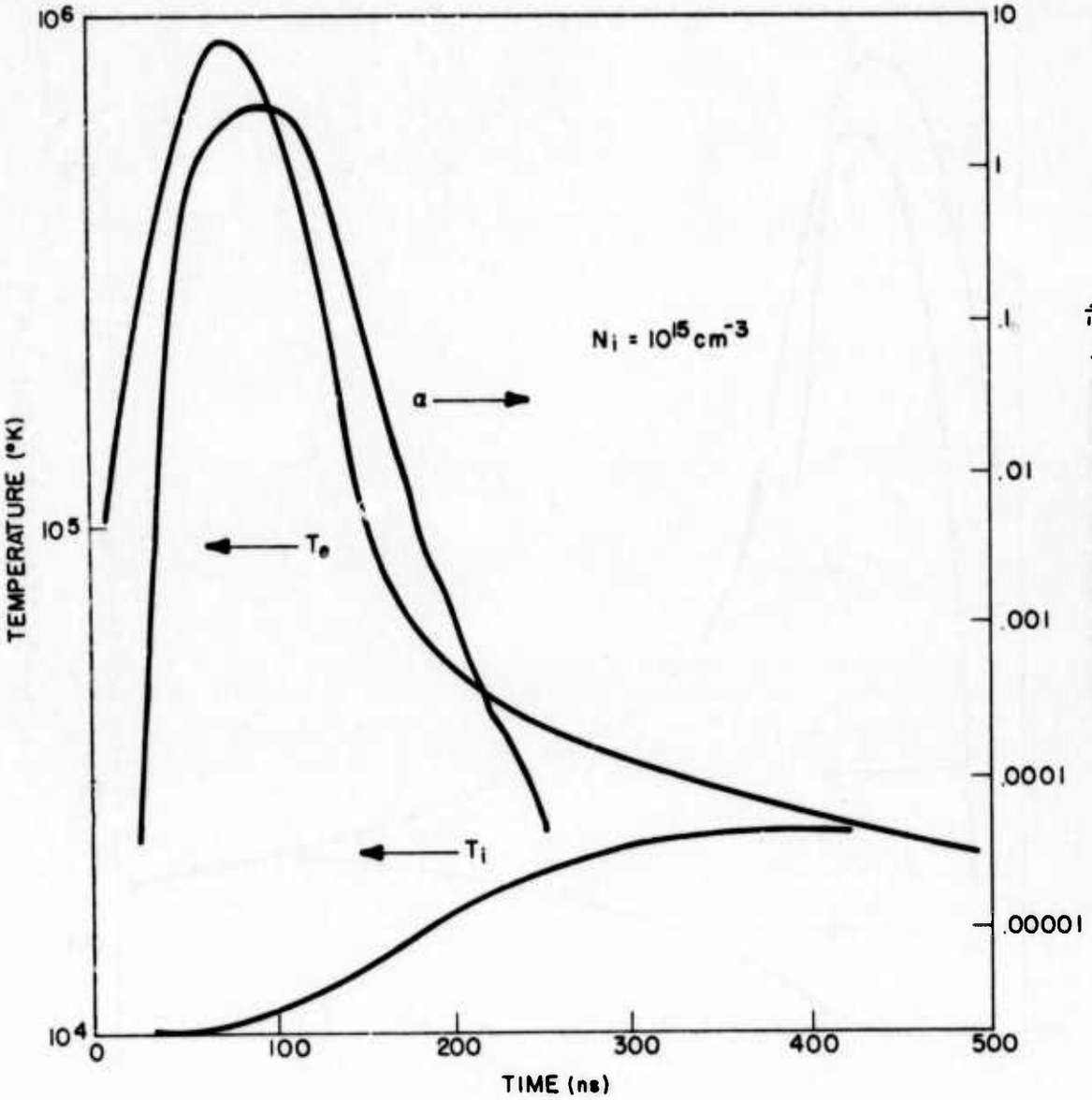

Figure 51 Gain coefficient and electron and ion temperatures for Hot-Spot run with initial ion density of 10^{15} cm^{-3}.

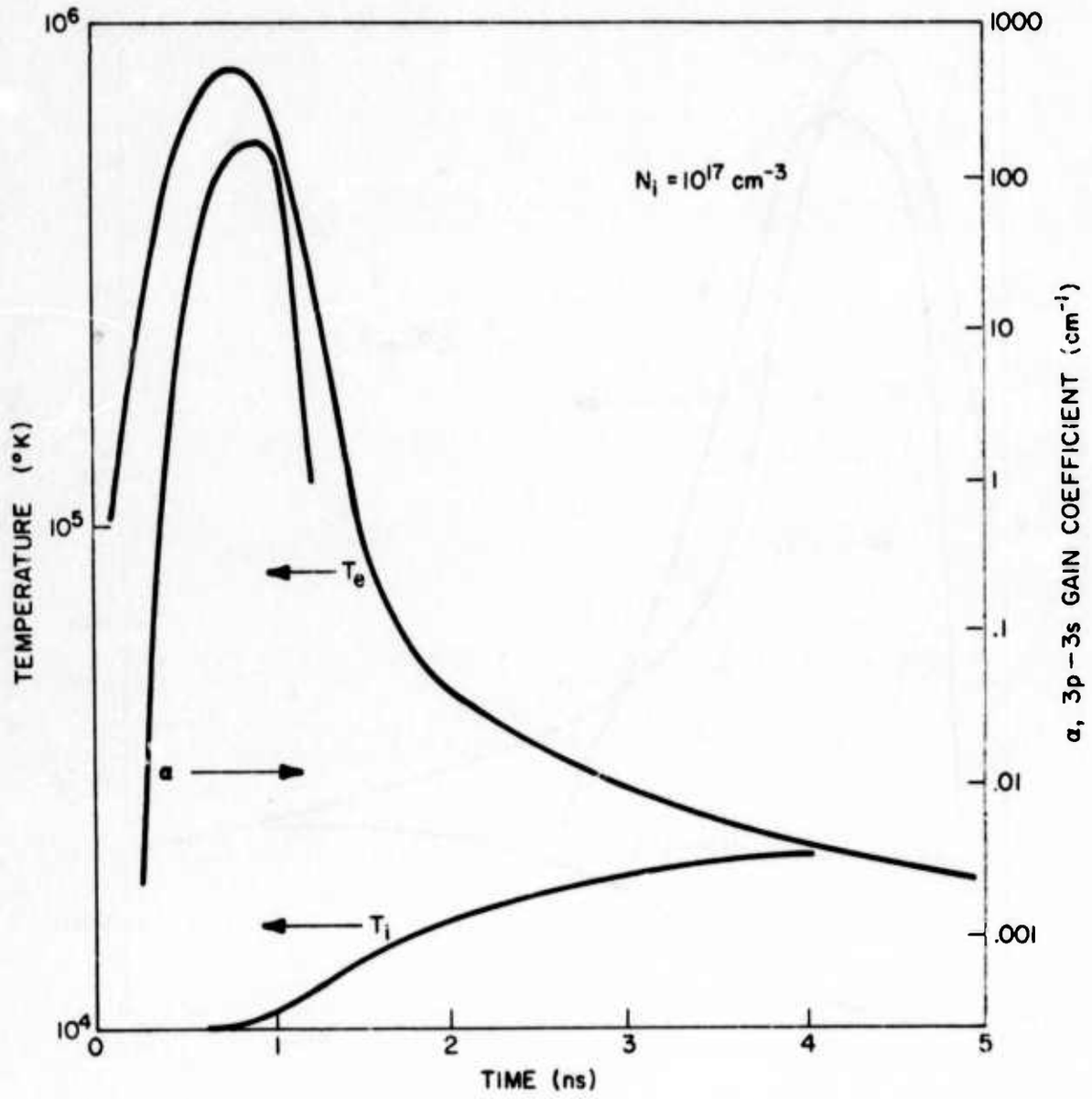

Figure 52 Gain coefficient and electron and ion temperatures for Hot-Spot run with initial ion density of 10^{17} cm^{-3}.

version of the Hot Spot model are at least simple estimates for the effects of radiation transport and magnetohydrodynamic motion. The extension of the O III scheme to more highly ionized species as well as the application of the code to model lasing on innershell transitions[5] are being studied. In general, working with the Hot Spot code will provide a better understanding of atomic processes important in producing a population inversion and lasing in plasmas heated by ultrashort laser pulses.

REFERENCES:

1. K. Whitney, J. Davis, and E. Oran, "K-Shell Line Radiation from Laser-Produced Aluminum Plasmas", NRL Memorandum Report 2644, June 1973.

2. K. Whitney and J. Davis, "Hot-Spot Model of K-Line Emission from Laser-Heated Plasmas", J. Appl. Phys. (to be published).

3. R. C. Elton, "Analyses of X-Ray Laser Approaches: 1. Extension of 3p - 3s Ion Lasers into the Vacuum-UV Region", NRL Memorandum Report 2799, May 1974.

4. J. Davis, P. Kepple, and M. Blaha, (to be published).

5. R. C. Elton, NRL Memorandum Report (to be published); also R. C. Elton, "Quasi-Stationary Population Inversion on K-Alpha Transitions", in Proc. of the Intl. Conf. on X-Ray Processes in Matter (Otaniemi, Finland, 1974), published in Physica Fennica, vol. 9, supplement S1, pp. 397-402, 1974.

VI. C. ANALYSIS OF INNERSHELL PHOTOIONIZATION PUMPING SCHEMES

For lasing in the x-ray spectral region, $2p \rightarrow 1s$, $K\alpha$-type transitions are most desirable because of the high photon energy. The pumping flux necessary to sustain a population inversion against spontaneous decay is, however, formidable[1], due to the large x-ray and Auger transition probabilities. The femtosecond risetimes required for pre-equilibrium operation in a self-terminating mode[2] are an additional severe problem. Stripping of outer electrons so that hydrogenic or helium-like ions are utilized would eliminate both the Auger contribution to the decay and the attenuation of the beam due to photoionization. In any case, however, such short-lived inversions could only be useful as amplifiers, since the coherence length is ≤ 1 μm, prohibiting cavity use without extremely well-synchronized repetitive operation or traveling wave pumping.

If, however, an inverted density can be maintained in a quasi-stationary mode for say, nanoseconds, operation with Bragg-reflecting resonators may be feasible. Even if cavities do not prove practical for intense x-ray laser beams, the reduction of pump pulse risetime

requirements in such a quasi-cw mode could be a deciding factor in achieving amplified spontaneous emission in the x-ray region. Stankevich[3] suggested such a quasi-cw operational possibility, providing that the total rate for transfer of L-vacancies (lower laser state) to the M-shell exceeds the total K-vacancy (upper laser state) decay rate. His sketchy analysis based upon early data indicated that sustained inversions on the $K\alpha_1$ and $K\alpha_2$ transitions was possible for elements with $Z \leq 36$ and 47, respectively. In order to validate his claims, an attempt has been made[4,5] to reproduce Stankevich's results with the data which he used and general agreement with his conclusions has been achieved as shown (dashed) in Figure 53, where rate ratios R_L/R_K greater than unity represent net gain. Using the same (gross) total-rate approach but with more recent and reliable data[6], it has been further found that gain may be achieved only for the $K\alpha_2$ transition and for $25 \leq Z \leq 45$. Also, the degree of inversion and the resultant gain are limited by a maximum excess L- over K- vacancy depletion rate of $\sim 30\%$. These new results are also plotted in Figure 53 for comparison.

As suggested above, Stankevick's analysis was quite unsophisticated due at least in part to the unavailability of basic atomic data. A more complete analysis would follow the binding energy diagram shown in Figure 54 for copper, which also may be interpreted conveniently as a "vacancy-level" diagram. Pumping (P) produces a K-vacancy followed by radiative (R) decay as well as Auger (Γ) decay. Cascading is indicated and leads to multiple vacancies and multiply-ionized species. The basic idea put forth by Stankevich has been further analyzed[4,5] at NRL and may be revived when it is realized that the creation of double LL- or LM_1 vacancy states following K-Auger transitions can produce a sufficient energy shift to avoid resonant absorption of the amplified K x-ray emission. In this refined model, it is only necessary for the total L-decay rate to exceed the K x-ray rate; significant rate excesses and net gain then become possible for both $K\alpha_1$ and $K\alpha_2$ transitions and for $13 \leq Z \leq 50$ as shown in Figure 55. This line shift model is based upon a delicate balance between (a) rapid Auger cascading to higher M-vacancy states with multiple ionization, associated (as outer electrons are lost) decay rate decreases and insufficient line shift; and (b) recombination which must proceed at a comparably high rate to prevent excessive depletion of amplifying atoms through ionization. This latter condition (b) places an upper limit on the temperature permitted ($kT \approx 30$-100 eV according to Stankevich[3]) and, in a continuously pumped medium, on the inversion period; hence the quasi-stationary nature of the inversion. The achievement of the proper balance will be found both by a full numerical model and from careful experimental diagnostics.

Based upon this new line-shift model, respective calculations[4,5] for Si, Ca, and Cu at wavelengths of 7.1, 3.4, and 1.5 Å, respectively, indicate first that only concentrated x-ray photon beams can provide the required pumping energy density. Electron impact pumping is

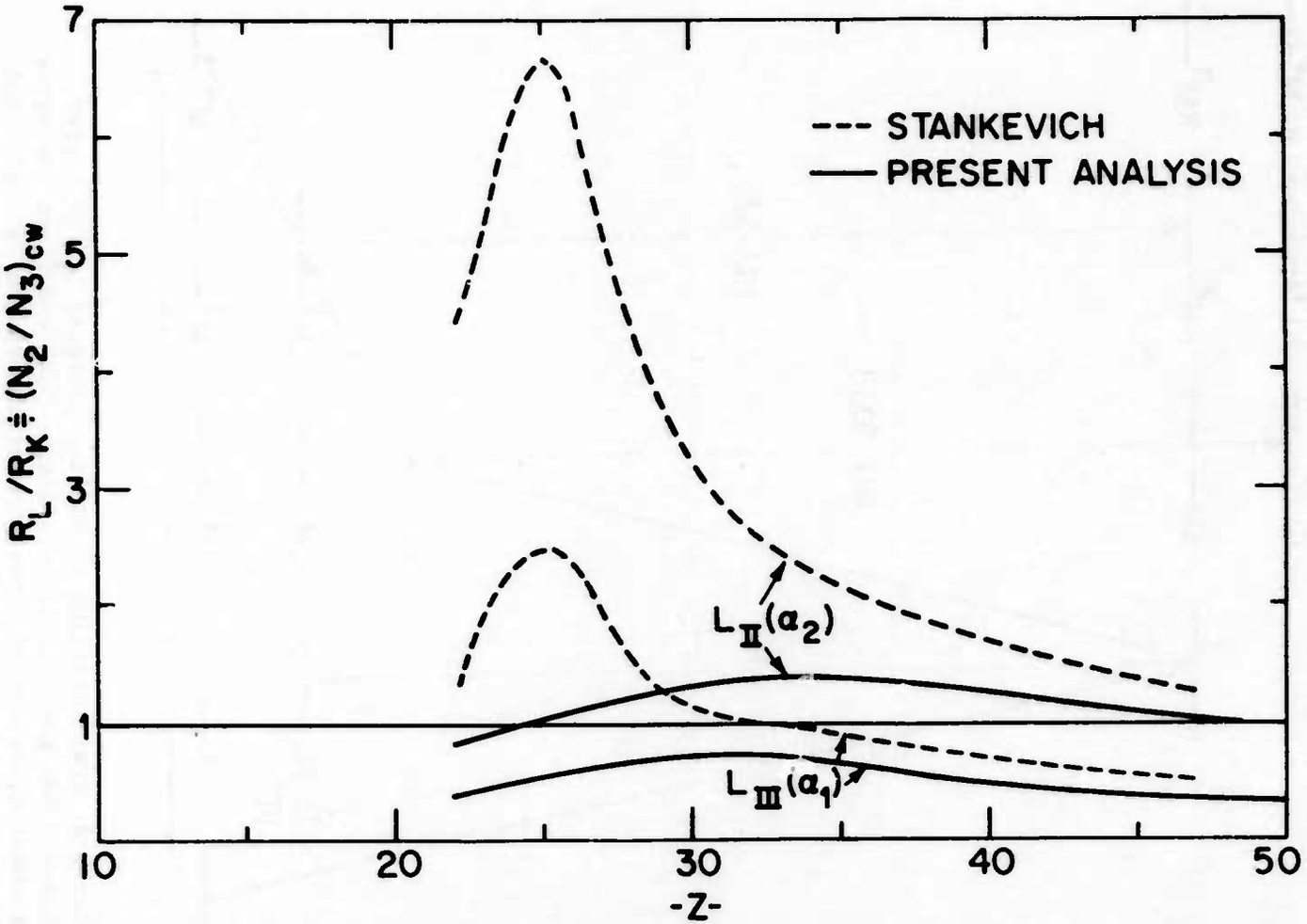

Figure 53 Ratio of rates R_L/R_K for total transitions out of a L and K vacancy states, respectively, versus atomic number Z. Values exceeding unity indicate gain. The model here assumes all K-vacancy decay transitions produce potential absorbers for laser radiation. Present analysis is based on recent data; an attempt to reproduce the results of Stankevich is shown dashed. Both $K \rightarrow L_{II}$ and $K \rightarrow L_{III}$, α_2 and α_1 transitions are shown.

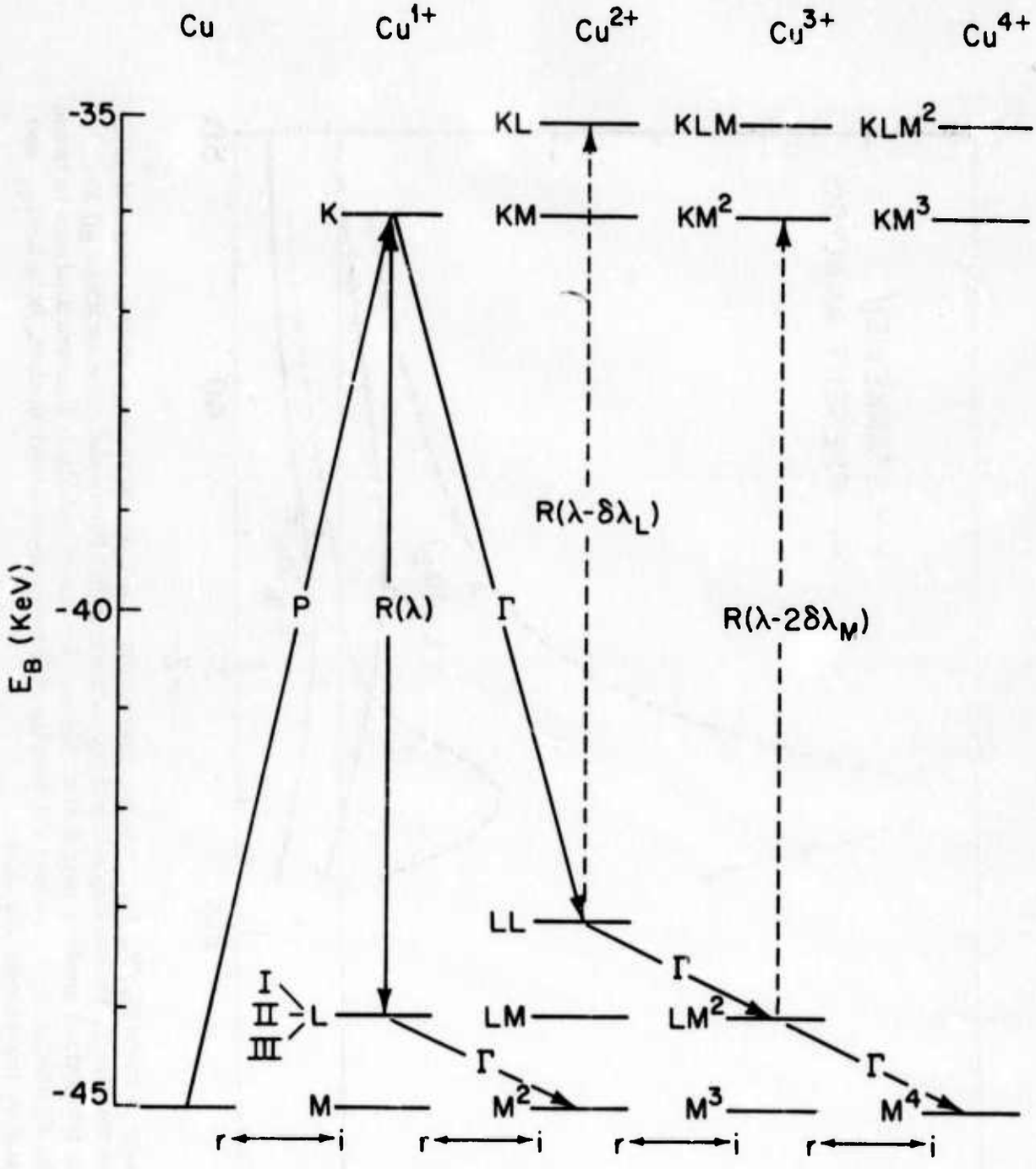

Figure 54 Vacancy diagram according to binding energies E_B for copper. K,L,and M designate shell vacancies. P,R, and Γ are the rates for pumping, radiative [emission or absorption (dashed)], and Auger transitions, respectively, $\delta\lambda_L$ and δL_M indicate line shifts with multiple vacancies. r and i designate alternate recombination and ionization transitions, respectively.

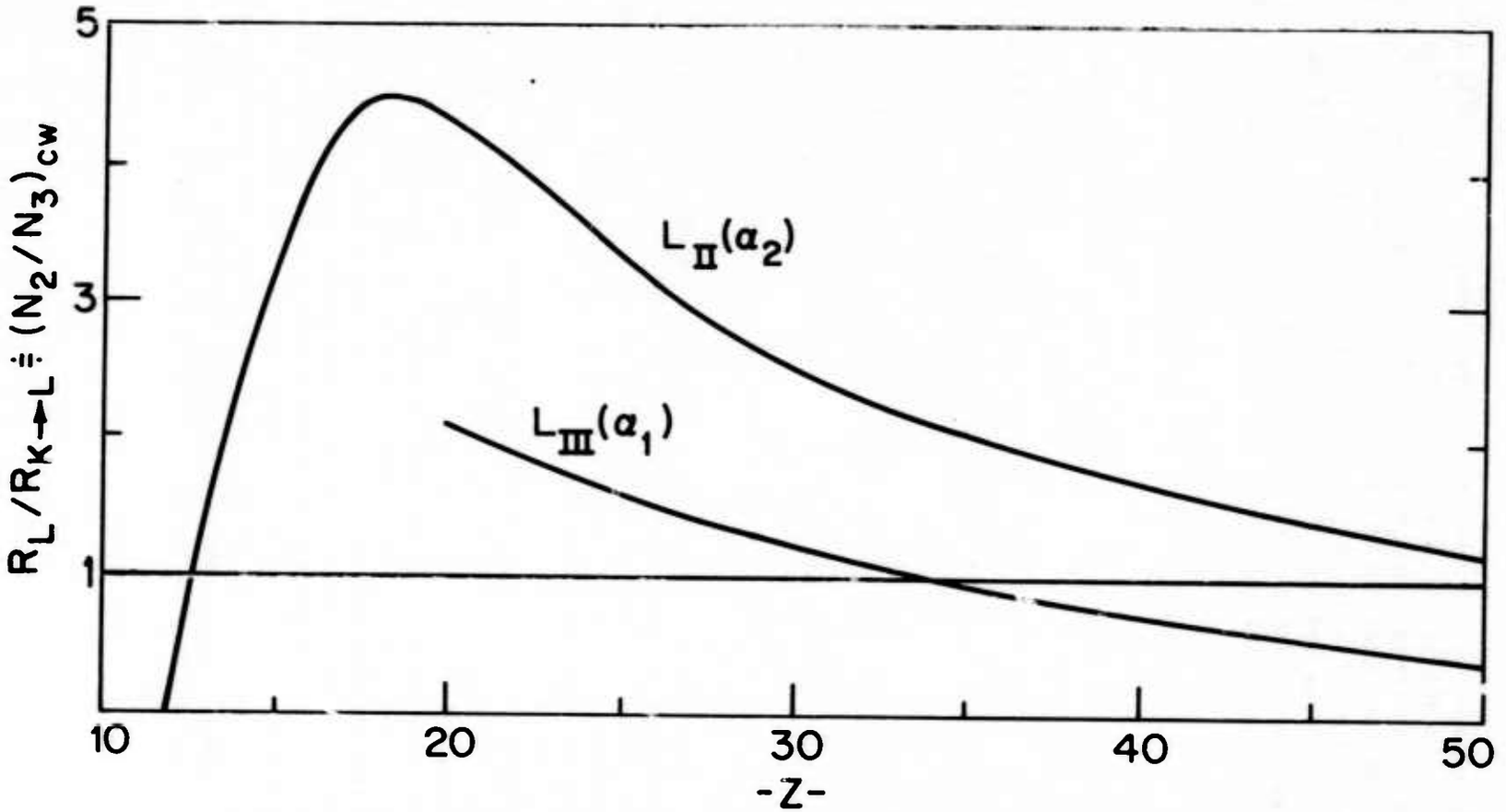

Figure 55 Ratio of rates $R_L/R_{K\to L}$ for total transitions out of a L-vacancy state and radiative decay out of a K-vacancy state versus atomic number Z. Values exceeding unity indicate gain. The model used assumes only radiative transitions produce absorbers, with Auger transitions generating shifted ion lines. Both $K\text{-}L_{II}$ and $K\text{-}L_{III}$, α_2 and α_1 transitions are shown.

limited in plasmas by the maximum electron density obtainable and in beams by the ability to focus the energy onto a sufficiently small area. For these three elements, the photon densities, N_ν, required to overcome photoionization losses in the beam, and the equivalent flux density F are listed in Table VIII, along with the resultant gain αL for a laser medium of length 300 μm and diameter 30 μm. With a 10 percent conversion efficiency, the indicated x-ray pumping flux requirements can be met by the IR laser powers P indicated. These

TABLE VIII. $K\alpha_2$ PUMPING REQUIREMENTS

ELEMENTS	λ (Å)	10^{-14} (Γ+A) (sec^{-1})	B	$10^{-20}N_\nu$ (cm^{-3})	$10^{-3}F$ (TW/cm^2)	$10^{20}\sigma_{pi}$ (cm^2)	αL	P(TW) $10^{-1}E$ (J)	kT_{BB} (keV)	$(\lambda_m)_{BB}$ (Å)
^{14}Si	7.1	6.7	0.6	2	4.8	9	70	4	0.5	5
^{20}Ca	3.4	11	0.8	4	21	4	30	9	0.7	4
^{29}Cu	1.5	21	0.6	20	230	2	15	200	1.2	2

pump power requirements are interestingly equivalent to 1 percent (useful fraction) of the total backbody radiation at the temperatures T_{BB} listed. These are quite achievable and also correspond to peak emission wavelengths $(\lambda_m)_{BB}$ listed which are good matches for the photoionization absorption bands.

In conclusion, the inclusion of the possibility of ionic line shift makes the quasi-cw inversion scheme appear viable, although the necessary balance between ionization to achieve line shifts and recombination to maintain a high density medium is delicate to maintain. The Auger and photoionization losses are severe and ultimately put a burden on the pumping source. It is clear that a more sophisticated model which includes plasma effects is needed for further analysis. Experimentally, the requirement is for a sufficiently intense photon source, tuned for a particular spectral region. For example, some experimental efforts could already be directed towards developing a pseudo-blackbody continuum of saturated L-emission lines from heavy elements; some vacuum-UV efforts on uranium plasma emission already exists.

REFERENCES

1. M. A. Duguay and R. M. Rentzepis, Appl. Phys. Letters 10, 350 (1967).

2. R. C. Elton, R. W. Waynant, R. A. Andrews, and M. H. Reilly, Naval Research Laboratory Report 7412 (May 1972).

3. Yu L. Stankevich, Sov. Phys.-Doklay 15, 356 (1970).

4. R. C. Elton, "Quasi-Stationary Population Iversion on Kα Transitions", Proceedings International Conference on X-Ray Processes in Matter, Helsinki, Finland July 1974, Physica Fennica 9, Suppl. S1, p. 397.

VI. D. MODELING OF RECOMBINATION AND PHOTON PUMPING SCHEMES

Two approaches to VUV and X-Ray lasers are considered here. The first is the use of a recombining plasma, which can be produced either by an electron or ion beam or from an expanding, laser produced, plasma. The recombination scheme shows promise if some mechanism can be found to cool the plasma sufficiently ($T \ll 100$ eV) while maintaining a "sufficient" electron density. The numerical calculations solve the standard set of rate equations which govern the time histories of the processes (Ref. 1):

$$N^z + 2e \xleftarrow{(1)} N^{z-1} + e + h\nu \xleftarrow{(2)} N^{z-2} + h\nu \quad .$$

The only species for which detailed calculations are done is for N^{z-1} (the hydrogenic ion) where each level is considered individually. For the bare portion and the helium-like species N^{z-2}, only total rates are considered. Included in the calculation for level (p) of N^{z-1} are 1) two- and three-body recombination from N^z and into N^{z-2}, 2) electronic ionization out of N^{z-1} and from N^{z-2}, 3) cascade, 4) electronic excitation and de-excitation and 5) stimulated emission and photoabsorption. Coupled to these rate equations (one for each discrete level in the hydrogen system) are the total rate equations for N^z, N^{z-1}, N^{z-2}, and N_e. In addition, the laser equation is included, namely the differential equation for the stimulated emission coefficient,

$$\frac{1}{E_{u\ell}} \frac{d\theta}{dt} = \gamma N_u A_{u\ell} + \theta \left[N_u - N_\ell \frac{g_u}{g_\ell}\right]$$

where θ is the emission coefficient, N_u and N_ℓ are the upper and lower levels of the transition of interest and $E_{u\ell}$ is a <u>modified</u> energy separation between the levels. Note that γ, which is merely a geometrical factor to account for pulse propragation in a real laser, has been set to unity for these calculations. This approximation has

little effect on the gain, but does affect the relative values of the photon energy in coherent and incoherent radiation. Thus when designing a practical laser, one must solve the radiation-transfer problem and include γ correctly; but for modeling purposes, the choice is not important. The above coefficients (1-5) can be found in the standard literature [1-4] To date, consideration has been given to the two cases $N_e = 10^{15}$ and 10^{17} for sodium (fully stripped) and $T_e = 0.1$, 0.5 and 1.0 eV. In all cases, inversion between levels 4 and 2 which lases at 40 Å (for example see Figure 56) has been obtained. The next project is to find the maximum laser gain as a function of temperature and electron (or ion) density, for several species such as boron, carbon, and aluminum (common targets in laser produced plasmas). This will be followed by an attempt to design a practical experiment which can show that lasing exists at these wavelengths.

The second possible x-ray laser pumping scheme considered is photon pumping of a gas or solid. The only species which seem to be amenable to this process, using current technology for light sources, are sodium vapor and aluminum (either solid or as a vapor). They have photoionization cross-sections[5] which lend themselves to being pumped by a broadband radiation source to produce inversion.

An example of gain (cm^{-1}) vs. time for a practical[6] experiment is shown in Figure 57. The peak power for a practical laser (with the geometrical factor $\gamma = 0.01$) is about 5 kW/cm^3 with the gain on the order of unity. The two cases presented are for an initial vapor density of 10^{14} and 10^{16} cm^{-3}. For each of these cases reduced (from blackbody level) fluxes ($\Phi = \varepsilon\Phi_{BB}$) have been used. The details of this model are given in Ref. (6).

REFERENCES

1. M. J. Seaton, "Radiative Recombination of Hydrogenic Ions", Month. Not. Roy. Astro. Soc. 119, 81 (1959).

2. H. W. Drawin,"Influence of Atom-Atom Collisions on the Collisional-Radiative Ionization and Recombination Coefficients of Hydrogen Plasmas", Z. Phys. 225, 483 (1969).

3. M. J. Seaton, Atomic and Molecular Processes, D. R. Bates, Ed., Academic (New York, 1962); H. Van-Regemorter, "Rate of Collisional Excitation in Stellar Atmospheres", Astro. Phys. J. 136, 906 (1962).

4. A. W. Ali, "Towards Shorter Wavelength Lasers and Breaking the 1000 Ångstrom Barrier I", NRL Mrmorandum Report 2792 (1974, unpublished).

5. W. D. Barfield, G. D. Korntz and W. F. Huebner, "Fits to New Calculations of Photoionization Cross Sections for Low Z Elements", J. Q. S. R. T. 12, 1409 (1972).

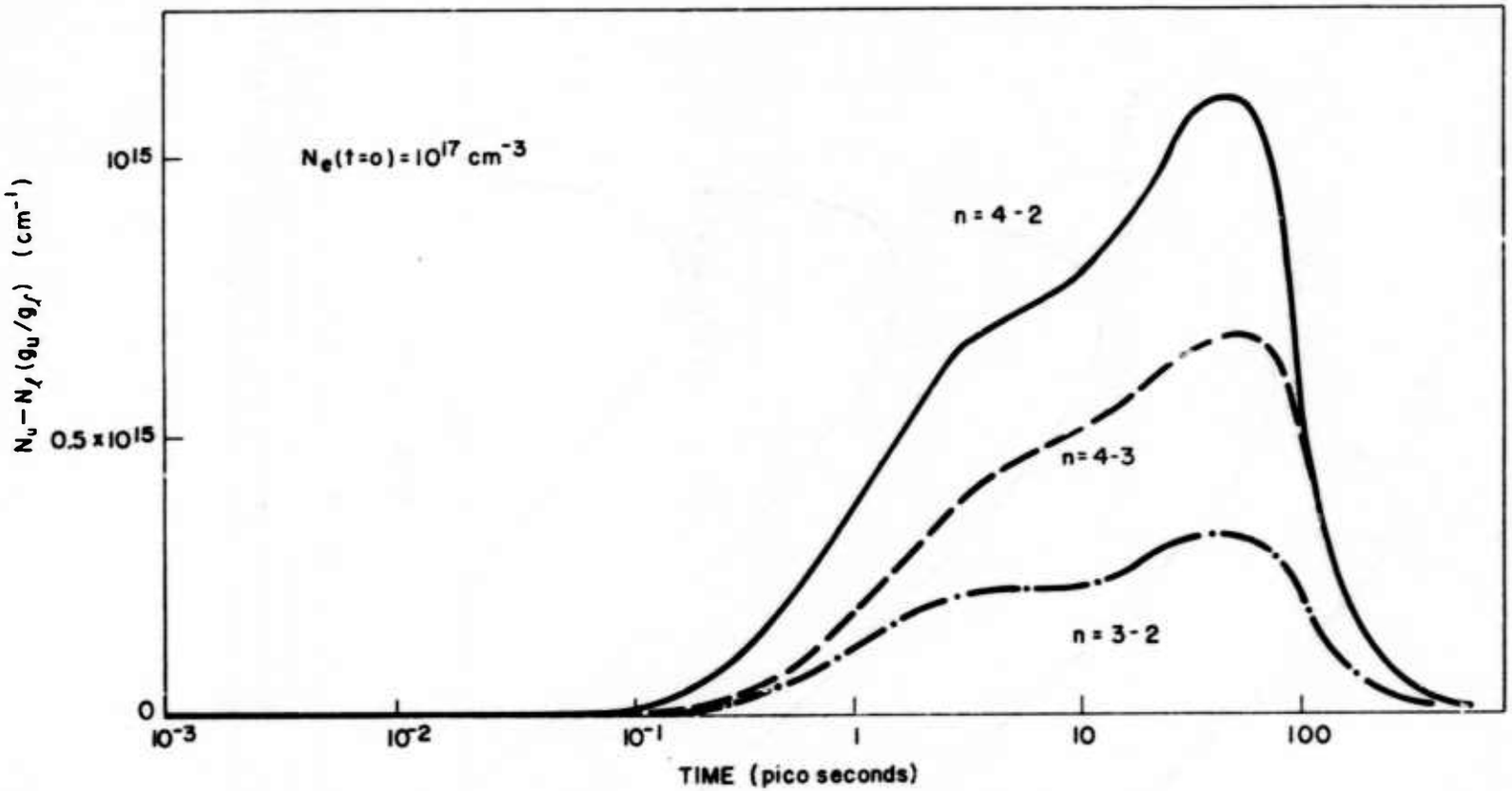

Figure 56 Population inversion density as a function of time (units are picoseconds) for the 40 Å line radiation emitted from the 4 to 2 transition of hydrogen-like sodium atoms.

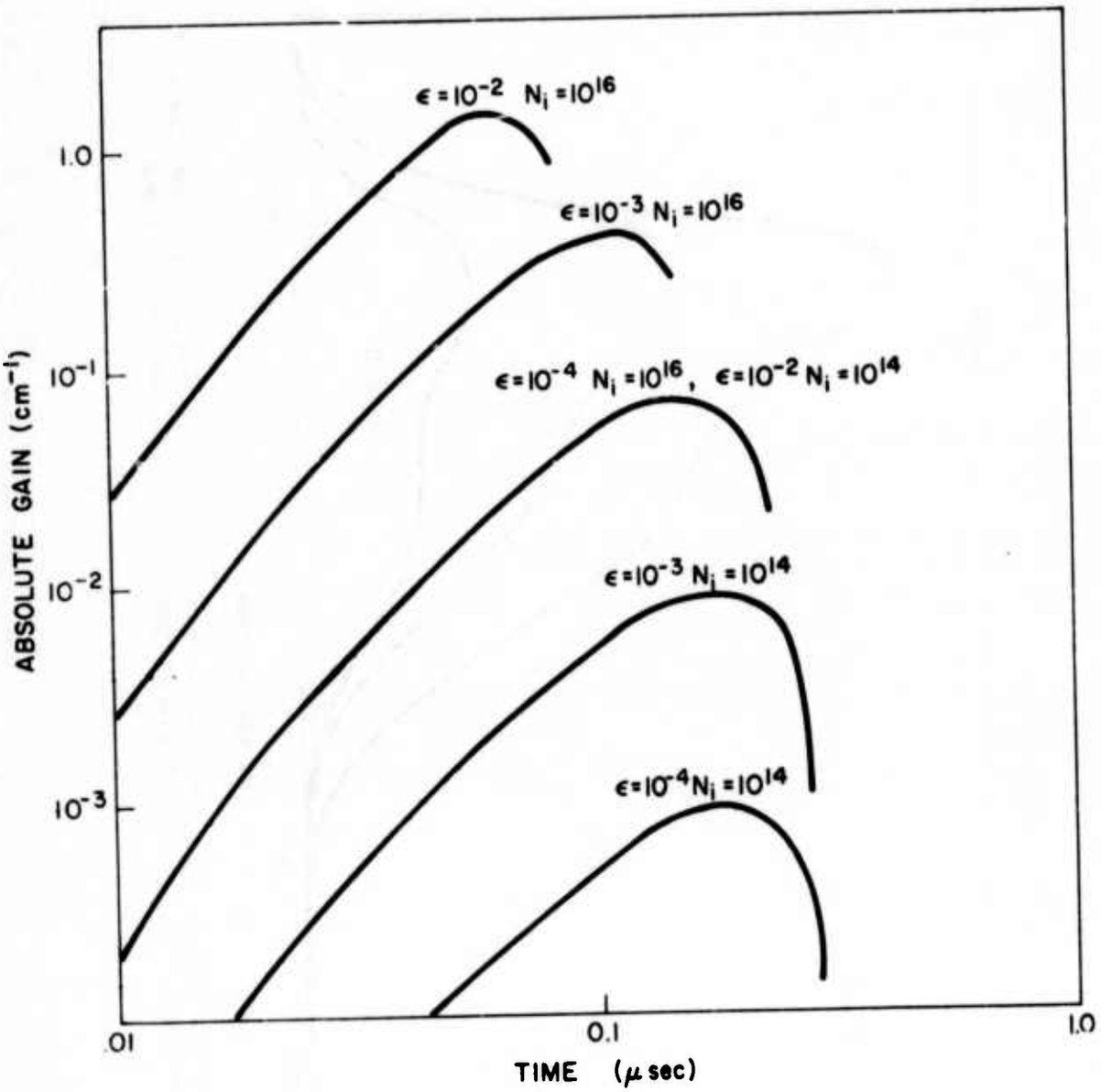

Figure 57 Logrithmic gain of the 372 Å line radiation given as a function of time (nanoseconds) for a given photon pump risetime τ of 1 nsec. The backbody pumping flux is reduced by a factor ϵ; and N_i is the ground state population density.

6. W. W. Jones and A. W. Ali, "Calculations For a VUV Laser from Sodium Vapor Pumped by Radiation from an Exploding Wire", NRL Memorandum Report 2807 (June 1974).

VI. E. THEORY OF X-RAY LINE WIDTHS IN PLASMAS

Whenever a plasma is created in the laser medium, either intentionally to achieve a high electron density for pumping purposes or unavoidably due to intense ionization pumping with Auger processes contributing to the free electron production, the effect on the line width must be considered, since the gain varies inversely with line width[1]. Enhanced broadening (over natural broadening) may be due to random Doppler shifts and to charged particle interactions (Stark broadening). Both are considered here for radiation in the Kα spectral region for various elements. The results are not only relevant to Kα innershell lines but to resonance lines of helium-like and hydrogenic ions; in fact, some Stark broadening data are taken for Ly-α lines for convenience and availability.

An estimate of the Doppler width $\Delta\lambda_D$ is obtained from[2]:

$$\Delta\lambda_D/\lambda \doteq \Delta\nu_D/\nu = 7.7 \times 10^{-5} \quad (\mathcal{T}T_i/\mu)^{\frac{1}{2}}, \qquad (1)$$

where $\mathcal{T}T_i$, the ion kinetic temperature, is in eV and μ is the atomic mass number of the element. As an approximation we can take $\mathcal{T}T_i = h\nu/4$ (ν the laser frequency) in an "equilibrium" plasma and $\lambda = \lambda(\text{Lyman-}\alpha)$, in order to evaluate $\Delta\lambda$ as a function of laser wavelength λ. The result is plotted in Figure 58.

The Stark widths for Kα transitions may be estimated[3], with sufficient accuracy for present purposes, from (a) an approximate formula for Holtsmark (quasistatic linear Stark effect) ion or electron broadening

$$\Delta\lambda_H \approx \frac{8\lambda^2}{\pi c} \quad \frac{h}{mZ_i} \quad N_e^{2/3} \bar{Z}_p^{1/3}, \qquad (2)$$

where $\bar{Z}_p$ is the average perturber charge and Z_i is the ion charge, and (b) from (1) for Lorentz (electron impact) broadening

$$\Delta\lambda_L \approx \frac{8\lambda^2}{cZ^2} \left(\frac{h}{m}\right)^2 \quad \frac{N_e}{v_e}, \qquad (3)$$

(plus a logarithmic factor ≈ 5), with the lesser of the two being more appropriate. In Eq. (3) v_e may be replaced by the mean thermal velocity for the electrons at the plasma temperature. The resulting Stark widths $\Delta\lambda_s$ are also plotted in Figure 58 as a function of wave-

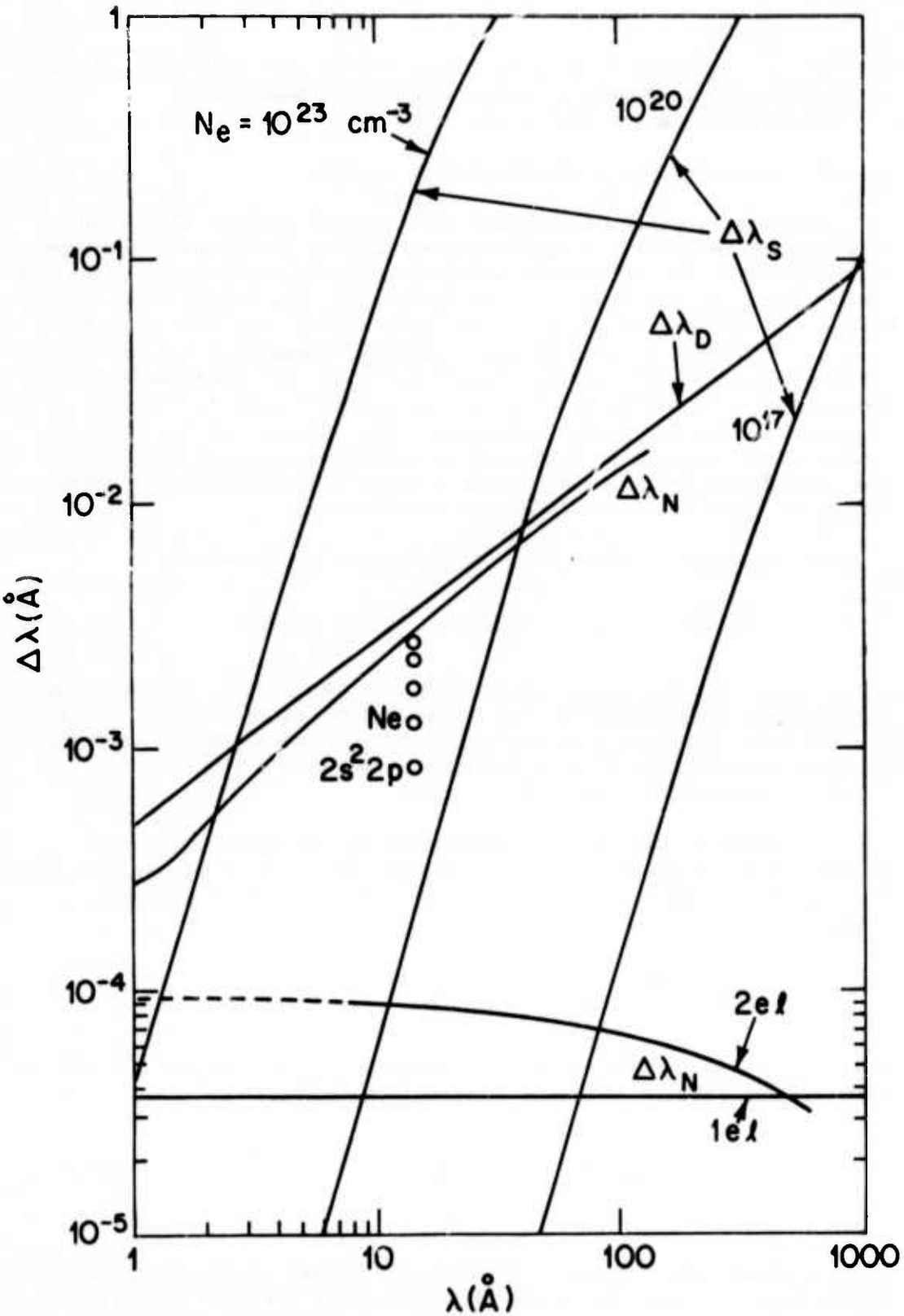

Figure 58 Estimates of line widths for Kα type transitions versus wavelength λ [with natural ($\Delta\lambda_N$), Doppler ($\Delta\lambda_D$) and Stark ($\Delta\lambda_s$) effects included]. The decrease in natural broadening with ionization is indicated for neon, and hydrogenic and helium-like ionic species are included.

length for three electron density values. The magnitudes of these two Stark broadening processes are approximately the same for present conditions. There is for some schemes an advantage in increasing the electron temperature preferentially over the ion temperature for increased electron collisional pumping without additional Doppler broadening; this will have the effect of decreasing the (Lorentz) width through ν_e in Eq. (3).

From Figure 58 a comparison is now possible between plasma line widths for Kα transitions and natural widths $\Delta\lambda_N$ ($\doteq \lambda^2 \Delta\omega/2\pi c$) determined from $\Delta\omega = \Gamma + X$, Γ being the Auger rate and X the X-ray decay rate, where the Auger data used here are from single K-vacancies in neutral atoms. This is somewhat contradictory to having an equilibrium plasma with sufficient electron energy to create K-vacancies, where multiple ionization is expected. Therefore the reduction in Auger width with multiple ionization is indicated for one case (neon, Kα = 14.6 Å). The possibility of frozen-in lower ionization stages in, for example, a rapidly expanding laser-produced plasma means that we must be prepared for multiple outer electrons, and indeed present innershell schemes usually depend directly on their presence. For general interest, also shown in Figure 58 are the natural widths $\Delta\lambda_N$ ($\Delta\omega$=A, the transition probability) for helium-like and hydrogenic species, where the latter is a straight line since Ly-α wavelengths were used, i.e., $A\alpha\lambda^{-2}$ and $\Delta\lambda_N\alpha\lambda^2 A$.

In summary, the data shown in Figure 58 indicate, for various degrees of ionization up to the one and two electron ions, the degree of line broadening to be expected.

It is clear that Doppler broadening remains comparable to innershell natural broadening (at least for a low degree of ionization) and therefore does not preclude a plasma approach in itself. Stark broadening even at solid densities ($\sim 10^{23}$ cm^{-3}) is not dominant for wavelengths shorter than 3 Å. From this we conclude that, e.g., laser pumping of innershell transitions (discussed elsewhere here) within the criterion for overcoming photoionization losses in the beam would be feasible in a plasma, as far as line broadening is concerned. Furthermore, a reduction in line width through avoidance of Auger processes would be no reason in itself for working with hydrogenic or helium-like species (the real advantage is the lack of photoionization losses in the medium itself).

REFERENCES

1. R. C. Elton, R. W. Waynant, R. A. Andrews, and M. H. Reilly, Naval Research Laboratory Report 7412, May 1972.

2. R. C. Elton, in Plasma Physics, Vol. 9A, "Methods of Experimental Physics", edited by H. R. Griem and R. H. Lovberg (Academic Press, New York, 1970).

3. H. R. Griem, "Spectral Line Broadening by Plasmas" (Academic Press, N.Y., 1974).

VII. SUMMARY

The x-ray laser program is at the point where a lot of major construction and development of experimental facilities is near completion. As a result this reporting period has seen an increase in the amount of work directly relevant to x-ray laser schemes as opposed to related physics and technology. This trend should continue. Two efforts were initiated during this period: the charge transfer experiment and the nonlinear mixing approach to shorter wavelengths. These efforts, therefore, have been mainly planning, design, and construction of hardware for the experiments.

The significant milestones reached during this period for each of the program areas are:

E-Collisional Pumping -

- Reliable operation of the short pulse laser facility has been attained with 25 psec, 0.2 Joule operation and synchronization with a Q-Switched laser with synchronization jitter of < 1 nsec.
- A series of laser-plasma characterization experiments using 25 psec pulses has been completed. The results agree well with numerical modeling of the experiment and verify the expected attainment of $T_e \gg T_i$ conditions.

Resonant Charge Transfer -

- An experiment using carbon and helium has been designed and is under construction.
- The NRL Glass Laser Facility has been converted to 40 psec operation.

Nonlinear Mixing Approach -

- The facility for generating tunable radiation in the vicinity of 1600 Å has been designed and is under construction.
- Development of a hydrogen amplifier at 1600 Å operating at 1 atm pressure is underway.

TW Pumping -

- The TW e-beam device has been completed and is being evaluated.

Preliminary results have been obtained with nitrogen and hydrogen.

Theory, Analysis, and Modeling -

- Analyses of e-collisional $3p \rightarrow 3s$ laser schemes and preferential innershell photoionization schemes have been completed.

- Modeling is underway and continuing for the $3p \rightarrow 3s$ collisional pumping scheme, photoionization pumping of sodium, and general recombination schemes.

Another very important result came out of this effort. This is the theory and experiment on a negative n_2 in cesium vapor at 1.06μm. This result is of great significance to high energy glass laser technology.

Finally, the details of a lot of the results presented in this report have been published as journal articles, reports, and conference proceedings. Appendix C lists these contributions which have come out of this program since its inception.

APPENDIX A - OPTICAL PULSE COMPRESSION

Optical pulse compression has been proposed as a possible technique for increasing laser efficiency and output energy, without the increase in peak intensity that could lead to self focusing or beam distortion[1,2]. The system proposed here would be suitable for generating energetic optical pulses in the 1-10 psec range for use in the NRL short pulse laser facility which is part of the x-ray laser program.

The basic idea of pulse compression[3,4] is to amplify a long pulse that has a variable carrier frequency (i.e., a chirp). If this propagates through a dispersive delay line beyond the final amplifier, it will be compressed in time if the delay is longer for the carrier frequencies in the earlier portions of the pulse. A highly dispersive delay line can be constructed from a pair of diffraction gratings[4], in which longer wavelengths are diffracted through larger angles, and consequently over longer propagation paths.

A large, effectively monotonic frequency chirp is provided by the Kerr liquid and saturable absorber combination shown in Figure 59. A pulse from the preamplifier is propagated through a total path length ℓ of CS_2[5], which is distributed over 5-10 well spaced cells K_1, K_2, --- K_n in order to avoid beam breakup due to small scale self focusing[6]. For an on-axis intensity $I(t,x)$, the resulting self phase modulation (SPM) produces a chirp or time-dependent frequency displacement

$$\omega_c(t) = -(*8\pi^2 n_2/n_o\lambda c)\ \ dD(t)/dt \qquad (1)$$

from the carrier frequency $2\pi c/\lambda$. Here

$$D(t) = \int_o^{\ell} I(t,x)\ \ dx \qquad (2)$$

is the so-called distortion parameter, and n_o and n_2 are respectively, the linear and nonlinear refractive indices defined by $n = n_o + n_2 \langle E^2 \rangle$. The integral, of course, extends only over the CS_2 cells.

For a Gaussian pulse of FWHM width Δt, $I(t,x) = I_o(x) \exp [-(41\ 2)\ t^2/\Delta t^2]$, and $\omega_c(t)$ has the form shown in Figure 60. The extremes of $\omega_c(t)$ occur at times $\pm t_m = \pm (1/81n2)^{\frac{1}{2}} \Delta t$, and the total chirp bandwidth is

$$\Delta\omega_c = \omega_c(t_m) - \omega_c(-t_m)$$
$$= 2\ (8\pi^2 n_2/n_o\lambda_c)\ \ (81n2/e)^{\frac{1}{2}}\ \ D(0)/\Delta t \quad . \qquad (3)$$

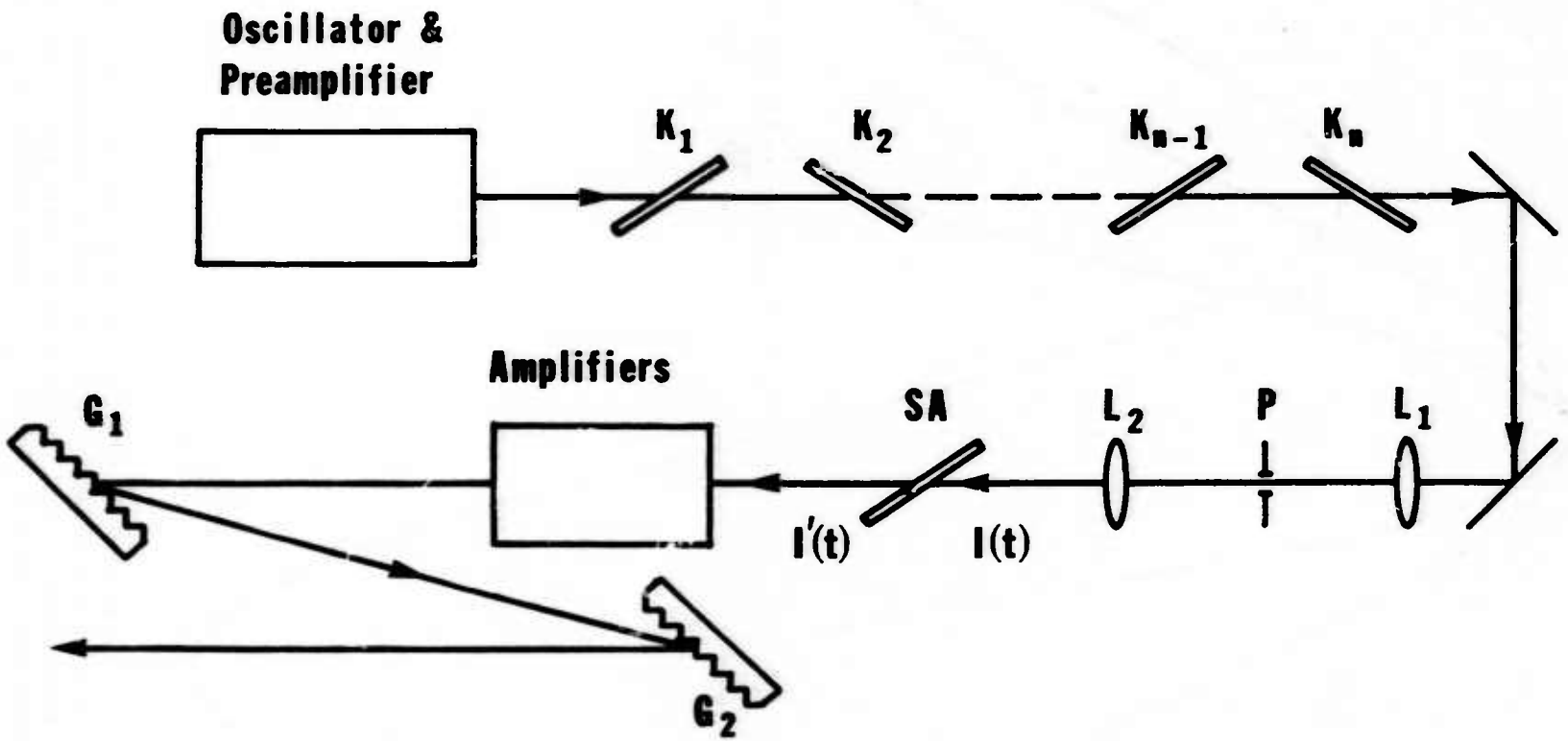

Figure 59 Proposed NRL optical pulse compression system.

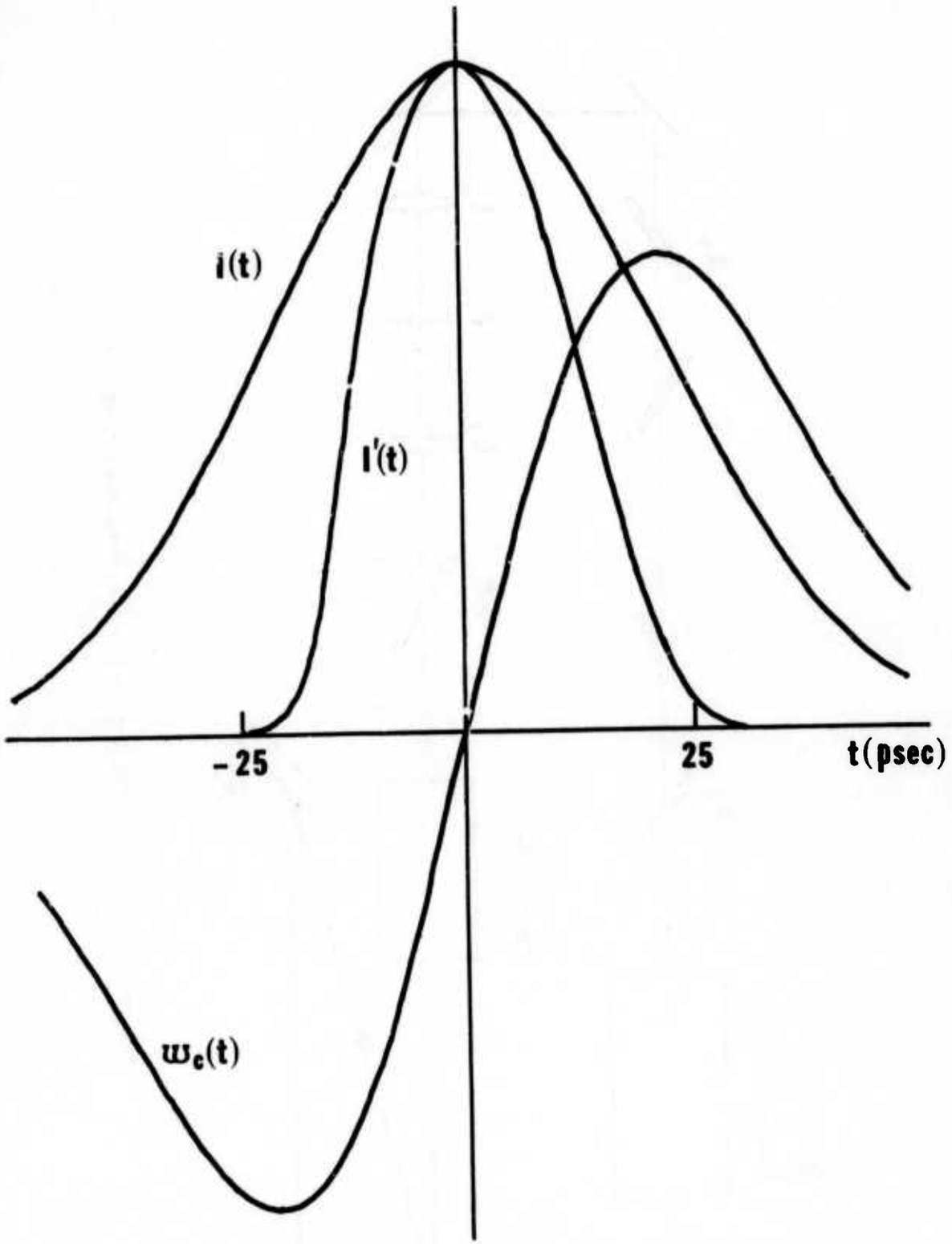

Figure 60 Action of the saturable absorber SA (Fig. 59) on a 50 psec chirped pulse, showing normalized input and output intensities I(t) and I'(t), respectively, and instantaneous chirp $\omega_c(t)$. The relevant parameters are I(0) = 1 GW/cm^2, I_s = 0.05 GW/cm^2, $T_c = 10^{-6}$, and T_1 = 6 psec. Net energy loss is 8dB.

For $\lambda = 1.06\mu m$, $\Delta\omega_c \Delta t \simeq 5.7\ D(0)$, where D(0) is expressed in units of GW/cm.

If the amplified version of I(t,x) were propagated through a grating pair[4] or other suitable dispersive delay line, the center portion $|t| < t_m$ could be optimally compressed; however, the falloff of $\omega_c(t)$ for $|t| > t_m$ would result in long leading and trailing edges on the output pulse[1,2,5]. An increase in the dispersion would not solve this problem, but would result only in the creation of large bumps on the leading and trailing edges. All such effects are highly undesirable for most short-pulse laser-plasma experiments. One could eliminate them by a saturable absorber located beyond the grating pair, but this would also attenuate the center portion, especially if the output pulse width Δt_1 is comparable to the relaxation time of the absorber dye. A better solution is to place the saturable absorber SA as shown in Figure 59. With this arrangement, the noncompressible outer portions of the pulse are eliminated, as shown in Figure 60, prior to the main amplifiers. The net energy attenuation is about 8 dB, but the loss can be easily recouped at this low signal level.

The output of SA can be written as

$$I'(t) = T_o\, e^{S(t)}\, I(t), \tag{4}$$

where I(t) is the input intensity, T_o is the low-signal transmission, and S(t) is a saturation parameter. S(t) is a solution of the equation

$$\dot{S}(t) = [1 - T_o e^{S(t)}]\ I(t)/I_s - S(t)/T_1 \tag{5}$$

(subject to the condition $S \to 0$ as $t \to -\infty$), where I_s is the saturation intensity, and T_1 is the dye relaxation time. For Kodak 9860, $I_s \simeq 50\ MW/cm^2$, and $T_1 \simeq 6$ psec.

From SA, the pulse, of width $\Delta t' \simeq \Delta t/2$, proceeds through the main amplifiers to the compressor gratings G_1G_2. Under favorable operating conditions, the additional bandwidth due to SPM in the amplifiers will be small in comparison to $\Delta\omega_c$, so that $\omega_c(t)$ remains monotonically increasing in time.

The minimum attainable pulsewidth from G_1G_2 is

$$\Delta t_1(\min) \simeq 4\ln 2/\Delta\omega_c\ , \tag{6}$$

and since $\Delta t' \simeq \Delta t/2$, the maximum compression ratio (using CS_2) is

$$\Delta t'/\Delta t_1(\min) \simeq \Delta\omega_c \Delta t'/4\ln 2 \simeq 1.0\ D(0). \tag{7}$$

With the lens-pinhole system of Figure 59, values of D(0) up to 20 GW/cm without severe beam distortion or breakup are expected.

Although this type of system is, in principle, applicable to any time regime, it appears to be most suitable for times $10 < \Delta t' < 50$ psec. For $\Delta t' < 10$ psec, the 6 psec relaxation time of the saturable dye significantly reduces the net transmission of SA. For $\Delta t' > 50$ psec, the required temporal dispersion (hence, the spacing) of the gratings becomes too large. The required spacing for gratings of blaze angle θ is

$$L \simeq \frac{4\pi C^2}{5.7} \quad \frac{\Delta t'}{D(0) \lambda \tan^2 \theta} 2 \qquad . \qquad (8)$$

E.g., if $\theta = 45^\circ$, $\lambda = 1.06\mu$, D(0) = 20 GW/cm, and $\Delta t' = 50$ psec, then $L \simeq 24$ meters.

One could compress longer pulses with a multistage Gires-Tournois interferometer[7], but the large time-bandwidth product would necessitate an inordinate number of stages in order to obtain enough dispersion, e.g., for D(0) = 20 GW/cm and $\Delta\omega_c \Delta t' \simeq 57$, one would require about 30 stages. An additional consideration is the fact that longer pulses can be amplified to higher energies; hence, more stages of amplification are required. This results in a larger SPM contribution from the amplifier material, and the total chirp may again become t iple-valued.

The pulse compression experiment outlined above will be set up in the near future, and preliminary experimental results should be available by late 1974. Eventually, it will be incorporated into the NRL short-pulse laser facility experiments.

REFERENCES

1. R.H. Lehmberg, "Compression and Shaping of Pulses from High Power Solid State Lasers", IEDM Technical Digest, p. 565 (Dec. 1973).

2. R. A. Fisher and W. K. Bischel, "Pulse Compression Via. Self-Phase Modulation for Improved High Power Operation of Nd:Glass Laser Amplifier Chains", Bull. Am. Phys. Soc. 18, 1586 (1973); "Pulse Compression for More Efficient Operation of Solid State Laser Amplifier Chains", Appl. Phys. Lett. 24, 468 (1974).

3. J. A. Giordmaine, M. A. Duguay, and J. W. Hansen, "Compression of Optical Pulses", IEEE J. Quantum Electrons, QE-4, 252 (1968).

4. E. B. Treacy, IEEE J. Quantum Electron. QE-5, 454 (1969).

5. R. A. Fisher, P. L. Kelley, and T. K. Gustafson, "Subpicosecond

Pulse Generation Using the Optical Kerr Effect", Appl. Phys. Lett. 14, 140 (1969).

6. A. Laubereau, "External Frequency Modulation and Compression of Picosecond Pulses", Phys. Lett. 29A, 539 (1969).

7. F. Gires and P. Tournois,"Interféromètre Utilisable pour La Compression d'Impulsions Lumineuses Modulées en Fréquence", C. R. Acad. Science (Paris) 258, 6112 (1964).

APPENDIX B - THE NRL GLASS LASER FACILITY

The U. S. Naval Research Laboratory glass laser capability has evolved over the past six years from the original purchased 2 GW (30 nsec) system operated in 1968 to the present subnanosecond pulse system which has operated extensively at 100 - 200 GW on target over the past two years. This evolution has been gradual with major emphasis on reliable and economical operation rather than on generating a few shots of very high peak power at the expense of reliability and it reflects the viewpoint that extensive, well diagnosed target interaction experiments must be carried out to master the physics of the laser matter interactions to a extent sufficient for the design of optimum laser-fusion targets. The NRL laser has had to operate frequently and dependably in order to calibrate and check out all the experimental packages needed to characterize the laser-target coupling on both the AEC (Atomic Energy Commission) and DNA (Defense Nuclear Agency) programs. During this evolution several significant achievements can be highlighted as not only critical in reaching our present status but also in terms of advancing the state of solid state laser technology to where the base now exists for the design of 10^3 - 10^4 Joule systems such as the one presently under construction at Lawrence Livermore Laboratory. These milestones were:

- recognition that narrow linewidth, high gain, crystalline neodymium host-materials have the potential for generating 20 psec to 1 nanosecond pulses without the nonlinear effects with plague glass oscillators, the calculation of expected oscillator performance, and the operation of an optimized, prototype Nd:YAG oscillator (1969-1970);

- operation of the first transmission-line KD*P Pockels cells which allowed 30 - 33 dB background suppression per stage (1971);

- design, construction, and operation of the first high gain, high efficiency disc amplifier. This amplifier was the first disc laser to offer significant advantages over rod amplifiers (1971);

- computer modeling of xenon flashlamp pumping of Nd glass (GENEFF CODE) and optical transfer (ZAP CODE) as well as modeling of the parasitic oscillation problem in laser discs and solution of this problem in the NRL system (1971-1972);

- experimental observation that Fresnel diffraction was triggering self-focusing well below the whole beam self-focusing threshold and the first use of apodization techniques to suppress Fresnel diffraction and allow high level, routine operation of a high power glass laser system (1972);

design, construction and installation of the first total back reflection isolation system using optimized Faraday rotators and Pockels cells to suppress any prepulse or prelase as well as to offer total laser protection from back reflection; and carrying out of experiments characterizing the observed backscatter (1973).

During the past year two more research efforts have achieved significant progress and have demonstrated the potential for further advances in the state of the art of generating high intensity pulses from solid state lasers. These efforts are concerned with parasitic oscillations and de-focusing in cesium vapor.

Parasitic oscillation has been demonstrated to limit the achievable gain in laser rod amplifiers to approximately half of what is expected with optimized optical pumping. Liquid solutions have been found which suppress this parasitic depletion in rods while not absorbing flash-lamp pump light. Thus it now appears possible to achieve $\alpha D \sim 0.65$ - .70 with these solutions while $\alpha D \sim 0.35$ was the highest gain previously attained. The result is a potential factor of 3 to 4 increase in the safe output intensity which could be generated by a rod system; this is sufficient to allow the use of economical and simpler rod amplifiers up through a 6 - 7 cm aperture rather than the much more expensive and complex disc amplifiers. For larger apertures, surface area to volume ratio constraints still demand disc amplifiers, but it now appears that a cheap, simple and reliable front end for a large system is practical.

Self-defocusing effect in cesium vapor at 1.064 μm of sufficient magnitude to offer the possibility of correcting nonlinear wavefront distortion (due to whole beam self-focusing) and self phase modulation in very high intensity laser beams has been demonstrated. This effect will allow separate correction of linear and nonlinear wavefront distortion in systems for laser fusion experiments; it also allows fundamental checks on self-focusing theory; and it may be very useful in satisfying longer-term needs for shaped, laser pulses.

These efforts are described in more detail in other sections of this report along with results on the new NRL-ILC disc amplifier which is 20% more efficient than the NRL prototype (1971) and an evaluation of the potential of the use of pulse compression and multiple pulse techniques to improve the overall efficiency and/or energy output of lasers for fusion applications.

A. GLASS LASER SYSTEM - PRESENT STATUS

The present overall configuration of the NRL laser system is similar to that previously reported. The mode locked Nd:YAG oscillator, Pockels cell pulse switch, and Nd:YAG preamplifiers are housed on one granite optical bench while the Nd:glass rod and disk amplifiers are

mounted on a parallel steel "I" beam. Two mirrors are used to turn the pulse from the output of the preamplifier section to the input of the power amplifier section. This configuration decouples the alignment of the two subsystems so that changes in the oscillator section such as the insertion (or deletion) of an etalon (to change the pulsewidth) will not necessitate realignment of the whole system but at most will involve realignment of the preamplifiers and turning mirrors. Figure 61 shows the system as it is now used.

There are significant changes since last year in the 44 mm disc amplifier and in the staging of the rod amplifiers. The 44 mm disc amplifier is a retrofit to the CGE 64 mm amplifier head and was designed as a sealed amplifier to minimize dirt and dust problems. It functions as an intermediate stage between the rod amplifiers and the 64 mm disc amplifier and has a small signal gain of 3.5. Figure 62 shows the construction of this amplifier.

The staging of the outputs from the rod amplifiers has been modified as a result of the success of the parasitic suppressing, liquid claddings. The output intensity from the 45 mm amplifier is unchanged at a maximum value of 1.3×10^{10} W/cm^2 but the output of the 32 mm amplifier has been decreased to $\sim 2.5 \times 10^9$ W/cm^2 (from 5×10^9 W/cm^2) and the output of the 23 mm amplifier to 2×10^8 W/cm^2 (from 10^9 W/cm^2). This staging should further improve component lifetime and should minimize the gain for small scale self-focusing in the rod section of the system.

The beam spatial profile evolves through the system in a reasonable fashion. The oscillator TEM_{oo} mode is truncated at the e^{-4} point before the YAG preamplifiers and is then retruncated at the first zero of the Airy's disc in the far field of the first aperture. This procedure is used rather than a "soft" aperture for several reasons:

- There does not appear to be any significant penalty. The spatial noise generated by the second truncation appears to be weaker than that generated by index inhomogeneities in the laser components; the damage patterns which accumulate over 500 - 1000 shots do not appear to be caused by the self-focusing of Fresnel fringes but are rather randomly distributed with the highest density of filaments in the center of the rod where the intensity is highest.

- This type of truncation aperture is easy to align.

- Suitable damage resistant "soft" apertures are not yet in routine commercial production.

When this situation changes it will be worthwhile to install a "soft" aperture in our system; until that point is reached it seems danagerous to make system operation depend on a component for which spares may not be readily available.

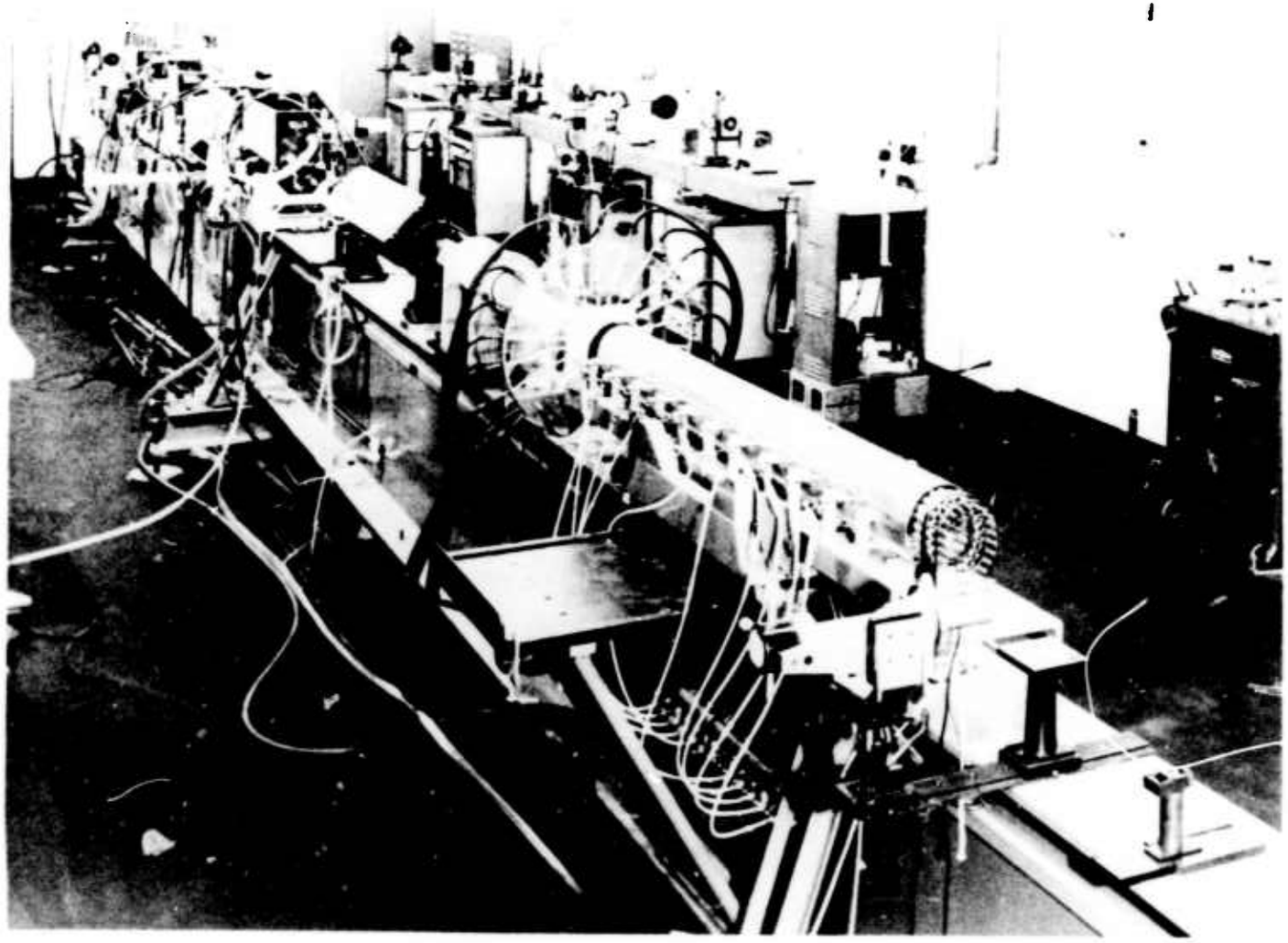

Figure 61 Present configuration of the NRL disc laser. The mode locked oscillator and preamplifiers are on the optical bench on the far side of the room while the CGE rod amplifiers, 44 and 66 mm disc amplifiers and optical isolators are on the Steel I-beam in the foreground.

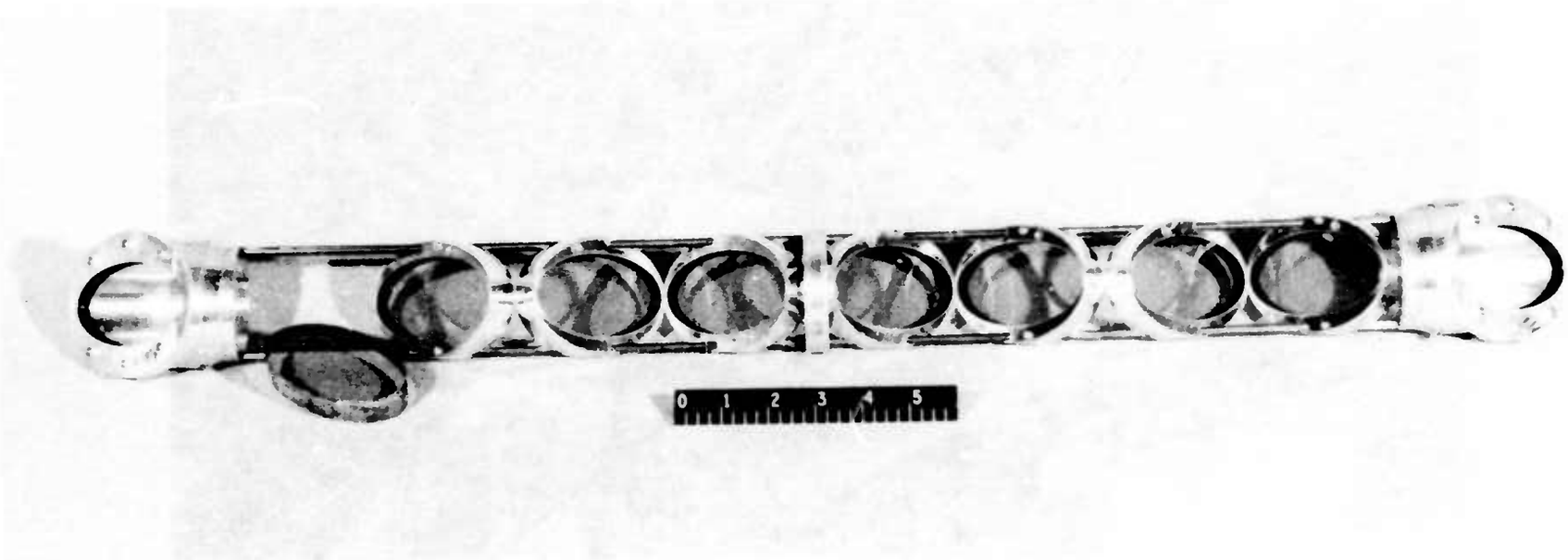

Figure 62a 44 mm aperture disc laser structure which was retrofitted into the CGE 64 mm laser head.

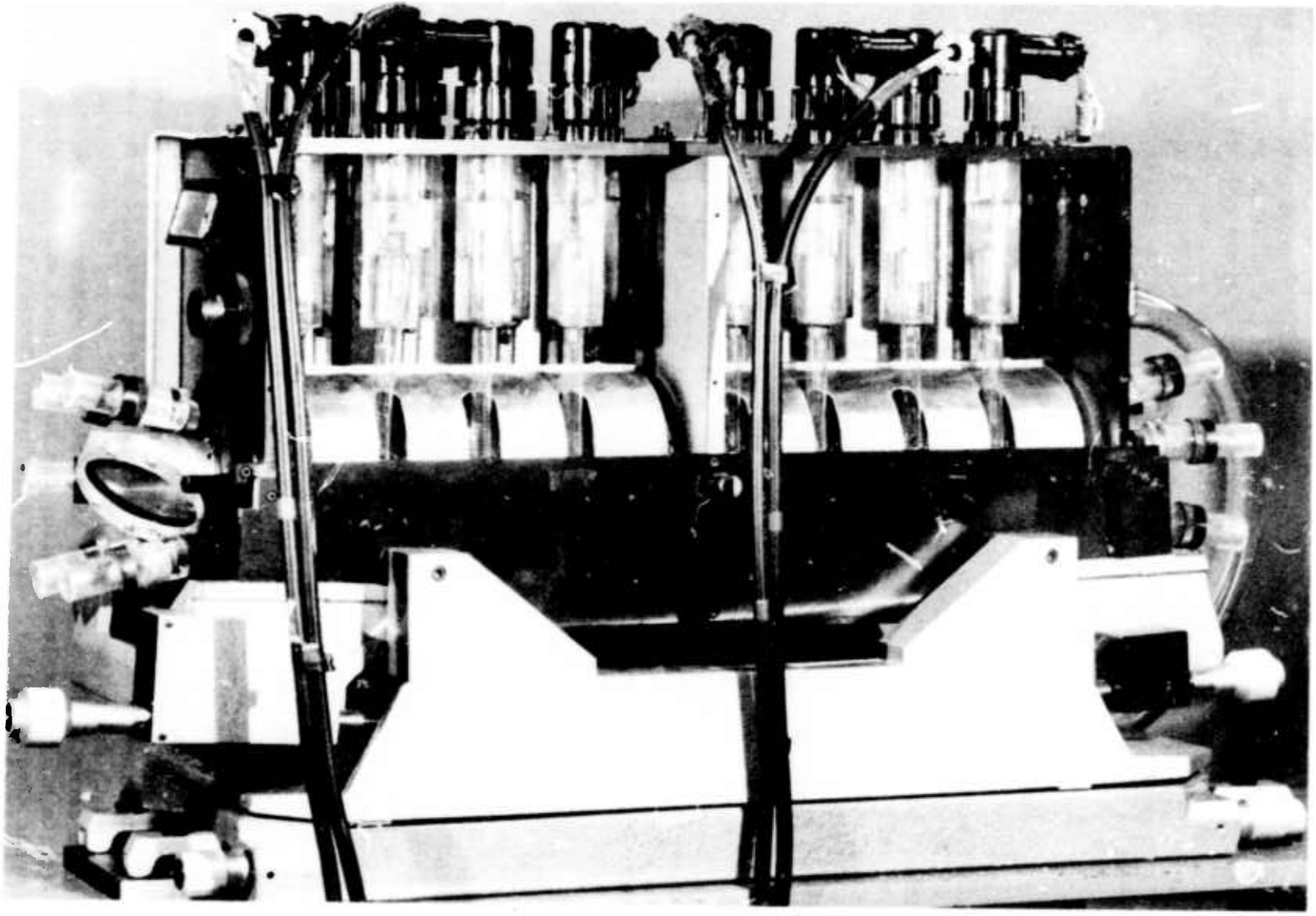

Figure 62b View of CGE V64A8 amplifier head with disc laser assembly installed. The assembly is sealed and has achieved a gain of 7%/cm.

The rod amplifiers have a strong radial variation of gain coefficient which results in a enhancement of the wings of the pulse as it diverges through them. Additionally, the 25 mm aperture Pockels cell isolator has a higher transmission at the edge than at the center. The approximately Gaussian character of the input profile is modified by these effects such that the beam profile out of the 45 mm amplifier most closely fits a shape function

$$F(r) = F(o)\ \exp[-(r/r_o)^5] \quad .$$

Figure 63 shows the results of measurements on the beam profile together with the best fits obtained for various shape functions. This function has about the fastest radial roll off which can be tolerated without severe spatial "ringing" on further amplification[1] due to the nonlinear index of refraction. At the output of the disc amplifier this profile is flattened more but does not have to propagate through any significant path of high n_2 material before the target (2 windows, 1 beam splitter, 1 lens) so that good energy extraction is obtained without beam breakup.

The wavefront shape is reasonable. Through the 45 mm rod the beam is a spherical wave to a very good approximation and can be collimated to a parallel wavefront with less than $\lambda/2$ depature from perfection. Figure 64 shows a shearing interferogram obtained at this point.

The disc amplifier and stacked plate polarizer introduce astigmatism into the beam because of cumulative polishing errors, and at present the astigmatism limits the best focal spot with the $f/14$ lens to ~ 100 μm and 30 μm with the $f/1.9$ aspheric lenses. Efforts are underway to reduce or eliminate this astigmatism by several means: The Fecker Division of Owens-Illinois has repolished laser discs to have a better surface finish with a more random residual than was shown in the initial discs; the new amplifier has a smaller number of discs (6 vs 11) operating at a higher gain and should show less distortion; for 100 psec or shorter operation the stacked plate polarizer can be replaced by available dielectric polarizers without damage problems; and a small residual astigmatism can be compensated by tilting the focusing lens.

Dynamic effects have been examined to determine their effect on focusing on target. The major effect noted was a dynamic shift of focus due to the rod amplifiers which at typical operating levels were determined by shearing interferometry to be equivalent to long focal length diverging lenses. The 23 and 32 mm amplifiers appear to be $\sim$ 16 meter lenses while the 45 mm amplifier appeares to be equivalent to a 35 meter lens. Also, the Pockels cell was equivalent to a 15 meter divergent lens. It is necessary to carefully collimate the laser and change the position of the collimating lens if the pump energy is changed.

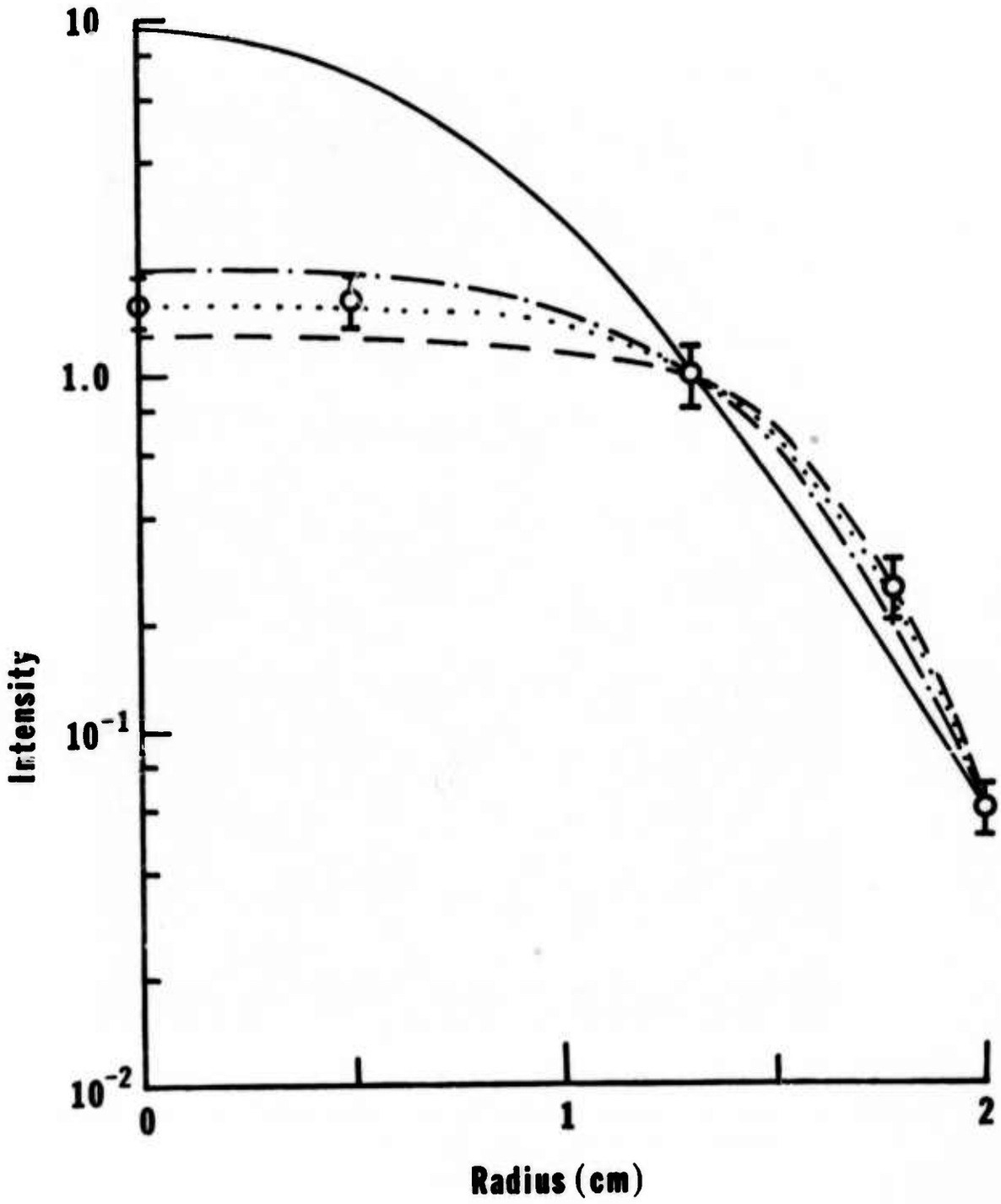

Figure 63 Measured beam profile out of the 45 mm rod amplifier at 7 Joules in a 250 psec pulse. Fits are shown for various shape functions $F = F(o) \exp [(r/r_o)^n]$ for n = 2(-); 4(-·-); 5(····); 6(---).

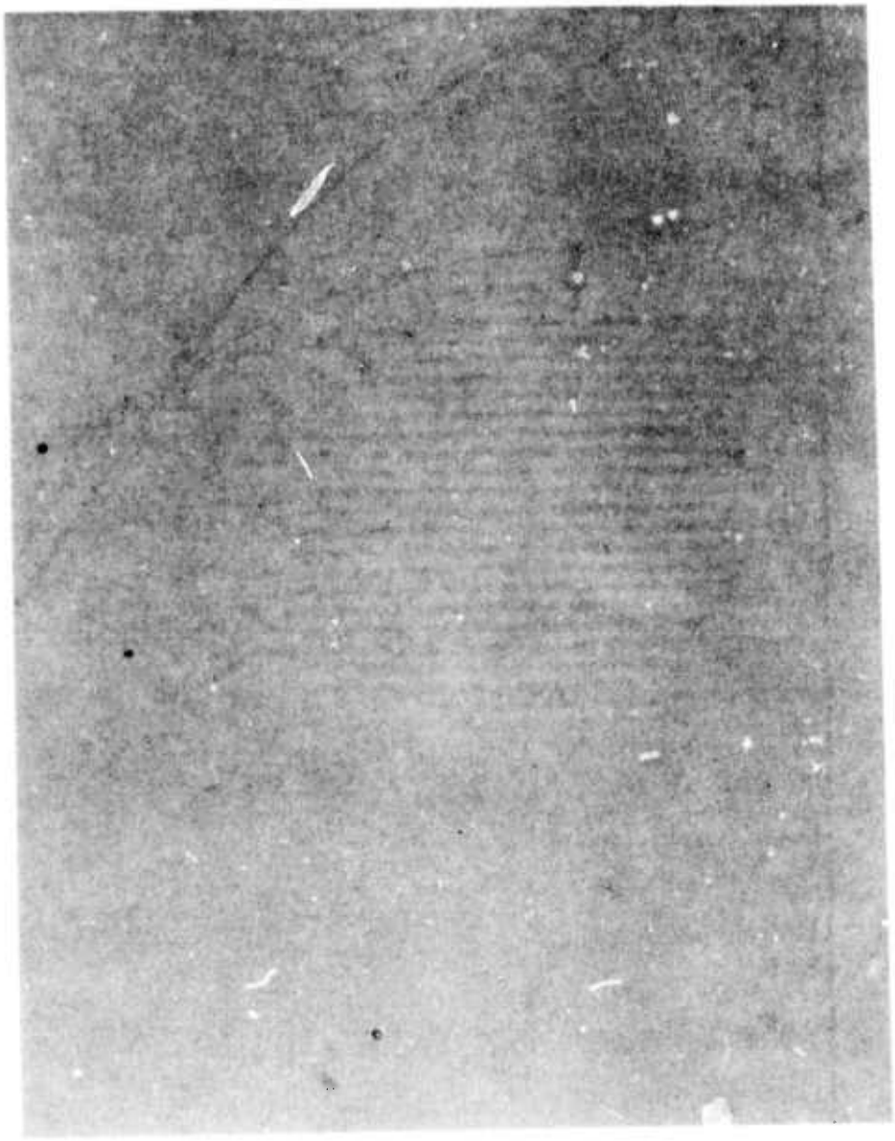

Figure 64 Shearing interferogram of the laser wavefront out of the system with a 20 J, 250 psec pulse.

No nonlinear shift of focus was noted with well behaved beams (although the dynamic testing of collimation would also result in setting for the best compensation of the nonlinear shift). Nonlinear effects were noticeable when the disc amplifier was operated with severely degraded disc surfaces. In this case less than 50% of the energy reached the target lens and the beam would not focus to less than 200 - 300 μm spots with the F/14 lens.

B. LASER OPERATION ON TARGETS

In FY-74 the NRL glass laser system was used for a wide variety of experiments in support of both the AEC and DNA interaction programs and the ARPA/NRL X-ray laser programs. Additionally, the laser system was run for a number of laser experiments and a number of shots were consumed by trouble shooting and realignment following changes in pulsewidth.

Median energies on targets at the different pulse widths were:

900 psec - 50 Joules

250 psec - 20 Joules

40 psec - 7 Joules.

The most intense shots were about twice these values. The intensities out of the laser were 30 - 40% higher with the pulse diagnostics and transmission losses accounting for the balance. The medium energies achieved in FY-74 are about twice those for FY-73 reflecting the degree of success achieved toward the program goal of increasing system output without sacrificing reliability. With the evolutionary modifications planned for FY-75 (sealed ILC disc laser in routine use and high gain 64 mm rod amplifier) it appears reasonable to plan for the same number of shots on target at median energies on target twice those achieved this year, i.e.:

15 - 20 J in 40 - 50 psec pulses

30 - 50 J in 100 psec pulses

100 - 150 J in 250 psec pulses.

There are at present no specific plans for experiments at longer pulse duration, but at a nominal nanosecond (900 psec) the system should be capable of routinely irradiating targets with more than 200 Joules.

Experience with component damage in the past year has been relatively benign with the exception of the prototype NRL disc amplifier in which disc surface damage has been a problem. Careful filtration of the N_2 purge gas and careful assembly has reduced but not eliminated the damage due to dust or foreign matter settling on disc surfaces

and being exploded by the flashlamps.* ZAP calculations[2] performed at LLL on the cerium absorption of pump light in ED-2 laser glass make it appear plausible that the surface of the discs are highly strained and that any cerium oxide polishing compound imbedded in the surfaces can cause localized failures. A set of cerium doped fused silica flashlamps is being procured to reduce the ultraviolet loading on the discs.

NRL experience with Pyrex shatter shields in the 44 mm disc amplifier was similar to that noted by LLL[3]; with careful annealing and cleaning there were no problems for 50 - 100 shots but as the flashlamps damaged the outside surface the inner surface began to ablate material; therefore fused silica tubing was substituted. There appeared to be some long term advantage in mounting the discs vertically to reduce the settling of dust and dirt on the disc surfaces. The ILC amplifier will be installed in this configuration.

The effect of disc surface damage on laser performance has been less dramatic than might be anticipated. For the first hundred shots the beam coherence was quite reasonable. Over the next 400 - 500 shots there will be a gradual deterioration in the level at which a high quality beam can be generated. At the end of this period the output level for a beam with a reasonable wavefront is decreased by a factor of 2 - 2.5 and the disc must be repolished to regain the initial output levels. This relatively benign situation is tracible to the abrupt staging of the amplifier (high gain per unit length) which only allows a short path length for build-up of small scale self focusing as well as the relatively long average air path between discs (13 cm). The new ILC amplifier should perform even more respectably because the gain is higher, the path length is shorter and more advanced sealing techniques are employed.

Rod amplifier damage rates have not been a serious problem (~ 1 final rod per 500 shots) and the index matching liquids should improve the situation since the 40% higher gain coefficient of the final amplifier allows operation with a reduced input. Indications to date are that the rate is increased but at this point the degree of improvement is not available. Earlier experience on damage vs intensity would lead to an expected improvement greater than a factor of two. Replacement of other components is required at a rate of once a year or less and is as correlatible with operator error as with the statistical damage probabilities for the components.

REFERENCES

1. LLL Laser Fusion Semi-Annual Report, UCRL-50021-73-2, p. 135.

2., 3, 4. ibid pp. 40, 13, 34.

* Additionally, flashlamp induced damage in the surfaces was noted.

APPENDIX C LIST OF PUBLICATIONS FROM THE ARPA/NRL X-RAY LASER PROGRAM

A. LASER TECHNOLOGY

1. "Self-Focusing in Mode-Locked Nd:Glass Laser Oscillators", R. C. Eckardt IEEE J. Quantum Electronics (Jan 1974).

2. "Temporal Development of Mode locked Oscillations in Nd:Glass Lasers", R. C. Eckardt, J. N. Bradford, and C. H. Lee, Opto-Electronics (Jan. 74).

3. "Characteristic of a Nd:Sodium Apatite Mode locked Oscillator", R. C. Eckardt, J. L. DeRosa, and J. P. Letellier, IEEE J. Quantum Electronics (August 1974).

4. "Characteristics of a Nd:CaLaSOAP Mode-Locked Oscillator", R. C. Eckardt, J. L. DeRosa, and J. P. Letellier, Technical Digest of 1973 International Electron Devices Mtg.

5. Numerical Calculations of Self-Focusing in Laser Oscillators", R. C. Eckardt, NRL Report (submitted).

6. "Computer Calculations of Temporal Development of Mode-Locked Laser Oscillations including Self Phase Modulation Effects in Nd:Glass", R. C. Eckardt, NRL Report (submitted).

7. "A Multiple Pulse Laser System with Hynchronized Mode-Locked and Q-Switched Outputs", J. Reintjes, R. C. Eckardt, and J. L. DeRosa, IEEE Intn'i Electron Devices Mtg., W shington, D. C. (Dec. 1974).

8. "Evaluation of High-Power Picosecond Pulses in a Pulsed Mode-Locked Laser", R. C. Eckardt, C. H. Lee and J. N. Bradford, VII Int'1. Quantum Electronics Conf. Montreal, Canada (May 1972).

B. TW UV LASER

1. "A Transverse Traveling-Wave Electron Beam Pump for Short Wavelength Lasers", R. Waynant, IEEE/OSA Conf. on Laser Eng. and Appl., Washington, D. C. (May 1973).

2. "Vacuum Ultraviolet Laser Emission from C IV", R. W. Waynant, Appl. Phys. Lett. 22, 419 (Apr. 73).

3. "New Laser Emission in the Vacuum Ultraviolet from C IV", R. W. Waynant, OSA Spring meeting, Denver 13-16 March 1973.

4. "Vacuum UV Laser Research at NRL", R. W. Waynant, III Vavilov Nonlinear Optics Conf., Novosibirsk, USSR (June 1973).

5. "Vacuum UV Laser Research at NRL", R. Waynant, Proceedings of III Vavilov Nonlinear Optics Conf.

6. "Increased Power from CO Laser Lines in the VUV", R. W. Waynant, submitted to Appl. Phys. Letters.

7. "Observations of Gain by Stimulated Emission in the Werner Band of Molecular Hydrogen", R. W. Waynant, Phys. Rev. Letters 28, 533 (1972).

8. "Laser Emission from the Werner Band of Hydrogen", R. W. Waynant, Proceedings of 24th Annual Gaseous Electronics Conference abstracted in Bull. Am. Phys. Soc. 17, 399 (1972).

9. "Gain in H_2 at 1160 Å", R. W. Waynant, 1972 Quantum Electronics Conference, Montreal, Canada, May 1972.

C. VACUUM SPARK

1. "Solar Flare and Laboratory Plasma Phenomena", T. N. Lee, Astrophysical Journal 190, 467-79 (1974).

2. "High Density Ionization with Intense Linear Plasma Focus Discharge", T. N. Lee, Conf. on Confinement of Plasmas, New York (March 1974).

3. "Non-Thermal Processes in a Linear Pinch Device", T. N. Lee, NRL Memorandum Report 2502 (1972).

4. "Diagnostics of a Vacuum-Spark Plasma", T. N. Lee and F. C. Young, APS Plasma Physics Mtg., Albuquerque, NM (Oct. 74).

D. LASER-PLASMA STUDIES

1. "X-Ray Emission from a Plasma Produced by a 25 psec Laser Pulse", T. N. Lee, J. Davis, J. R. Reintjes, R. H. Dixon, R. C. Eckardt, K. Whitney, J. L. DeRosa, R. A. Andrews, and R. C. Elton, APS Spring Mtg., Washington (Apr. 1974).

2. "Laser Produced Mg Plasma", T. N. Lee and D. Nagel, J. of Applied Physics (submitted).

3. "Towards X-Ray Lasers with VUV Amplification on 3p→3s Transitions", R. C. Elton, T. N. Lee, J. Davis, J. Reintjes, R. H. Dixon, R. C. Eckardt, K. Whitney, J. L. DeRosa, L. J. Palumbo, and R. A. Andrews, Intn'l Conf. on X-Ray Processes in Matter, Helsinki (July 74).

4. "Effect of Pre-pulse in 25 ps Laser Produced Plasma", J. F. Reintjes, T. N. Lee, R. C. Eckardt, J. L. DeRosa, R. A. Andrews and R. C. Elton, APS Plasma Physics Mtg., Albuquerque, NM (Oct. 1974).

5. "Further Evidence of Laser X-Ray Emission from $CuSO_4$-Doped Gelatin", R. Elton, L. Palumbo, R. Andrews, R. Eckardt, and J. Bradford, Appl. Optics 12, 155 (1973).

6. "Evidence for Collimated X-Ray Emission from Laser-Heated Copper Sulfate", J. N. Bradford, R. C. Elton, R. Eckardt, L. Palumbo, and R. A. Andrews, Div. of Plasma Phys. Mtg. of APS, Monterey, Calif. (Nov. 1972).

7. "Recent Supporting Evidence of X-Ray Laser Emission from $CuSO_4$-Doped Gelatin", L. Palumbo, R. A. Andrews, R. Elton, J. N. Bradford, R. Eckardt, Div of Electron and Atomic Phys. Mtg. of APS, Stanford, Calif. (Nov. 1972).

8. "Further Comments on Collimated X-Ray Emission from Laser-Heated $CuSO_4$-Doped Gelatin", J. N. Bradford, R. C. Elton, T. N. Lee, R. A. Andrews, L. J. Palumbo, and R. C. Eckardt, Appl. Optics 12, 1095 (1973).

9. "Soft X-Ray Emission from Double-Electron Radiative Transitions in Plasma Ions", R. C. Elton and L. J. Palumbo, NRL Memorandum Report 2457 (1972).

E. ANALYSIS

1. "Research Toward X-Ray Lasers", R. A. Andrews, Gordon Research Conference on Nonlinear Optics and Lasers, Santa Barbara, CA (Jan. 1974).

2. "Radiative Energy Losses Due to Anamolous Bremsstralung Emission Following Dielectronic Capture", L. J. Palumbo and R. C. Elton, APS - Division of Plasma Physics Mtg., Philadelphia (Nov. 1973).

3. "Investigation of $3p \rightarrow 3s$ Lasing in the VUV Region", R. C. Elton, IV Intern'l Conf. on VUV Radiation Physics, Hamburg, W. Germany (July 74).

4. "Lasers", R. C. Elton, Electron-Positive Ion Workshop, Boulder, Colo. (July 74).

5. "Quasi-Stationary Population Inversion on K_α Transitions", R. C. Elton, Intern'l Conf. on X-Ray Processes in Matter, Helsinki (July 74).

6. "Extension of $3p \rightarrow 3s$ Ion Lasers into the VUV Region", R. C. Elton, submitted to Applied Optics.

7. "Analysis of VUV and X-Ray Lasers Pumped by a TW Source", submitted as NRL Memo Rept.

8. "Analysis of X-Ray Laser Approaches: 1. Extension of 3p-3s Ion Lasers into the VUV Region", R. C. Elton, NRL Memo Rept. 2799 (May 1974).

9. "X-Ray Lasers: The Problems, Possible Approaches and Current Status", R. C. Elton, Invited Paper, Meeting of Optical Society of America, Denver, 13-16 March 1973.

10. "The Problems, Progress and Outlook for X-Ray Lasers", R. C. Elton, Invited Paper, Spring Meeting of American Physical Society, Washington, D.C., 23-26 April 1973.

11. "X-Ray and Vacuum-UV Lasers -- Current Status and Prognosis", R. A. Andrews, R. C. Elton, M. H. Reilly and R. W. Waynant, NRL Report 7412, May 1972.

12. "Approaches to High Photon Energy Lasers", D. J. Nagel, Intern'l Conf. on X-Ray Processes in Matter, Helsinki (July 74).

13. "Analyses of X-Ray Laser Approaches: 2. Quasistationary Inversion on Kα Innershell Transitions", R. C. Elton, NRL Memo Rept. (August 1974). 1974).

F. MISCELLANEOUS

1. "Atomic and Ionic Emission Lines below 2000 Å-Hydrogen through Krypton", R. L. Kelly and L. J. Palumbo, NRL Report 7599.

2. "Radiative-Auger Transitions in Soft X-Ray Emission", R. C. Elton and L. J. Palumbo, Phys. Review A9 1873 (May 1974).

3. "Plasma Turbulence in a Linear Discharge Pinch", T. N. Lee, and R. Dixon, APS-Division of Plasma Physics Mtg., Philadelphia (Nov. 1973).

4. "Experimental Work on X-Ray Lasers at NRL", by R. C. Elton, Conference on New Laser Concepts, Key Largo, Florida, November, 1972.

5. "X-Ray Lasers - Current Thinking", R. A. Andrews, NRL Memo Rept. No. 2677.

6. "X-Ray Lasers-Current Thinking", R. A. Andrews, Invited Paper, 1973 Mtg. Materials Research Council, LaJolla, Calif., 19-20 July, 1973.

7. "The NRL-NPGS Compilation of Vacuum Ultraviolet Spectra", R. L. Kelly and L. J. Palumbo, 1973 Fall Mtg. of Optical Soc. of Amer., Rochester, N.Y., Oct. 1973.

8. "Two Photon Resonantly Enhanced Self-defocusing in Cs Vapor at 1.06 μ", R. H. Lehmberg, J. Reintjes, and R. C. Eckardt, IEEE Intern'l Electron Devices Mtg., Washington (Dec. 1974).

9. "Two Photon Resonantly Enhanced Self-defocusing in Cs Vapor at 1.06μ", R. H. Lehmberg, J. Reintjes, and R. C. Eckardt, Appl. Phys. Lett.

10. "Publication Problems of the NRL-NPGS Compilation of Computer-Based Data", L. J. Palumbo and R. L. Kelly, 1973 Fall Mtg. of Optical Soc. of Amer., Rochester, N.Y., Oct. 1973.